The Science of Hysteresis, Volume 3; I. Mayergoyz and G.Bertotti (Eds.); Elsevier (2005)

CHAPTER 4

Hysteresis in Piezoelectric and Ferroelectric Materials

***Dragan Damjanovic**, Ceramics Laboratory, Materials Science and Engineering Institute, School of Engineering, Swiss Federal Institute of Technology – EPFL, 1015 Lausanne, Switzerland*

Contents

4.1 INTRODUCTION

Piezoelectric and ferroelectric materials are widely used in many areas of technology and science. The sensors based on the piezoelectric effect transform mechanical signals into electrical signals and are used as accelerometers, and for measurements of pressure and vibration. The piezoelectric actuators transform electrical signals into mechanical signals and are used in displacement actuators and force generators. Ferroelectric materials are a special class of piezoelectrics, which exhibit, in general, a large piezoelectric response. Besides piezoelectric applications, optical, thermal and electrical properties of ferroelectrics are exploited in a large number of devices and components [1–3], including capacitors and nonvolatile

The Science of Hysteresis Volume 3
I. Mayergoyz and G. Bertotti (Eds.)
ISBN: 0-123-69432-3
3 volume set ISBN: 0-1248-0874-3

memories where electrical voltage is used to displace electrical charge. Except in memory applications, which are based on polarization switching and hysteretic polarization–electric field relationships, hysteresis is undesired in high-precision sensor, actuator and capacitor applications. Yet, with a few very special exceptions, the ferroelectric materials with the highest piezoelectric properties are usually the ones with the strongest electromechanical hysteresis. The control, description, and understanding of electromechanical (piezoelectric) and ferroelectric hystereses present thus an important, and, as we shall try to demonstrate throughout this chapter, difficult undertaking from both the practical and theoretical point of view.

There are different approaches to how to reduce the hysteresis in piezoelectric devices. A material scientist may attempt the challenging task of minimizing the hysteresis by designing the material on a microstructural or even atomic level, while keeping the high piezoelectric response. A device engineer will try to construct an active feedback system that will reduce hysteresis of the output signal by controlling the driving-field input signal. In each case, the control process is greatly facilitated if the physical origins of the hysteresis are known. From the fundamental point of view, the interest in piezoelectric hysteresis includes the fact that it appears between mixed variables such as electric field and mechanical strain, or mechanical pressure and electric charge. This electromechanical coupling is responsible for some unusual hysteretic phenomena, such as clockwise hysteresis that is not encountered in hysteretic processes that relate purely electric (e.g. electric polarization–electric field), elastic (strain–stress) or magnetic (magnetization–magnetic field) variables.

Origins and mechanisms of the piezoelectric hysteresis are complex and, as illustrated in Fig. 4.1, they manifest themselves in qualitatively different forms. We shall see that a study of hysteresis can give valuable information on different physical processes that take place in ferroelectric materials, e.g. domain-wall pinning, defect ordering, and nature of defects. In that sense, this chapter will approach hysteresis from the materials science point of view. The first part of the chapter will mainly discuss piezoelectric hysteresis in ferroelectric materials; however, the formal approach, wherever given, is quite general and is valid for nonferroelectric piezoelectric materials as well.

The polarization–electric field hysteresis in ferroelectric materials is discussed in some detail in the last part of the chapter. It is a wide subject, ranging from the nonswitching dielectric hysteresis that encompasses a huge number of dielectric relaxation phenomena to processes related to polarization switching. The hysteresis in ferroelectric and dielectric properties will be discussed through a few selected examples. Throughout

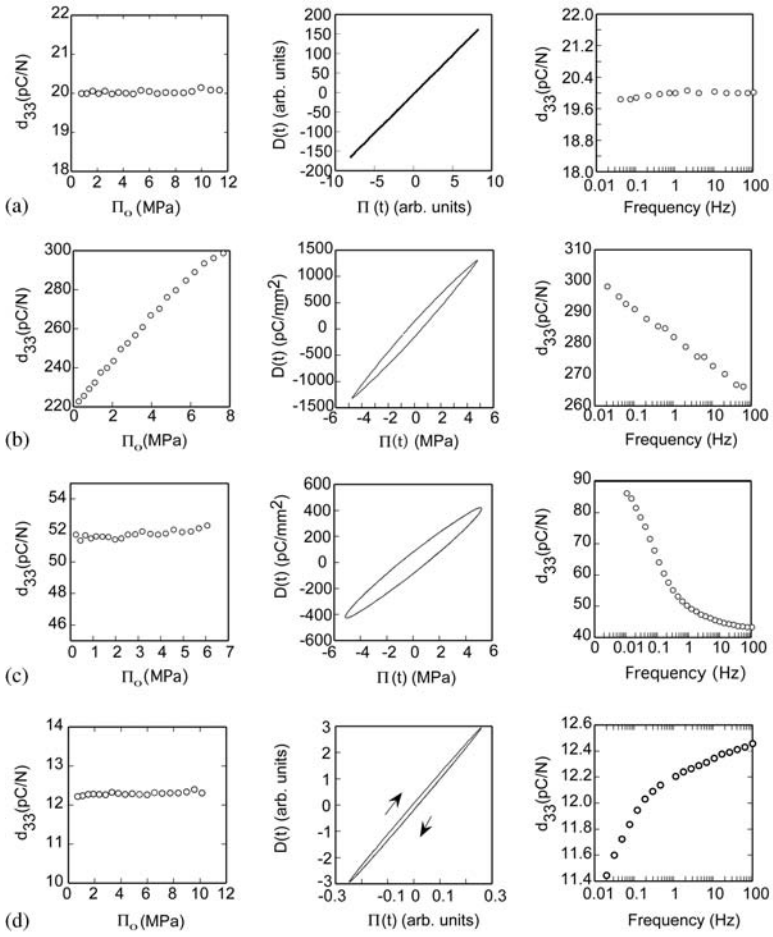

FIGURE 4.1 Field dependence, hysteresis, and frequency dispersion associated with the direct piezoelectric effect in (a) $SrBi_4Ti_4O_{15}$, (b) Nb-doped PZT, (c) (Pb, Sm)TiO_3, and (d) Mn doped $SrBi_4Ti)_4O_{15}$ (courtesy of Cyril Voisard) ceramics. Arrows in (d) indicate the clockwise sense of hysteresis rotation for this material. The hystereses are measured under compressive pressure and are subsequently centered numerically.

the text, attempts will be made to demonstrate how a study of hysteresis may be a powerful tool to get insight into microscopic processes taking place in ferroelectric and piezoelectric single crystals, ceramics and polymers.

With a few exceptions, mainly in the field of actuators [4–6], and in the studies of ferroelectric switching [7–9], the experimental investigations of piezoelectric and ferroelectric hysteresis are carried out by applying a periodic, constant-amplitude signal; thus, the most commonly adopted approach in describing the hysteresis in ferroelectrics and piezoelectrics is in terms of looping and phase angle rather than in terms of branching. As we shall see later, this approach, even though restricted [10], can nevertheless give rich information on different hysteretic processes in ferroelectric and piezoelectric materials. First of all, some of the most important and interesting hysteresis processes in piezoelectric and ferroelectric materials are manifested simply by the frequency-dependent phase angle between the driving field and the linear material response. Secondly, in many nonlinear (field-dependent) cases that will be discussed in detail, the processes that in the first approximation can be described as rate independent are in fact accompanied by a weak frequency dependence of the hysteresis parameters, so that the description of the hysteresis in terms of the phase angle and looping becomes convenient. The simultaneous occurrence of the nonlinear, rate-independent, and linear, rate-dependent, processes in a material makes the analysis of associated hystereses very challenging from both the experimental and theoretical points of view. Finally, in piezoelectric materials, the simple, linear hysteresis originating from the relationship $R = mF_0 \sin(\omega t - \delta)$, (where F is the general driving field (input), R is the material response (output) and m the material coefficient) can exhibit interesting properties, such as the clockwise and horizontal hystereses (with its axes parallel to R and F axes), that are not observed in F-R processes that relate conjugate work variables. The author believes that this unusual, even though mathematically simple, hysteretic behavior deserves to be treated in some detail in a general book on hysteretic phenomena.

It is difficult to make self-contained a relatively short text that treats a subject of such complexity as hysteresis. To bridge unavoidable gaps in the text, references that contain more detailed and complementary information are given whenever possible. The choice of examples given in the text is necessarily biased by the author's own research, interest, and preferences. It must be mentioned that a rigorous theoretical treatment of the piezoelectric hysteresis is, unfortunately, still lacking and the number of experimental studies dealing with the subject from the physical point of view is rather limited. Owing to recent activities in the field of ferroelectric memories, understanding of ferroelectric hysteresis is much more advanced.

The chapter starts with a somewhat extended introduction into ferroelectric and piezoelctric properties. An appendix is provided, which

defines most important variables that are not defined in the text and which also gives a short thermodynamic derivation of piezoelectric constitutive equations.

4.2 BASIC DEFINITIONS

4.2.1 DEFINITION OF THE DIELECTRIC, PIEZOELECTRIC, AND ELASTIC COEFFICIENTS

In this section the basic dielectric, elastic, piezoelectric, and ferroelectric properties and relations necessary for further reading are defined. The reader interested in more details should consult classical textbooks [1,11]. Most of the properties discussed in this text are tensors; however, the scalar treatment is sufficient for most examples discussed later in the text and the tensor indices are often omitted. In those cases where direction of the effect is important, the matrix description based on the Voigt convention [11] is used for tensors of the third and fourth rank.

Application of an electric field, E_i (V/m) ($i = 1, 2, 3$) on an insulating material polarizes the material by separating positive and negative charges. A macroscopic manifestation of the charge separation is the surface charge, described by the electric polarization vector, P_i (C/m^2). The field and polarization are related by:

$$P_i = \chi_{ij} E_j \tag{4.1}$$

where χ_{ij} (F/m) are components of the tensor of the dielectric susceptibility. The total surface-charge density that is induced in the material by the applied field is given by the dielectric displacement vector, D_i (C/m^2), which includes both charges associated with polarization of the material (P_i) and charges created by the polarization of free space ($\varepsilon_0 E_i$):

$$D_i = \varepsilon_0 E_i + P_i = \varepsilon_0 E_i + \chi_{ij} E_j = \varepsilon_0 \delta_{ij} E_j + \chi_{ij} E_j = (\varepsilon_0 \delta_{ij} + \chi_{ij}) E_j = \varepsilon_{ij} E_j \tag{4.2}$$

where $\varepsilon_{ij} = \varepsilon_0 \delta_{ij} + \chi_{ij}$ is the dielectric permittivity of the material and δ_{ij} is Kronecker's symbol ($\delta_{ij} = 1$ for $i = j$, $\delta_{ij} = 0$, for $i \neq j$). Scalar $\varepsilon_0 = 8.854 \times 10^{-12}$ F/m is known as the dielectric permittivity of vacuum. For most ferroelectric materials $\varepsilon_0 \delta_{ij} << \chi_{ij}$ and $\varepsilon_{ij} \approx \chi_{ij}$. In practice, the relative dielectric permittivity, $\kappa_{ij} = \varepsilon_{ij}/\varepsilon_0$, also known as the dielectric constant of the material, is more often used than the dielectric permittivity. Typical values of κ in piezoelectric materials are 10–10 000. Relations (4.1) and (4.2) are valid only in the linear approximation.

The relationship between the stress Π_m (N/m^2) applied upon an elastic material and the resulting strain x_{mn} (-) is given, in the linear approximation, by Hooke's law:

$$x_m = s_{mn}\Pi_n \tag{4.3}$$

where $m, n = 1, 2, \ldots, 6$ (see Appendix A) and s_{mn} is the elastic compliance. The inverse relationship $\Pi_m = c_{mn}x_n$ defines the elastic stiffness tensor c_{mn} (N/m^2). In most ferroelectric materials, values of s are of the order of $10–100 \times 10^{-12}\,m^2/N$.

Piezoelectric materials are a class of low-symmetry [11] materials that can be polarized, in addition to an electric field, also by application of a mechanical stress. The linear relationship between the stress Π_m applied on a piezoelectric material and the resulting charge density D_i is known as the *direct* piezoelectric effect and may be written as:

$$D_i = d_{im}\Pi_m \tag{4.4}$$

where d_{im} (C/N) are piezoelectric coefficients. d is a third-rank tensor. This effect is used, for example, in accelerometers for seat-belt tension systems and pressure sensors. The charge density–pressure relationship in a typical piezoelectric ferroelectric (e.g. soft Pb(Zr, Ti)O_3 or PZT) presents hysteresis as shown in Fig. 4.1(b).

Piezoelectric materials have another interesting property: they change their dimensions (they contract or expand) when an electric field E is applied to them. This *converse* piezoelectric effect describes the strain that is developed in a piezoelectric material due to the applied electric field:

$$x_m = d_{km}E_k = d^t_{mk}E_k \tag{4.5}$$

where t denotes the transposed matrix. The units of the converse piezoelectric coefficient are m/V. This effect is the basis of displacement actuators used in, e.g. scanning systems in electronic microscopes and fuel injection valves in cars. Typical hysteretic behavior of a piezoelectric actuator based on PZT ceramics is shown in Fig. 4.2. Values of d range from 2 to $> 2\,000$ pC/N or pm/V in, respectively, quartz and $Pb(Mg_{1/3}Nb_{2/3})O_3$-$PbTiO_3$ single crystals.

The piezoelectric coefficients d for the direct and the converse piezoelectric effects are thermodynamically identical, i.e. $d_{\text{direct}} = d_{\text{converse}}$. Note that the sign of the piezoelectric charge D_i and piezoelectric strain x_m depends on the direction of the mechanical and electric fields and piezoelectric coefficients. It is common to call a piezoelectric coefficient,

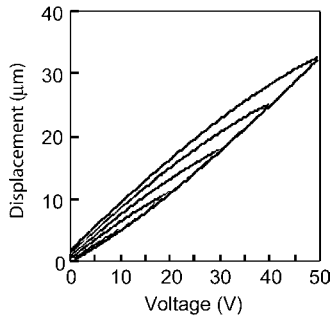

FIGURE 4.2 Displacement–voltage hysteresis in a typical piezoelectric ceramic actuator. (Courtesy of E.L. Colla).

measured in the direction of the applied field, the longitudinal coefficient, and that measured in the direction perpendicular to the field the transverse coefficient. Other piezoelectric coefficients are known as shear coefficients. All piezoelectric coefficients can be either positive or negative.

There are a number of symmetry conditions imposed on ε, s and d coefficients by the symmetry of the stress and strain tensors, thermodynamic relations and crystal symmetry. These conditions limit number of independent and nonzero coefficients. For example, the piezoelectric effect cannot exist in centrosymmetric materials [11].

4.2.2 PIEZOELECTRIC CONSTITUTIVE EQUATIONS AND COUPLING OF ELECTRIC AND MECHANICAL PROPERTIES

Electric charge in a polar material may be induced by an external electric field Eqn. (4.1), or by a stress through the piezoelectric effect, Eqn. (4.4). Similarly, the mechanical strain in a piezoelectric material may be induced by an electric field through the converse piezoelectric effect, Eqn. (4.5), or by an external stress through Hooke's law, Eqn. (4.3). This coupling of different effects places important experimental constraints on property measurements. Assume, for example, that an electric field is applied on the major surfaces of a piezoelectric plate. If the sample is laterally mechanically free to change its dimensions, the resulting longitudinal strain (parallel to the field) is due to the pure piezoelectric effect, Eqn. (4.5). If the sample is partially clamped, so that it cannot expand laterally (for example, a thin film deposited on a thick substrate), the resulting longitudinal strain will be a sum of the piezoelectric strain, Eqn. (4.5), and the mechanical strain Eqn. (4.3) that opposes the piezoelectrically induced lateral strain and which is defined by the clamping conditions [12,13].

The coupling between the elastic and electrical parameters of a material can be introduced formally using the thermodynamic approach (see Appendix B). The results are equations of state that give relations between material parameters measured under different experimental conditions. These relations are essential for modeling and understanding the response of piezoelectric materials. A more detailed discussion can be found in [1,14]. For isothermal processes, combination of Eqns. (4.2)–(4.5) written in the matrix notation leads to:

$$x_m = s_{mn}^{T,E}\Pi_n + d_{im}^{T,\Pi}E_i, \tag{4.6}$$

$$D_i = d_{im}^{T,E}\Pi_m + \varepsilon_{ij}^{T,\Pi}E_j, \tag{4.7}$$

where superscripts indicate variables held constant. Thus, the pure piezoelectric strain (charge) is obtained only under conditions of zero stress (zero electric field). Equations (4.6), (4.7) are known as the piezoelectric constitutive equations. Other combinations of electric and mechanical variables give three additional sets of constitutive equations (see Appendix B).

4.2.3 FERROELECTRIC MATERIALS

Polar materials possess an effective electric dipole moment in the absence of an external field. In general, the individual dipoles are randomly oriented in the space. In so-called pyroelectric materials, all dipoles are oriented in the same sense, creating surface charge, which is a measure of the macroscopic spontaneous polarization, P_S. Ferroelectrics are a special case of polar materials where spontaneous polarization P_S possesses at least two equilibrium states; the direction of the spontaneous polarization vector may be switched between those orientations by an electric field. The crystal symmetry requires that all ferroelectric materials must be pyroelectric and all pyroelectric materials must be piezoelectric. Today, the majority of piezoelectric materials in practical use, with the important exception of quartz, are ferroelectrics. The modern definition of ferroelectric polarization can be found in some recent texts [15], but for our purposes we can limit ourselves to the simple approach given here.

Most ferroelectric materials undergo a structural phase transition from a high-temperature nonferroelectric (or paraelectric) phase into a low-temperature ferroelectric phase. Some ferroelectrics, like barium titanate, $BaTiO_3$, undergo several phase transitions into successive ferroelectric phases. The transition into a ferroelectric phase usually leads to strong anomalies in the dielectric, elastic, thermal and other properties of the material [1,16,17], and is accompanied by changes in the dimensions of the crystal unit cell. The associated strain is called the spontaneous strain, x_S

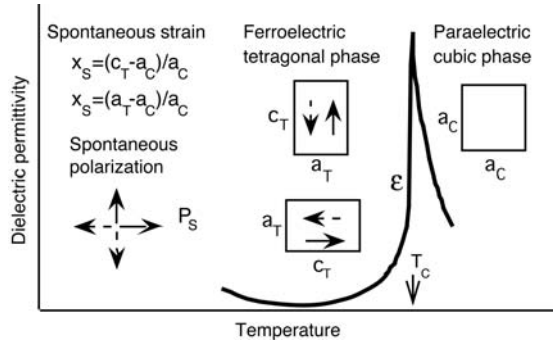

FIGURE 4.3 Illustration of the changes in a two-axial ferroelectric material as it transforms from a paraelectric cubic into a ferroelectric tetragonal state.

It represents the relative difference in the dimensions of the ferroelectric and paraelectric unit cells. Some changes that can occur in a ferroelectric material that transforms from a paraelectric cubic into a ferroelectric tetragonal phase are illustrated in Fig. 4.3. Readers interested in the theoretical treatment of ferroelectricity and related phenomena should consult one of the many textbooks on the subject [1,14,16,17].

4.2.4 FERROELECTRIC DOMAINS

To introduce ferroelectric domains, and avoid a too general discussion, we take as an example lead titanate, $PbTiO_3$. Lead titanate is a perovskite crystal that transforms from a nonferroelectric cubic to a ferroelectric tetragonal phase at 490°C. Perovskite crystals have a general formula ABO_3 where valence of A cations takes values from +1 to +3 and of B cations from +3 to +6. As shown in Fig. 4.4, the structure may be viewed as consisting of BO_6 octahedra surrounded by A cations. Most of the ferroelectric materials that are of practical interest have a perovskite structure and many, such as lead zirconate titanate, $Pb(Zr, Ti)O_3$, are solid solutions of $PbTiO_3$. The spontaneous polarization in $PbTiO_3$ lies along the c_T-axis of the tetragonal unit cell and the crystal distortion is usually described in terms of the shifts of O and Ti ions relative to Pb [18]. In the ferroelectric phase, the crystal is spontaneously strained with $a_T(= 0.390\,\text{nm}) < a_C < c_T(= 0.415\,\text{nm})$ where a_T and a_C are the a-axes of the tetragonal and cubic unit cells, and c_T is the c-axis of the tetragonal cell.

The spontaneous polarization in a ferroelectric crystal (or a grain in a ferroelectric film or ceramic) is usually not uniformly aligned throughout the material along the same direction. The six directions (including

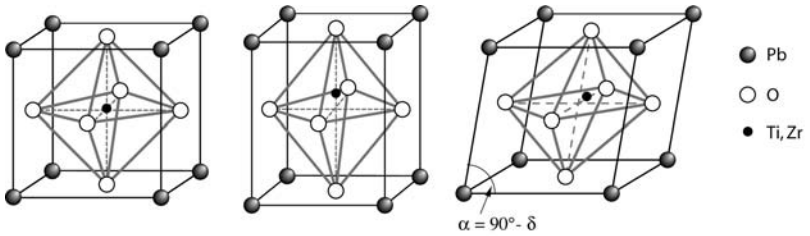

FIGURE 4.4 Perovskite crystal in its paraelectric cubic (left), ferroelectric tetragonal (middle), and rhombohedral (right) states. $PbTiO_3$, which is cubic in the paraelectric phase and tetragonal in the ferroelectric phase, can adopt rhombohedral structure when modified by about 50 per cent Zr.

positive and negative orientations) along the three a_C-axes of the cubic cell in $PbTiO_3$ are equivalent, and spontaneous polarization may arise with equal probability along any of them when the crystal is cooled through the ferroelectric phase-transition temperature. Directions along which the polarization will develop depend on the electrical and mechanical boundary conditions imposed on the sample, as discussed below. The regions of the crystal with uniformly oriented spontaneous polarization are called ferroelectric domains. The region between two domains is called a domain wall. The walls that separate domains with oppositely oriented polarization are called 180° walls and those that separate regions with mutually perpendicular polarization are called 90° walls (Fig. 4.5). Because c_T- and a_T-axes in a tetragonal crystal are different, the angle between polarization directions on each side of a 90° domain wall is slightly smaller than 90° [19]. In the domain-wall region, the polarization changes from one domain to another continuously but steeply [19]. The ferroelectric domain walls are therefore much narrower than the domain walls in ferromagnetic materials. Observations with transition electron microscopy show that the width of the domain walls in ferroelectric materials is of the order of 1–10 nm [1,19,20], that is, as little as 2–3 crystal unit cells. The width of the domains increases with increasing temperature, as the phase transition is approached [21].

The ferroelectric domains form to minimize the electrostatic energy of the depolarizing fields and the elastic energy associated with the mechanical constraints to which the ferroelectric material is subjected as it is cooled through the paraelectric–ferroelectric phase transition [1,22,23]. Onset of spontaneous polarization at the transition temperature leads to the formation of surface charges. This surface charge produces an electric field, called the depolarizing field E_d, which is oriented oppositely to

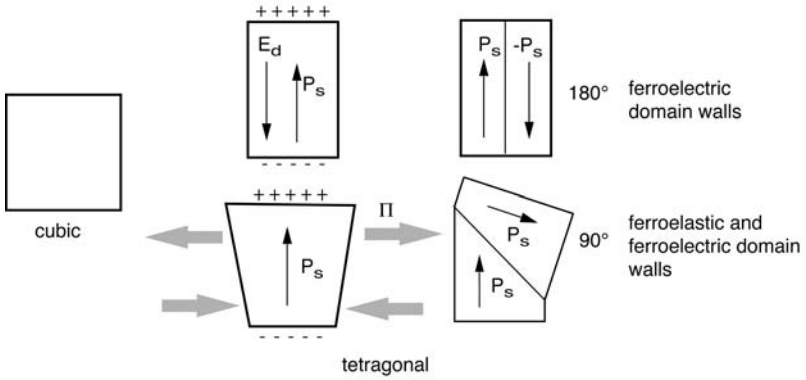

FIGURE 4.5 Illustration of the formation of 180° and 90° ferroelectric domain walls in a tetragonal perovskite ferroelectric. Tetragonal distortion is exaggerated. Effects of the depolarizing field, E_d, and the stresses, Π are minimized by the creation of domain walls.

P_S (Fig. 4.5). The depolarizing field will form whenever there is a nonhomogeneous distribution of the spontaneous polarization, for example, due to the fall-off of the polarization near the surface of the ferroelectric (polarization is zero outside the ferroelectric and nonzero inside) or due to a change in the direction of the polarization at grain boundaries. The depolarizing field may be very strong (of the order of MV/m) rendering the single-domain state of the ferroelectric energetically unfavorable [1,22]. The electrostatic energy associated with the depolarizing field may be minimized if: (i) the ferroelectric splits into domains with oppositely oriented polarization, Fig. 4.5, or (ii) the depolarizing charge is compensated by electrical conduction through the crystal or by charges from the surrounding material (for example, from atmosphere or the electric circuit to which the material is connected). The depolarizing field often cannot be completely compensated, and as grown ferroelectric crystals often exhibit reduced or even zero pyroelectric and piezoelectric effects due to the presence of ferroelectric domains.

Splitting of a ferroelectric crystal into domains may also occur due to the influence of mechanical stresses, as shown in Fig. 4.5 [23,24]. Assume that a part of the $PbTiO_3$ crystal is mechanically compressed along the [100] cubic direction as it is cooled through the phase-transition temperature. To minimize the elastic energy, the long c_T-axis of the tetragonal cell will develop perpendicularly to the stress. In the unstressed part of the crystal, the polarization may remain parallel to the direction of the stress (short a_T-axis perpendicular to the stress). The domain walls in $PbTiO_3$ may

therefore separate regions in which polarization orientation is antiparallel (180° walls) or perpendicular (90° walls) to each other. Both 90° and 180° walls may reduce the effects of depolarizing electric fields but only formation of 90° walls may minimize the elastic energy. A combination of electrical and elastic boundary conditions to which a crystal is subjected as it is cooled through the ferroelectric phase-transition temperature usually leads to a complex domain structure with many 90° and 180° walls. Since domain walls themselves carry energy, the resulting domain-wall configuration will be such that the sum of the domain-wall energy, crystal surface energy, and elastic and electric fields energy is minimal [1,23].

The domain walls that differ in orientation from the spontaneous polarization vector are called ferroelectric domain walls and those that differ in orientation from the spontaneous strain tensor are called ferroelastic domain walls. In $PbTiO_3$, the 180° walls are purely ferroelectric because they differ only in orientation of the polarization vector. The 90° walls are both ferroelectric and ferroelastic, as their differ in orientation of both the polarization vector and the spontaneous strain tensor [24].

The types of domain walls that can occur in a ferroelectric crystal depend on the symmetry of both nonferroelectric and ferroelectric phases of the crystal [25]. In the rhombohedral phase of the lead zirconate titanate, $Pb(Zr, Ti)O_3$, Fig. 4.4, and $BaTiO_3$, for example, the direction of the polarization develops along the body diagonals (direction $\langle 111 \rangle$) of the paraelectric cubic unit cell. This gives eight possible directions of the spontaneous polarization with 180°, 71° and 109° domain walls. Criteria that may be used to derive possible types of domain walls in a ferroelectric material were derived by Fousek and Janovec [25].

4.2.5 FERROELECTRIC HYSTERESIS AND POLING OF FERROELECTRICS

Owing to the complex set of elastic and electric boundary conditions at each grain, the ferroelectric grains in polycrystalline materials are always split into many domains. If the direction of the spontaneous polarization through the material is random or distributed in a such way as to lead to zero net macroscopic polarization, the piezoelectric effects of individual domains will cancel out and such materials will not exhibit piezoelectric effect, which requires at least noncentrosymmetric symmetry of the material [11]. Polycrystalline ferroelectric materials (ceramics) may be brought into a polar state by applying a strong electric field (10–100 kV/cm), usually at elevated temperatures. This process, called poling, can reorient domains within individual grains along those directions that are permissible by the crystal symmetry and that lie as close as possible to the direction of the field. A poled polycrystalline ferroelectric exhibits piezoelectric

properties, even if many domain walls are still present. As-grown ferroelectric single crystals usually contain many domains and may exhibit weak piezoelectric properties. A single crystal that does not contain domains is said to be in a single-domain or monodomain state. The single-domain state in single crystals may be achieved by poling.

Note again that, by definition, the poling, i.e. polarization reversal by a field, is possible only in ferroelectric materials. A piezoelectric non-ferroelectric polycrystalline material (e.g. quartz) with randomly oriented grains cannot be poled and exhibits macroscopic piezoelectric properties.

After the removal of the poling field (at zero field) a ferroelectric material possesses macroscopic polarization, called remanent polarization, P_R. The maximum remanent polarization that may be achieved in a polycrystalline material depends on many factors, including available domain states, electromechanical boundary conditions at grain boundaries and sample surface, and imperfections such as elastic and charged defects in the material.

A defining, and the most important, characteristic of ferroelectric materials is polarization reversal (or switching) by an electric field. We have seen that the natural state of a ferroelectric material is a multidomain state. Application of an electric field will reduce (in ceramics) or completely remove (in crystals) domain walls. One consequence of the domain-wall switching in ferroelectric materials is the occurrence of the ferroelectric hysteresis loop, Fig. 4.6. At small values of the alternating electric field, the polarization increases linearly with the field amplitude, according to relation (4.1). This corresponds to segment AB in Fig. 4.6. In this region, the field is not strong enough to switch domains with unfavorable direction of polarization. As the field is increased, the polarization of domains with unfavorable direction of polarization will start to switch along directions that are crystallographically as close as possible to the direction of the field, rapidly increasing the measured charge density (segment BC). The polarization response in this region is strongly nonlinear and Eqn. (4.1) is no longer valid. Once all the domains are aligned (point C) the ferroelectric again behaves as a linear dielectric (segment CD). When the field strength starts to decrease, some domains will back-switch, but at zero field the polarization is nonzero (point P_R). To reach the zero polarization state, the field must be reversed (point F). A further increase of the field in the negative direction will cause a new alignment of dipoles and saturation (point G). The field strength is then reduced to zero and reversed to complete the cycle. As already mentioned above, the value of polarization at zero field is called the remnant polarization, P_R. Typical values are 0.001 to 1 C/m^2 [1]. The field necessary to bring the polarization to zero is called the coercive field, E_C. In most widely used ferroelectric ceramics

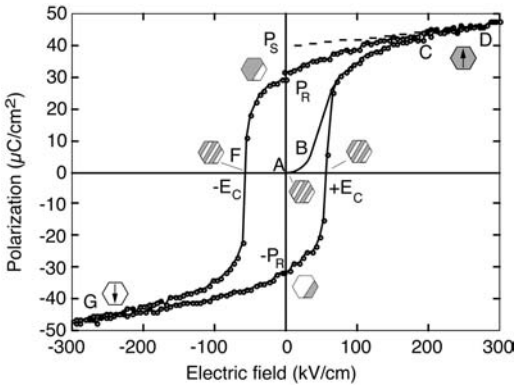

FIGURE 4.6 Ferroelectric (P–E) hysteresis loop. The hexagons with gray and white regions represent schematically repartition of two polarization states in the material (e.g. in grains of a ceramic) at different fields. The symbols are explained in the text. The loop shown is measured on a (111)-oriented 1.3 μm thick sol-gel $Pb(Zr_{0.45}Ti_{0.55})O_3$ film. (Courtesy of David V. Taylor).

and crystals its value is of the order of 0.1–10 MV/m. In single crystals, the spontaneous polarization P_S may be estimated by taking the intercept of the polarization axis with the extrapolated linear segment CD. It should be mentioned that the coercive field, E_C, that is determined from the intercept of the hysteresis loop with the field axis is not an absolute threshold field [22]; if a low electric field is applied over a (very) long time period the polarization will eventually switch. Note that in an experiment only changes of the polarization, such as $\Delta P = 2|P_R|$ induced by electric field, or the temperature derivative of polarization, $\partial P/\partial T$, can be measured, but not the absolute value of polarization.

An ideal hysteresis loop is symmetrical, so the positive and negative coercive fields and positive and negative remanent polarizations are equal. The coercive field, spontaneous and remanent polarization, and shape of the loop may be affected by many factors including the thickness of the sample, presence of charged defects, mechanical stresses, preparation conditions, and thermal treatment. Their effects on the hysteresis loop will be discussed in Section 4.5.

The hysteresis shown in Fig. 4.6 is obtained under switching conditions. Under ideal conditions and in a single-crystal material, the whole domain-wall structure is wiped out by the field at point D and new domains with orientation opposite to those of P_R start nucleating at the

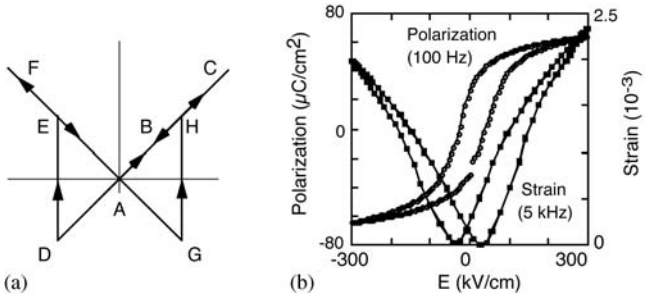

FIGURE 4.7 Strain–electric field (x–E) hysteresis loop (butterfly loop) in ferroelectrics: (a) idealized loop in a crystal in which polarization reverses only by 180°, and (b) the polarization and strain loops measured on a (111)-oriented, 322 nm thick, sol-gel $Pb(Zr_{0.53}Ti_{0.47})O_3$ thin film (Courtesy of David V. Taylor).

sample surface once the field reverses direction. The mechanisms of domain nucleation and propagation depend on many factors. For example, different mechanisms are observed in the same composition of PZT in bulk and thin-film form (Section 4.5) [26].

In addition to the polarization–electric field hysteresis loop, the polarization switching by electric field in ferroelectric materials leads to the strain–electric field hysteresis, as shown in Fig. 4.7. The strain–electric field hysteresis loop, which resembles the shape of a butterfly and is called the butterfly loop, is due to three types of effects. One is the normal converse piezoelectric effect of the lattice, and the other two are due to switching and movement of domain walls. Let us consider as an example a monodomain single crystal and assume that polarization can be instantaneously switched by 180° reversal only. To illustrate how the strain in the crystal changes during the field cycling we can use the following simple, but instructive, description [27].

At zero field (point A in Fig. 4.7(a)), the strain of the crystal is taken to be zero. The electric field is then applied in the direction of the spontaneous polarization. As the field is increased, the crystal expands through piezoelectric effect, according to Eqn. (4.5) and the strain traces line ABC. The expansion continues until the maximum field is reached (point C). At point C the field starts to decrease, but is still parallel to P_S. The strain of the sample traces the same line but in the opposite direction (from C to A). At point A the strain is again zero. The field then changes its direction, becoming antiparallel to P_S. As the field strength increases in the negative direction, the crystal contracts with respect to point A, according to Eqn. (4.5). At point D the field is large enough to switch the direction

of polarization. After switching, the polarization becomes parallel to the field, and the strain again becomes positive (point E). During a further increase of the field in the negative direction, strain increases to point F, and then decreases back to point A as the field is decreased in accordance with Eqn. (4.5). The reversal of the polarization and sudden change of the strain happens again at point G. Ideally, the strain–field curve is linear, indicating that the strain is purely piezoelectric except at the switching points D and G.

In reality, the strain–field relationship is more complicated, as shown in Fig. 4.7(b) for a PZT thin film. Samples usually contain a number of non-180° domains. The movement and switching of non-180° walls may involve a significant change in dimensions of the sample, in addition to the pure piezoelectric response of the material within each domain. The switching of *a*- and *c*-axes of a tetragonal unit is, for example, accompanied by a strain of approximately one per cent in $BaTiO_3$ ($a =\sim 3.994$Å, $c =\sim 4.034$Å at 20°C, [28]) and six per cent in $PbTiO_3$ ($a = 3.902$Å, $c = 4.156$Å at room temperature [18]). Clearly, there is no question of achieving such large strains in a ferroelectric material because only some parts of the sample contain non-180° walls, their orientation may be unfavorable and some of these walls will never switch under realizable experimental conditions. The contribution to the strain from the switching and movement of non-180° domain walls may, however, be comparable to the piezoelectrically induced strain. This has recently been shown experimentally by comparing total electric-field-induced strain and strain due to 90° domain-wall switching in a $Pb(Zr, Ti)O_3$-based ceramic [29]. The jump from one polarization orientation to another in real materials is less sudden than schematically shown in Fig. 4.7(a) because the coercive field may vary for different domains. During the field cycling, a residual (or remanent) strain may be observed at zero field if domains on average do not switch to their original positions at zero field [30,31]. The nonhysteretic, linear portion of the strain–field relationship may not even be observed in many experiments because the single-domain state may not be reached until very high fields. On the other hand, the contribution to the strain from the displacement of domain walls is strongly nonlinear and hysteretic, and it is this part of the strain–electric field relationship that is most often experimentally observed.

There is a tendency in the recent literature on thin ferroelectric films to refer to the relationship between the piezoelectric *coefficient* and the electric bias field as 'piezoelectric hysteresis'. In analogy to magnetic, ferroelectric and elastic hystereses, the term 'piezoelectric hysteresis' in this text is reserved for the strain–electric field and charge density–pressure relationships.

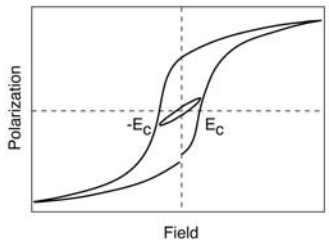

FIGURE 4.8 Switching and nonswitching ferroelectric hystereses. (Courtesy David V. Taylor).

4.2.6 CONTRIBUTION OF DOMAIN-WALL DISPLACEMENT TO THE ELECTROMECHANICAL PROPERTIES

In this work we shall mostly discuss the piezoelectric and dielectric hystereses under nonswitching conditions. Experimentally, this means that the maximum applied field is lower (Fig. 4.8) than the coercive field E_C that would be measured under the same experimental conditions (e.g. the same temperature, frequency, number of cycles and waveform). In other words, it is assumed that during a 'nonswitching' experiment, the domain structure on average remains the same, while domain walls may move on a small scale by bending, jumps and local switching. We thus make an implicit assumption that domain-wall displacement is the main source of the dielectric, elastic and piezoelectric hystereses. As we shall see later, this is a reasonable assumption in most cases encountered in practice, however, examples will be given where other mechanisms control hysteresis in electromechanical properties.

Contribution of domain-wall displacement to the properties of ferroelectric materials is a very complex problem [17]. Understanding the mechanisms of domain-wall nucleation and displacement during the switching process is relatively advanced [26,32–34]. It is, however, questionable whether the description of domain-wall displacement under switching conditions can be straightforwardly extrapolated to the subswitching case where the driving field is weaker, domain-wall structure does not change (at least not 'on average'), and the nucleation process is probably absent.

There is very little direct evidence on how weak-to-moderate (subswitching) field displacement of domain walls contributes to the electrical, elastic, and piezoelectric properties. Yang *et al*. [35] have observed pinning and bowing of a single 180° domain wall in $LiTaO_3$ single crystals using a polarization-sensitive collection mode near-field-scanning optical microscope, Fig. 4.9. In most of the older literature, a domain wall is usually

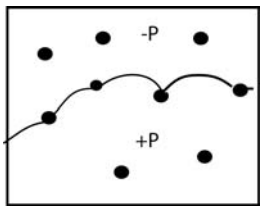

FIGURE 4.9 Schematic presentation of bowing of a pinned domain wall as proposed by Yang *et al*. [35]. The dots represent pinning centers and arcs the bowed portion of the domain wall.

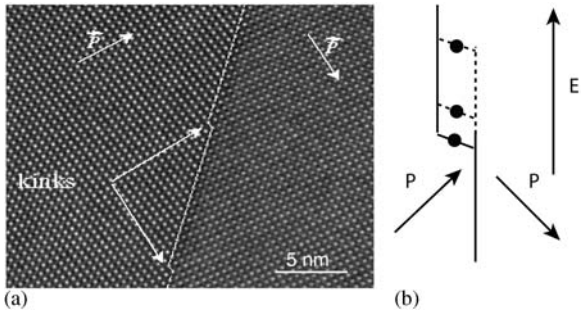

FIGURE 4.10 (a) Kinks in a 90° domain wall in lead titanate observed by high-resolution transmission electron microscopy (courtesy P. Stadelmann), and (b) schematic representation of the possible motion of the domain wall under an external field. The black dots represent pinning defects.

assumed to move as a membrane subjected to a restoring force through a viscous medium [36–40]. Other modes of domain-wall movement may be envisioned. It is known that under large, switching fields, domain-wall jumps (Barkhausen jumps) take place [1]. It is not unreasonable to assume that parts of domain walls move in the form of local Barkahausen jumps even under macroscopic nonswitching conditions, as suggested in Fig. 4.10. One recent result discusses direct observation of such domain-wall dynamics in (BaSr)TiO_3 thin films, using atomic force microscopy [41]. Calculations [42] and indirect experiments [43] show that the domain-wall contributions may account for as much as 50 per cent of the total observed dielectric or piezoelectric effect.

Displacement of ferroelastic–ferroelectric walls (such as 90° walls) can contribute to dielectric, piezoelectric and elastic effects. Movement of 180° walls contributes directly to the polarization. In the case of 180° wall displacement, the induced strain changes with twice the frequency of the

applied electric field [44], so that this movement does not contribute directly to the piezoelectric effect (according to the linear equation (4.5) strain and field should change with the same frequency). The contribution of different types of domain walls to the electromechanical properties has been reported by several authors (see, for example, [45,46]).

Identification of microscopic hysteretic mechanisms in ceramics is difficult (see Section 4.3.3 on lead titanate), while in single crystals an easy test can distinguish whether hysteresis has its origin in domain-wall displacement or in another process. The properties are measured in a crystal that is partially poled, i.e. it contains some domain walls. Then, the crystal is completely poled to remove domain walls and properties are measured again. In most cases the difference in the response between the poled and unpoled crystal can be safely attributed to domain-wall-related mechanisms [47].

One approach toward understanding various contributions to electromechanical hystersis is to investigate processes that lead to hysteresis reduction. For this reason, different methods to control electromechanical hysteresis in ferroelectric materials are discussed in some detail in Section 4.4.4.

4.3 PIEZOELECTRIC HYSTERESIS IN LINEAR SYSTEMS

It was stated in the Introduction that we shall start our discussion on piezoelectric hysteresis by first considering different processes that lead to the phase angle (phase 'lag') between corresponding mechanical and electric variables. For reasons that will become clear later, we shall prefer the term 'phase angle' rather than 'phase lag'. It should be noted that in a linear system driven by a periodic signal with constant amplitude (typical experimental situation, although not typical situation in practice), knowledge of the phase angle and of the response amplitude gives complete information on the hysteresis. This is equivalent to expressing relevant material coefficients in complex form. The case of nonlinear systems is much more complicated and the phase angle and amplitude of the fundamental and all higher harmonics is necessary for a full description of the response (see Section 4.4). Thus, a measurement of the hysteresis loop always contains at least as much or more information than just the knowledge of the response magnitude and the phase angle. Unfortunately, in most of the first studies of piezoelectric relaxation, especially those in polymer materials [48], only information on complex material coefficients is given, i.e. the response is treated as linear with a phase angle.

Historically, investigations of piezoelectric hysteresis began by theoretical models followed by experimental studies of the relaxation and of the piezoelectric phase angle. For a historical review, the reader may consult [49,50]. In these early publications the hysteresis itself is rarely, if ever, mentioned. With few exceptions [51–53], the first experimental studies were focused on the piezoelectric relaxation in polymers (for a review see [48]). In solid ferroelectrics, the piezoelectric phase angle and hysteresis have in the past been studied mostly in the context of device control, where mechanisms of the hysteresis have not been of primary concern [4,5,54]. Only relatively recently have the first studies of the piezoelectric hysteresis in solid ferroelectrics and the first attempts to develop a physical description of its microscopic mechanisms appeared [43,55–60].

One of the first derivations of the frequency dependence of piezoelectric coefficients was proposed by Meixner and Reik [61] in the framework of irreversible theromodynamics, followed by Nowick and Heller [62] and subsequently by other authors in the field of solid-state ferroelectrics [49,58,63,64] and polymers [48,65–67]. Treatment of nonlinear piezoelectric hysteresis is more recent [55,57,59,60] and is still insufficiently developed.

In the rest of this section we shall discuss several models and experimental results of studies of linear piezoelectric hysteresis. Piezoelectric and dielectric hysteresis in nonlinear materials will be discussed in Section 4.4 and ferroelectric hysteresis is the subject of Section 4.5.

4.3.1 Debye-type Piezoelectric Relaxation. Bistable Model of Piezoelectric Relaxation

The bistable model for piezoelectric relaxation has been proposed in various forms by several authors, including Nowick and Heller [62], Arlt [49] and Smits [64]. A piezoelectric material is assumed to have defects or species (generalized defects) that are both elastic [62] and electric dipoles. Examples of such defects are 90° domain walls and ionic substitution–ionic vacancy dipoles, as shown in Fig. 4.11.

An often discussed dipole example is the $Fe_{Ti}^{-1} - V_O^{+2}$ pair, where a double-charged oxygen vacancy would be shared by two single-charged acceptor cations, see Section 4.5.2. Double-charged acceptor substitution is another possibility. Exact charges of defects are often unknown, particularly in the case of transition metal oxides that can adopt several valence states. Without an external field, these simultaneously elastic and dielectric dipoles are randomly distributed along equivalent crystallographic directions, giving zero net strain and polarization. In ceramics, due to random orientation of the grains, dipoles are distributed randomly in the space

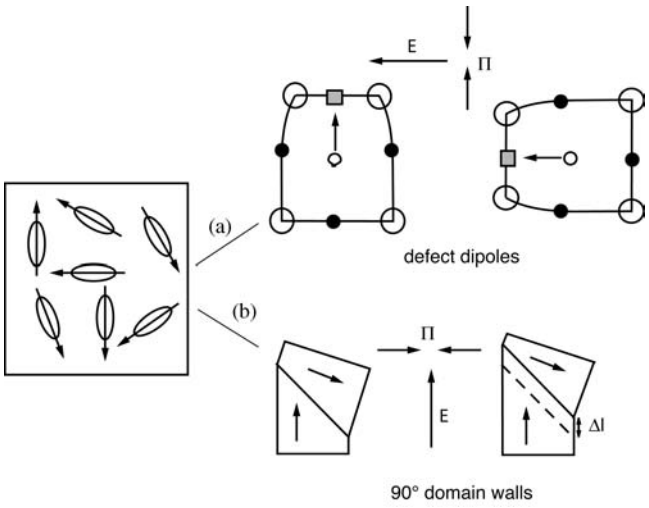

FIGURE 4.11 Schematic representation of elastic and electric dipoles. On the left, generalized elastic dipoles are represented by ellipses and electric dipoles by arrows. (a) Defect dipoles, such as an acceptor-oxygen vacancy pair, and (b) non-180° domain walls. Arrows show external electric and stress fields, which reorient generalized dipoles.

while their orientation within a single domain is dictated by the crystallographic constraints [62].

We next show how a simple bistable model can lead, through the piezoelectric coupling of elastic and dielectric effects, to relaxation and hysteresis in the piezoelectric properties. The derivation given below closely follows the standard procedure for this type of problem [49,64]. In the presence of an external electric field E, the electric energy W_e of the electric dipole μ is:

$$W_e = -\mu E, \tag{4.8}$$

and in the presence of an elastic stress Π, the energy of an elastic dipole λ is defined as:

$$W_m = -\lambda \Pi. \tag{4.9}$$

If the number of equally oriented dipoles per unit volume is n, then the electric and elastic energy densities are, respectively:

$$w_e = -n\mu E, \tag{4.10}$$

$$w_m = -n\lambda \Pi. \tag{4.11}$$

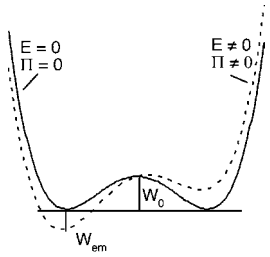

FIGURE 4.12 Bistable potential with and without external elastic, Π, and electric, E, fields. W_0 is the height of the barrier and W_{em} the energy change due to the field application.

The total polarization P and strain x per unit volume due to the defect contribution are:

$$P = n\mu, \tag{4.12}$$

$$x = n\lambda. \tag{4.13}$$

It is understood that relationships (4.8)–(4.13) are, in general, tensor equations.

To simplify the discussion further, it is assumed that defects are one-dimensional and at the same time electric and elastic dipoles. This is a contradiction which, however, does not violate the general character of the results and which disappears in a three-dimensional model [49,62,64]. Defects now have only two possible 'orientations', described by the two potential wells in Fig. 4.12. If elastic and electric external fields are zero, both wells are at the same energy level and are occupied by $n/2$ defects per unit volume. If external electric field E and elastic field Π are now applied, one well is lowered in energy by the amount $W_{em} = |\mu E + \lambda\Pi|$ and the other increased by the same amount (Fig. 4.12).

The number of jumps of defects from well 1 to well 2 per unit time is given by thermodynamic statistics [64,68] as:

$$v_{12} = A \exp[-(W_0 + (\mu E + \lambda\Pi))/kT], \tag{4.14}$$

where W_0 is the height of the potential barrier and A is a constant. In the weak-field limit $|\mu E + \lambda\Pi| << kT$ and Eqn. (4.14) becomes:

$$v_{12} = v[1 - (\mu E + \lambda\Pi)/kT], \tag{4.15}$$

where $v = A \exp[-W_0/kT]$ is the number of jumps per unit time in the absence of fields E and Π. W_0 is called the activation energy. The frequency of jumps from well 2 to well 1 is given by $v_{21} = v[1 + (\mu E + \lambda\Pi)/kT]$.

At equilibrium, $n_1 v_{12} = n_2 v_{21} = (n - n_1)v_{21}$, where n_1 and n_2 are the equilibrium populations of wells 1 and 2, respectively. Since the total concentration of defects is $n = n_1 + n_2$, it follows that:

$$n_1 - n_2 = (n_1 + n_2)[(\mu E + \lambda \Pi)/kT]. \tag{4.16}$$

According to Eqns. (4.12)–(4.13), the contributions of the defects to the equilibrium polarization and strain are:

$$\begin{aligned} \Delta P &= (n_1 - n_2)\mu, \\ \Delta x &= (n_1 - n_2)\lambda, \end{aligned} \tag{4.17}$$

which gives, using Eqn. (4.16):

$$\begin{aligned} \Delta P &= \frac{n\mu^2}{kT} E + \frac{n\mu\lambda}{kT} \Pi, \\ \Delta x &= \frac{n\mu\lambda}{kT} E + \frac{n\lambda^2}{kT} \Pi. \end{aligned} \tag{4.18}$$

In the absence of equilibrium, the number of particles entering wells 1 and 2 can be written as:

$$\frac{\mathrm{d}n_1}{\mathrm{d}t} = -\frac{\mathrm{d}n_2}{\mathrm{d}t} = n_2 v_{21} - n_1 v_{12}. \tag{4.19}$$

Together with Eqn. (4.15) and corresponding expression for v_{21} one obtains:

$$\left(\frac{\mathrm{d}n_1}{\mathrm{d}t} - \frac{\mathrm{d}n_2}{\mathrm{d}t} \right) \mu = 2(n_2 v_{21} - n_1 v_{12})\mu = 2\nu[(n_2 - n_1)\mu + n(\mu^2 E + \lambda\mu\Pi)/kT], \tag{4.20}$$

and, together with Eqn. (4.17):

$$\frac{\mathrm{d}\Delta P(t)}{\mathrm{d}t} = -\frac{1}{\tau}\Delta P(t) + P_{\mathrm{eq}}, \tag{4.21}$$

where $P_{\mathrm{eq}} = n(\mu^2 E + \lambda\mu\Pi)/kT$ and $\tau = 1/(2\nu)$. Expression (4.21) indicates that the rate of change of polarization (or strain, if the equivalent expression for strain is used) is proportional to the distance from the equilibrium; incidentally, this represents the simplest way in which time-dependent material response $R(t)$ (e.g. polarization or strain) may approach the equilibrium value R_{eq} [68]. A similar equation can be derived for $\Delta x(t)$,

finally giving:

$$\begin{aligned}\Delta P(t) + \tau\frac{\mathrm{d}\Delta P}{\mathrm{d}t} &= \frac{n\mu^2}{kT}E + \frac{n\mu\lambda}{kT}\Pi,\\ \Delta x(t) + \tau\frac{\mathrm{d}\Delta x}{\mathrm{d}t} &= \frac{n\mu\lambda}{kT}E + \frac{n\lambda^2}{kT}\Pi.\end{aligned} \tag{4.22}$$

For periodic fields $E = E_0\mathrm{e}^{\mathrm{i}\omega t}$ and $\Pi = \Pi_0\mathrm{e}^{\mathrm{i}\omega t}$, $\mathrm{d}(\Delta P)/\mathrm{d}t = \mathrm{i}\omega\Delta P$ and $\mathrm{d}(\Delta x)/\mathrm{d}t = \mathrm{i}\omega\Delta x$. Now, if constitutive equations (4.6) and (4.7) are added to Eqns. (4.22), using superscript ∞ for the parameters of the perfect material (or for $\omega \to \infty$), the following result is obtained:

$$\begin{aligned}D = D^\infty + \Delta P &= \left[\varepsilon^\infty + \frac{n\mu^2}{kT(1+\mathrm{i}\omega\tau)}\right]E + \left[d^\infty + \frac{n\mu\lambda}{kT(1+\mathrm{i}\omega\tau)}\right]\Pi,\\ x = x^\infty + \Delta x &= \left[d^\infty + \frac{n\mu\lambda}{kT(1+\mathrm{i}\omega\tau)}\right]E + \left[s^\infty + \frac{n\lambda^2}{kT(1+\mathrm{i}\omega\tau)}\right]\Pi.\end{aligned} \tag{4.23}$$

The total complex piezoelectric coefficient d can then be written as:

$$d = d^\infty + \frac{\Delta d}{1+\mathrm{i}\omega\tau}, \tag{4.24}$$

where $\Delta d = n\mu\lambda/kT$. After separation of the real and imaginary components and defining $d^0 - d^\infty = \Delta d$ where d^0 is the value of d at $\omega = 0$, one obtains:

$$d = d^\infty + \frac{d^0 - d^\infty}{1+\omega^2\tau^2} - \mathrm{i}\frac{(d^0 - d^\infty)\omega\tau}{1+\omega^2\tau^2}. \tag{4.25}$$

Equation (4.25) has the same form, Fig. 4.13, as the well-known Debye equation. Note that the maximum in d'' occurs at $\omega\tau = 1$. Frequency ω_m at which d'' is maximum is called relaxation frequency and $\tau = 1/\omega_m$ is known as relaxation time. Clearly, s and ε coefficients will, according to Eqns. (4.23), behave in the same way as the piezoelectric coefficient, except that $\Delta s = n\lambda^2/kT$ and $\Delta\varepsilon = n\mu^2/kT$. It is also plausible to expect that piezoelectric relaxation is subjected to the same types of deviation from the ideal Debye-type relaxation as the elastic and dielectric properties ([69], and Section 4.3.3).

Equations (4.23) indicate that a material that contains defects that are simultaneously elastic and electric dipoles (such as ferroelastic domain walls), and which experiences the simple relaxation in elastic and dielectric properties, will exhibit the same type of relaxational behavior in its piezoelectric properties. This is a general result obtained by several authors and is observed under different experimental conditions: a process that in a piezoelectric material contributes to both elastic and dielectric response

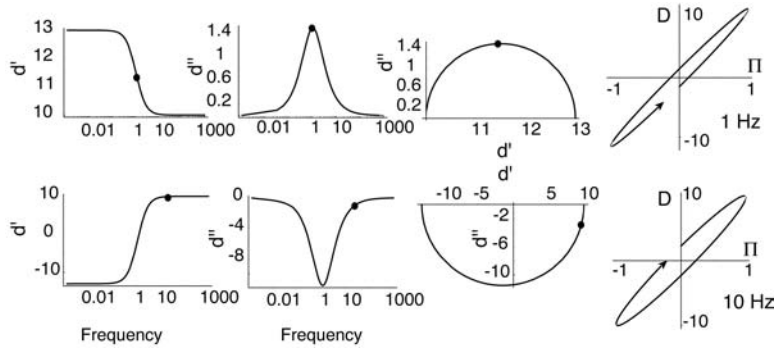

FIGURE 4.13 Some of the possible frequency dependences of the piezoelectric coefficients described by Eqn. (4.25). Numerical values of parameters in Eqn. (4.25) are chosen arbitrarily to illustrate different possibilities. The dots indicate frequencies at which the hystereses were taken. See also [65].

will contribute to the piezoelectric properties as well [40,47–49,64,70]. Experimentally, this is manifested by similar frequency or temperature dependences of the complex elastic, dielectric and piezoelectric coefficients [40,48,66,71], Fig. 4.14. However, the implication contained in the above derivation that a material *must* contain defects that are both elastic and electric dipoles in order to exhibit piezoelectric relaxation should be taken with care. As will be shown in Section 4.3.4 for the case of heterogeneous (composite) piezoelectrics, each component of a heterostructure may exhibit, for example, the dielectric relaxation only while the whole composite exhibits both the elastic and piezoelectric relaxations. The elastic and piezoelectric relaxations of the composite are then just a consequence of the piezoelectric coupling, whereas the physical origin of the loss is purely dielectric [58,72].

Relations (4.23) are derived by using constitutive equations (4.6)–(4.7) where dependent variables x and D are extensive variables. Experimentally, this choice is often the most convenient one. Other combinations of independent and dependent variables (Eqns. (B12)–(B17)) lead to the same type of equations as expressions (4.23) for the g, h and e coefficients [49,64,73]. It is interesting that in the same material some of the piezoelectric coefficients may be real while the others are complex (see [48,64,66,73] and Section 4.4.4).

Equations (4.23) and (4.25) give the first indication of unusual behavior of piezoelectric relaxation: the frequency-dependent parts of the elastic and dielectric terms are always positive definite (they contain terms $\Delta\varepsilon \propto \mu^2$

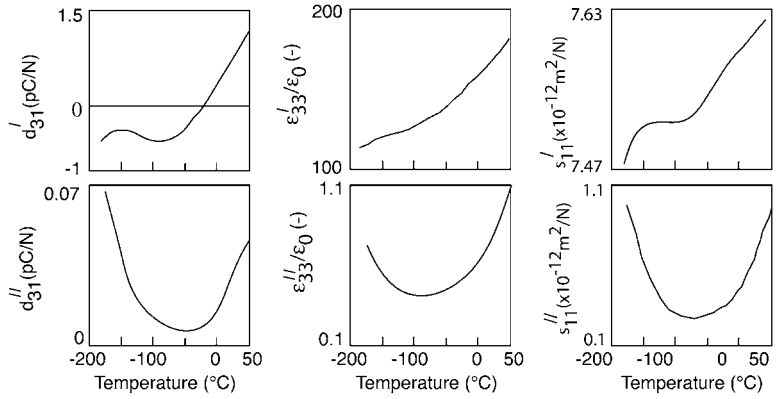

FIGURE 4.14 Similar temperature dependence of the complex piezoelectric, dielectric and elastic coefficients in a (Pb, Sm)TiO_3 ceramic, measured by the resonance technique. For details see [71].

and $\Delta s \propto \lambda^2$), whereas the piezoelectric term contains term $\Delta d \propto \mu\lambda$, which, being a product of components of the electric and elastic dipole tensors, can, in principle, be either positive or negative. In addition, Δd does not have to have the same sign as the corresponding d^{∞} coefficient [62–65]. Such a case has been observed experimentally in $AgNa(NO_2)_2$, see Section 4.3.3.2. For a more general and rigourous thermodynamic treatment of these issues the reader may consult [62,74]. Note that moduli $\beta = 1/\varepsilon$ and $c = 1/s$, which correspond to compliances ε and s, will naturally have $\Delta\beta < 0$ and $\Delta c < 0$.

Figure 4.13 summarizes selected frequency dependences and hystereses that can result from Eqn. (4.25). In agreement with the requirement that the power loss must be positive [75], the dielectric and elastic hystereses, relating conjugate work variables D and E, and x and Π (for positive compliances), always rotate in the counterclockwise sense. This is not the case for the piezoelectric hysteresis, Fig. 4.13, which for the same coefficient can be either counterclockwise or clockwise. This does not violate the second law of thermodynamics since neither (x, E) nor (D, Π) are pairs of conjugate work variables. In other words, while in elastic (x versus Π) and dielectric (D versus E) hystereses the products $x\Pi$ and ED have units of energy density, products xE and ΠD of the corresponding piezoelectric hystereses do not have energy-density units. In this sense, it is instructive to follow arguments of Holland [70] presented in the next section to see how piezoelectric coupling affects total power dissipation in a piezoelectric material. Experimental evidence of clockwise piezoelectric hysteresis will then be

presented in subsequent sections. Note also that the bistable model has been considered so far in the limit of the weak field. Once the field becomes comparable or higher than kT, there will be another, rate-independent and nonlinear contribution to hysteresis. Those effects will be discussed in Section 4.4.

The bistable model is not the only model that leads to relaxation equations of the type (4.25). To describe the contribution of vibrating domain walls to the piezoelectric, elastic and dielectric properties of tetragonal ferroelectric ceramics, Arlt *et al*. [39,40], for example, have assumed that moving domain walls are subjected to a restoring force and a frictional (rate-dependent) force in addition to an external periodic force. The governing equation in that case is:

$$\tau \frac{\mathrm{d}\Delta l}{\mathrm{d}t} + \Delta l = -\frac{1}{Ac}\left(\frac{\partial W_E}{\partial \Delta l} + \frac{\partial W_M}{\partial \Delta l}\right), \tag{4.26}$$

where Δl is the domain-wall displacement, A is the vibrating domain-wall area, c is the restoring force constant, the relaxation time is $\tau = b/2c$, and b is the friction constant. Energies of electric μ and elastic λ dipoles (i.e. the elastic and electrical energy of 90° domain walls) are defined as $W_E = -\mu_i E_i/2$ and $W_M = -\lambda_{ij}\Pi_{ij}/2$. For the particular case considered, these authors obtained that the contribution of domain walls to the permittivity, elastic compliance and piezoelectric coefficients can be expressed in periodic electric and elastic fields as:

$$\begin{aligned} \varepsilon^{\Pi}_{33D} &= P_S^2 F(\omega, c, A) f_\varepsilon, \\ S^{E}_{33D} &= x_S^2 F(\omega, c, A) f_S, \\ d_{33D} &= x_S P_S F(\omega, c, A) f_d, \end{aligned} \tag{4.27}$$

where subscript D denotes domain-wall contribution, P_S and x_S are spontaneous polarization and strain, f are geometrical factors that describe orientation of domain walls, and

$$F(\omega, c, A) = 1/[2c(1 + \mathrm{i}\omega\tau)]. \tag{4.28}$$

Equations (4.27) therefore have the same form as expression (4.24) obtained from the bistable model. We shall see later in Sections 4.3.3 and 4.3.4 that other mechanisms can lead to the same mathematical expressions for the piezoelectric relaxation as Eqn. (4.25), even though the physical origins of the relaxation are different. Thus, care is needed when attributing a particular model to experimental data.

4.3.2 Complex Piezoelectric Coefficients and Energy Dissipation

It is known from the theory of dielectric and elastic materials that the imaginary components of dielectric permittivity ε, and elastic compliance s, are directly related to the dissipation of electric and elastic energy in a material. Holland [70] has shown that the expression for the total energy dissipation in a piezoelectric material is modified by a term that is a function of the imaginary components of the piezoelectric coefficients. His approach is outlined below.

Holland uses a generalized Poynting vector S that, in a piezoelectric material, has an additional elastic term:

$$S = \frac{1}{2}(E \times H^* - \Pi u^*), \tag{4.29}$$

where E and H are vectors of electric field and magnetic displacement, respectively, Π is the stress tensor, and u is the velocity vector of an elemental volume of the material. An asterisk denotes the complex-conjugate tensor. Therefore, the first term in Eqn. (4.29) represents as usual the electromagnetic energy flux and the second term is the elastic energy flux. The density of the power dissipation in the material is defined as:

$$P_d = -\mathrm{Re}(\mathrm{div} S) \tag{4.30}$$

where Re denotes the real part of the expression. Using Maxwell equations for a nonconductive medium, $\mathrm{curl}\, E = -\mathrm{i}\omega B$ and $\mathrm{curl}\, H = \mathrm{i}\omega D$, where $B = \mu_0 H$ is the magnetic field vector, and Newton's second law, $\mathrm{div}\Pi = -\omega^2 \rho \delta$, where ρ is the density of the material and δ displacement vector of the elemental volume under a periodic field [76], Eqn. (4.30) becomes:

$$P_d = \frac{\omega}{2}\mathrm{Im}(E_i d^*_{im} \Pi_m + E_i \varepsilon^*_{ij} E^*_j + \Pi_m s^*_{mn} \Pi^*_n + \Pi_m d^*_{jm} E^*_j), \tag{4.31}$$

where electric displacement D and strain $x = \mathrm{grad}\delta$ are eliminated using the constitutive relations (4.6) and (4.7).

The stress Π and the field E may be represented by a generalized force (or field) vector $F_p = [\Pi_m, E_i]$, where $p = [m, i] = 1, 2, \ldots, 9$. Material coefficients ε, d and s then form a 9 x 9 matrix of complex coefficients $m_{pq} = m'_{pq} - i m''_{pq}$:

$$[m_{pq}] = \begin{bmatrix} s_{mn} & d_{mi} \\ d_{jm} & \varepsilon_{kl} \end{bmatrix}. \tag{4.32}$$

Equation (4.31) can now be rewritten in the form:

$$P_d = \frac{\omega}{2}\mathrm{Im}(F_p m^*_{pq} F^*_q) = \frac{\omega}{2}|F_p||F_q|(m''_{pq}\cos\theta_{pq} + m'_{pq}\sin\theta_{pq}), \qquad (4.33)$$

where $|F_p| = \sqrt{(\mathrm{Re}\,F_p)^2 + (\mathrm{Im}\,F_p)^2}$ is the modulus of the force F_p and θ_{pq} is the phase angle between F_p and F_q. Since sine is an odd function, terms containing $\sin\theta_{pq}$ and $\sin\theta_{qp}$ cancel out. Hence,

$$P_d = \frac{\omega}{2}|F_p||F_q|m''_{pq}\cos\theta_{pq}. \qquad (4.34)$$

The power dissipation function P_d therefore consists of pure elastic terms $|\Pi_m||\Pi_n|s''_{mn}\cos\theta_{mn}$, pure electric terms $|E_i||E_j|\varepsilon''_{ij}\cos\theta_{ij}$, and coupled terms $|\Pi_m||E_i|d''_{mi}\cos\theta_{mi}$. Mechanical and electric energy losses are represented by the imaginary components of the elastic compliance and dielectric permittivity. Imaginary components of the piezoelectric coefficients are responsible for the mixed terms.

Power dissipation P_d in a passive material must always be greater than or equal to zero. This limits the possible values of the imaginary components m''_{pq}. To find which conditions m''_{pq} must satisfy in order that $P_d \geqslant 0$, Holland assumes that the components of the generalized field F are all mutually independent [77]. These components can be then chosen so that phase angle $\theta_{pq} = 0$ or π. Equation (4.34) then may be written as $P_d = \frac{\omega}{2}F_pF_qm''_{pq}$ where F_p and F_q are real numbers. Since F_p are all independent, $P_d \geqslant 0$ only if m'' is a positive-definite matrix. This means that all principal minor determinants of m'' must be greater than or equal to zero [70,78]. For a 9 x 9 matrix there are $2^9 = 512$ minor principal determinants. For a matrix of mth order, nth order minor principal determinants are obtained by crossing any m–n rows and m–n columns that are obtained by reflecting crossed rows with respect to the main diagonal of the original matrix. The positiveness of the first-order principal determinants gives that all elements on the main diagonal of m'' must be nonnegative:

$$m''_{pp} \geqslant 0. \qquad (4.35)$$

This is an expected result since the diagonal elements of m'' represent elastic and dielectric losses. Inspection of all principal determinants shows that there are no conditions on the sign of the imaginary components of the piezoelectric coefficients, while there are conditions on their magnitude. Therefore, terms $|\Pi_m||E_i|d''_{mi}\cos\theta_{mi}$ in Eqn. (4.34) represent power loss when $d''_{mi}\cos\theta_{mi} > 0$ and partial reduction of the power loss when $d''_{mi}\cos\theta_{mi} < 0$. The latter case does not violate the law of conservation

of energy as long as the total $P_d \geqslant 0$. This is ensured if all minor principal determinants of m'' are nonnegative.

While there are no constraints on the sign of the imaginary components of the piezoelectric coefficients, their absolute values are clearly limited. For example, the condition $m''_{pp} m''_{qq} \geqslant (m''_{pq})^2$ must be satisfied to have $P_d \geqslant 0$. Thus, for example, in the case of the point group 6mm (poled ferroelectric ceramics), the positive-definite value of m'' requires that:

$$s''_{11}\varepsilon''_{33} \geqslant (d''_{31})^2, \quad s''_{33}\varepsilon''_{33} \geqslant (d''_{33})^2, \quad s''_{44}\varepsilon''_{11} \geqslant (d''_{15})^2, \tag{4.36}$$

where superscripts E and Π are dropped out. According to Eqn. (4.36), if a material has zero elastic or dielectric energy losses, the corresponding imaginary components of the piezoelectric coefficients will be zero as well. This agrees with the discussion in the previous sections where it was indicated that a material must contain defects that relax under both elastic and electric fields in order to show piezoelectric relaxation. We shall see later that this condition has to be taken with care. In complex systems, for example, if either elastic or dielectric dissipation alone is present, the piezoelectric and dielectric or elastic dissipation will still, in general, be nonzero due to electromechanical coupling.

The above very simplified approach has been discussed by other authors. Lakes [50] has investigated energy losses in piezoelectric materials at subresonant frequencies and found that relations among imaginary components of the elastic compliance s, dielectric permittivity ε and piezoelectric coefficient d depend on the geometry of the piezoelectric solid. In addition, Lakes showed that electric field and elastic stress cannot, in general, be taken as independent and that the relation between them also depends on the geometry of the piezoelectric material. Lakes' findings do not, however, make Holland's results invalid; it is always possible to apply upon a piezoelectric solid of the given geometry a set of electric and elastic fields with such configurations that the phase angle between them vanishes. The situation here is similar to that with electromechanical coupling factors defined by Berlincourt *et al*. [79]. For simple geometries these coupling factors depend only on properties of the material; for a more complicated system of stresses and electric fields, coupling factors become dependent on external variables. The most important result of Holland's analysis is that the power dissipation density P_d in piezoelectric materials depends on the piezoelectric phase angle that may be either positive or negative.

In the next sections we shall discuss some specific examples of piezoelectric hysteresis and relaxation, and demonstrate experimental evidence of clockwise hysteresis, and reduction of power loss due to piezoelectric coupling.

4.3.3 EXPERIMENTAL EXAMPLES OF DEBYE AND QUASI-DEBYE PIEZOELECTRIC RELAXATION IN FERROELECTRIC CERAMICS AND SINGLE CRYSTALS

In this section we discuss three examples of the Debye-like piezoelectric relaxation: two in ferroelectric ceramics with compositions $Pb_{0.85}Sm_{0.1}Ti_{0.98}Mn_{0.02}O_3$ (PSmT) and $Pb_{0.76}Ca_{0.24}TiMnO_3 + 0.3\%$ wt MnO_2 (PCaT), and the third in $AgNa(NO_2)_2$ single crystals. PSmT and PCaT are interesting because the large piezoelectric relaxation observed is quite unexpected for lead-titanate-based materials. The simple structure and composition of these materials suggest that the relaxation is probably of extrinsic origin, for example, due to moving defects such as domain walls or charged defects. Difficulties in identifying the origins of the piezoelectric relaxation will be demonstrated using these compositions. The relaxation in $AgNa(NO_2)_2$ is much better understood and is associated with displacement of NO_2^- radicals, which from part of the crystal cell; it is thus of intrinsic character. It is exactly in this intrinsic relaxation of $AgNa(NO_2)_2$ that some unusual hystereses, such as horizontal hysteresis and clockwise hysteresis, can be deduced from the experimental data.

Piezoelectric Relaxation in Modified Lead-Titanate Ceramics

$PbTiO_3$ is an interesting material for high-frequency transducers used in acoustic emission, Doppler probes, and medical imaging. Pure lead-titanate ceramics are difficult to manufacture as they tend to break on cooling from the sintering temperature ($> 1\,000°C$) because of the high spontaneous strain that develops at the phase-transition temperature (490°C, see Sections 4.2.3 and 4.2.4). Doping with rare earths (e.g. Sm) or alkaline earths (e.g. Ca) reduces the spontaneous strain of $PbTiO_3$ and has the additional beneficial effect of increasing the d_{33}/d_{31} ratio [71,80]. The high piezoelectric anisotropy is useful for reducing the coupling between the lateral and thickness vibrational modes. The role of Mn is to decrease the conductivity and thus to improve the poling of the ceramics. The longitudinal and transverse direct piezoelectric coefficients d_{33} and d_{31} in these compositions are nearly linear with the driving pressure, however, they exhibit a strong Debye-like frequency dependence and hysteresis, as shown in Fig. 4.1(c) for the d_{33} in PSmT. The Cole–Cole (d'' versus d') plot, which for an ideal Debye-process leads to a perfect semicircle with its center on the d' axis, reveals a high-frequency tail in these materials, Fig. 4.15, which suggests a broad distribution of the relaxation times [69]. In that case, the Debye equation (4.24) is replaced by an empirical equation with general

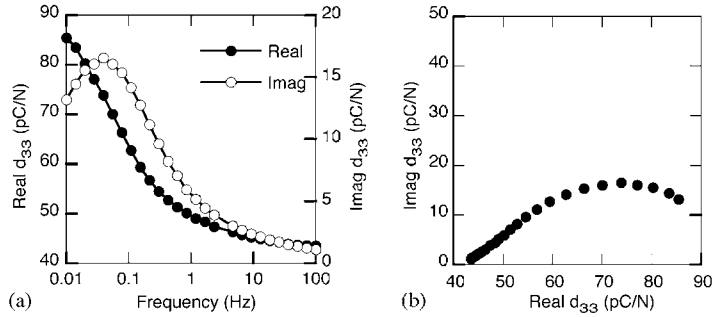

FIGURE 4.15 (a) Frequency dependence of the complex direct longitudinal piezoelectric coefficient $d_{33} = d' - id''$, and (b) its Cole–Cole plot in PSmT ceramics at room temperature.

form:

$$d = d^{\infty} + \frac{\Delta d}{[1 + (i\omega\tau)^{\alpha}]^{\beta}} \tag{4.37}$$

where $0<\alpha\leqslant 1$ and $0<\beta\leqslant 1$ are so-called stretching exponents. For $\alpha = \beta = 1$ Eqn. (4.37) is identical to the Debye equation; for $0<\alpha\leqslant 1$, $\beta = 1$ it is known as the Cole–Cole; for $0<\beta\leqslant 1$, $\alpha = 1$ as the Davidson–Cole; and for α, $\beta\leqslant 1$ as the Havriliak–Negami equation [81,82]. Plot d'' versus d' is called Cole--Cole plot. Without going into details of the theoretical treatment of relaxation phenomena, it should be mentioned that the fractional exponents are obtained when diffusion processes that control relaxation occur in a disordered medium. Such systems have recently been successfully treated within the framework of the fractional Fokker–Planck equation [83,84].

The problem of the origin of the piezoelectric relaxation in ferroelectric materials is nontrivial, and the modified lead titanates are a good example to illustrate some of the difficulties encountered in the identification of the mechanisms underlying the relaxation and the hysteresis. It will be seen later that this task is even more complex when nonlinear processes are included. In PSmT ceramics, the possible relaxing species include vibrating domain walls, and reorientation of dipole pairs consisting of Sm^{+3} cations on a Ti^{+4} site (donor) and lead vacancies, V_{Pb}^{-2}, created to compensate the donor charges. As shown in Section 4.3.1, both mechanisms could lead to the same functional dependence of the piezoelectric coefficient on frequency, even though the physical origins are different. One way to

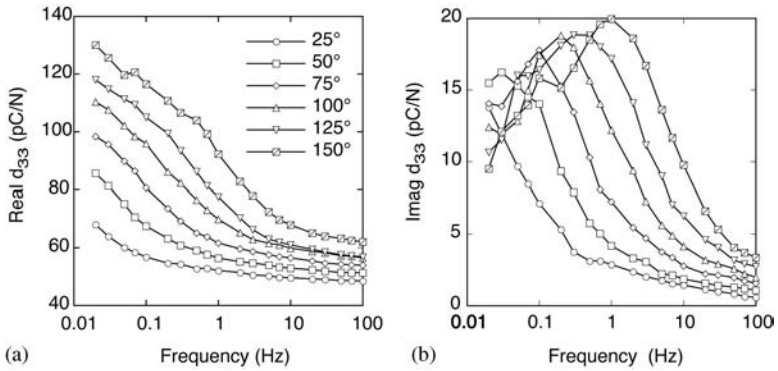

FIGURE 4.16 Relaxation of the complex direct longitudinal piezoelectric coefficient $d_{33} = d' - \mathrm{i}d''$ in PSmT ceramics at different temperatures. (Courtesy Jamasp Jhabvala).

discriminate between the various possibilities is to look at values of the relaxation parameters, such as relaxation strength, Δd, activation energy, and relaxation time, and compare the theoretical predictions of the particular model with the experimental values. A brief analysis of relaxation in modified lead-titanate ceramics is given below, with the intention to illustrate the approach and difficulties for this particular case where physical origins of the hysteresis and relaxation are still not clear. The reader interested in sophisticated tools for the analysis of relaxation spectra can consult [85] and references therein.

When d_{33} of PSmT is measured as a function of the temperature and frequency, one obtains the behavior typical for a thermally activated process, Fig. 4.16, where the peak in the imaginary component occurs at higher frequencies as the temperature is increased [82]. Such behavior is the consequence of the fact that the mean relaxation time follows the Arrhenius law, $\tau = \tau_0 \exp(E/kT)$, as derived in Section 4.3.1. The activation energy can then either be calculated by fitting the appropriate relaxation equation with expression (4.37) or can be estimated by plotting for each temperature the frequency $\omega_{\max} = 1/\tau$, at which the maximum of the d''_{33} occurs [85]. In the case of PSmT, the activation energy is around 0.4 eV and $\tau_0 \approx 10^{-6}$ sec ($\omega_{\inf} \approx 10^6\,\mathrm{s}^{-1}$), as shown in Fig. 4.17. The activation energy associated with the relaxation in the dielectric permittivity has been measured or investigated theoretically in many perovskites and it ranges from 0.075 eV for polaronic processes at low temperatures [86] via ~ 1 eV for the most common relaxation due to motion of oxygen vacancies to several eV for displacement of A and B cations [87]. For ions jumps, the value of the

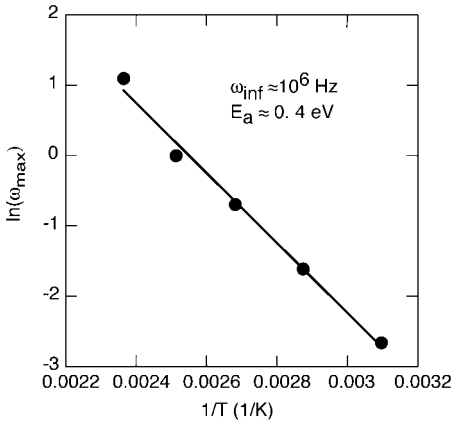

FIGURE 4.17 Arrhenius behavior of the relaxation frequency maximum, $\omega_{\max} = \omega_{\inf} \exp(-E_a/kT)$ in PSmT. (Courtesy Jamasp Jhabvala).

pre-exponential factor τ_0 is of the order of phonon frequencies (10^{12} Hz), much higher than that observed in PSmT [88]. On the other hand, recent first-principle calculations predict that the energy barrier for displacement of 90° domain walls is extremely small in pure and defect-free $PbTiO_3$, of the order of kT (0.02 eV) at room temperature [89]. It is probable that the presence of imperfections associated with dopants and the grain boundaries may increase this barrier in ceramic PSmT with respect to the pure single crystalline $PbTiO_3$.

Perhaps the best argument that speaks in favor of the domain walls as the relaxing species in PSmT is the piezoelectric behavior of PCaT. Figure 4.18 shows relaxation in two samples of PCaT from the two different sources, one from the author's own laboratory and the other from [90], but with approximately the same Ca content. One sample shows relaxation comparable to that in PSmT, whereas the hysteresis and relaxation are much weaker in the other sample. The nature and concentration of the additives used to control the conductivity of the sample with the strong relaxation are not known, but is probably below 1% wt. $(Pb, Ca)TiO_3$ is prepared assuming that Ca occupies only site A in the perovskite cell, but it is possible that Ca spontaneously distributes itself between the A and B sites [71]. If this is indeed the case, addition of Ca would create lead vacancies and holes/oxygen vacancies as the charge compensating defects. Reorientation of these defects is then a possible source of the piezoelectric relaxation. The arguments against the relaxation due to ionic displacement and in favor of domain-wall displacement are the following. Since the two

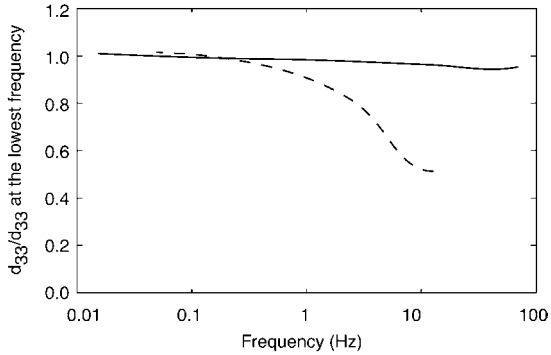

FIGURE 4.18 Relaxation and hysteresis in d_{33} of two PbCaT ceramics with the same concentration of Ca. The dashed line is generated after [90]. The full line describes unpublished data from the author's laboratory. (Courtesy of Jamasp Jhabvala).

samples have approximately the same concentration of the Ca-dopant, any ionic relaxation should be somehow related to the presence of a small concentration of other cations or impurities. It is, however, difficult to see how a small variation in the additive concentration (such as MnO_2, [71]) could explain the strong difference in the behavior of the two samples, if the relaxation is due to ionic motion of the Ca-created defects. Equally, it is unlikely that the strong relaxation could be a consequence of the ionic or electronic hopping associated with the presence of the low concentration of Mn cations or impurities. On the other hand, even small concentrations of dopants in perovskite ferroelectrics can be very effective in creating pinning centers for the domain walls (see [28] and Section 4.5.2). Thus, in the absence of more systematic and detailed experimental results, one can, using these hand-waving arguments, speculate that the relaxation in PSmT and in one of the PCaT samples could be due to domain-wall displacement. However, the nature of the domain-wall displacement in these materials is qualitatively different from that in highly nonlinear soft PZT (compare Figs 4.1(b) and 4.1(c)). Finally, it is significant that elastic relaxation in Ca and Sm-modified $PbTiO_3$ also exhibits activation energy of approximately 0.4 eV [91].

In PSmT, the α and β parameters from Eqn. (4.37) are in the range from 0.6 to 0.9, indicating that the relaxation takes place in a somewhat disordered medium. Examples of piezoelectric relaxation in strongly disordered material will be discussed in Section 4.4.2.

Piezoelectric Relaxation in $AgNa(NO_2)_2$ Single Crystals

The piezoelectric relaxation in this material is of interest for two reasons. Firstly, the relaxation occurs in monodomain single crystals so that displacement of domain walls can be eliminated as a possible cause of the relaxation and hysteresis. Secondly, the Debye-type piezoelectric relaxation observed in this material exhibits unusual characteristics. The real component of the complex longitudinal piezoelectric coefficient d_{22} changes its sign with temperature and frequency, Fig. 4.19. From the data presented in Fig. 4.19, one can predict unusual hysteresis behavior. For example, at $-13°C$ and 20 kHz, where $d'_{22} > 0$, $d''_{22} < 0$, the hysteresis rotates clockwise. When $d'_{22} = 0$, $d''_{22} < 0$ the hysteresis is horizontal, i.e. its axes lie parallel to the strain–electric field axes. The hystereses calculated from the data in Fig. 4.19 are discussed and shown in Section 4.3.5 (Fig. 4.30).

The unusual behavior of $AgNa(NO_2)_2$ can be explained qualitatively by deriving its dielectric, elastic and piezoelectric properties within the framework of thermodynamic theory [92]. This crystal undergoes a paraelectric–ferroelectric phase transition at 38°C. In the ferroelectric phase NO_2^- polar molecules are ordered, and thus contribute, in addition to the ionic and electronic polarization, to the total polarization of the crystal. While the relaxation of the ionic and electronic contributions takes place at infrared and optical frequencies [1,93] the relaxation of NO_2^- radicals occurs around 50 kHz. The origin of the unusual piezoelectric properties of $AgNa(NO_2)_2$ is in competing effects of the three contributions to the polarization. The ionic and electronic components are constant at low frequencies, but change with temperature as the phase-transition temperature is approached. The dipolar contribution changes with both temperature and frequency. In alternating fields, the dynamic dielectric, elastic and piezoelectric coefficients can be written, in the one-dimensional case, as:

$$\varepsilon^{T,\Pi}(\omega) = \varepsilon_\infty^{T,\Pi}(\omega) + \frac{p(\mu)^2}{A(T)} \frac{1}{1 + i\omega\tau^{T,E}} = \varepsilon_\infty^{T,E}(\omega) + \frac{\varepsilon_0^T - \varepsilon_\infty^T}{1 + i\omega\tau^{T,E}}, \quad (4.38)$$

$$s^{T,E}(\omega) = s_\infty^{T,E}(\omega) + \frac{S^2}{A(T)} \frac{1}{1 + i\omega\tau^{T,E}} = s_\infty^{T,E}(\omega) + \frac{s_0^T - s_\infty^T}{1 + i\omega\tau^{T,E}}, \quad (4.39)$$

$$d^T(\omega) = d_\infty^T(\omega) + \frac{p(\mu)S}{A(T)} \frac{1}{1 + i\omega\tau^{T,E}} = d_\infty^T(\omega) + \frac{d_0^T - d_\infty^T}{1 + i\omega\tau^{T,E}}, \quad (4.40)$$

where $p(\mu)$ is a function of the radical dipole moment and coefficients of the crystal free energy, $A(T)$ is a function of the temperature, and S is another function of the coefficients of the crystal free energy. Note that the predicted relaxation time is the same for all three coefficients; this was indeed

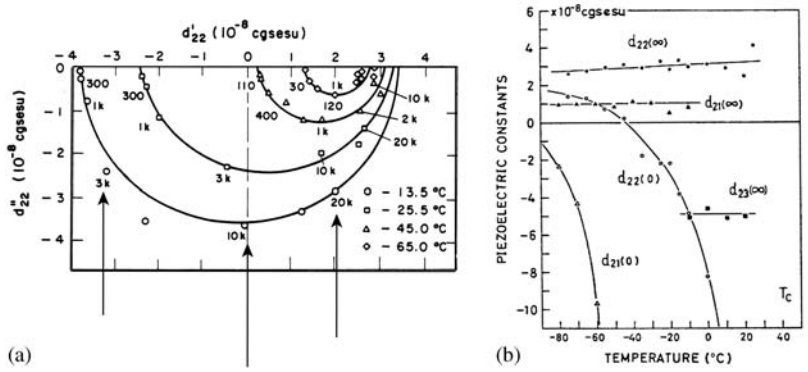

FIGURE 4.19 Relaxation of the d_{22} piezoelectric coefficient in $AgNa(NO_2)_2$ monocrystals. (a) Cole–Cole plots at different temperatures, and (b) the temperature dependence of the static (d^0) and high-frequency (d^∞) piezoelectric d_{22} constants. Arrows in (a) indicate frequencies used for calculations of hystereses loops shown in Fig. 4.30. (From [63] with kind permissions of T. Yamaguchi and H. Nishimori, Chairperson of the publication committee of the Physical Society of Japan.)

observed experimentally [63]. A change of the sign of the piezoelectric coefficient is then a consequence of the competing evolutions of d_∞ and d_0 with temperature, Fig. 4.19(b). As could be expected, Eqns (4.38)–(4.40) have the same form as Eqns (4.23) in Section 4.2.1. The change of sign is possible only in the piezoelectric coefficients while ε and s are positive definite.

4.3.4 CLOCKWISE PIEZOELECTRIC HYSTERESIS IN A HETEROGENEOUS PIEZOELECTRIC

Let us consider two piezoelectric materials connected in series, Fig. 4.20. For simplicity, it is assumed that both samples are ferroelectric ceramics, with their polar axes oriented in the same sense (head-to-tail) perpendicular to the plane of the layers. The surface charges due to ferroelectric polarization are considered to be completely compensated. If a pressure Π is applied parallel to the polar axes, the surface-charge density, D_i, is produced in each layer i through the direct longitudinal piezoelectric effect, $D_i = d_i\Pi$, where d_i is the corresponding piezoelectric coefficient. It is further assumed that all effects arising from lateral piezoelectric effects, different elastic properties of the two materials, and mechanical deformation caused by the electric fields through the converse piezoelectric effect,

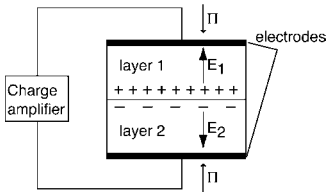

FIGURE 4.20 Bilayer structure consisting of two piezoelectrics oriented in the same sense. Arbitrarily assigned positive and negative piezoelectric charges are marked at the interface. For the given configuration, the net charge at the interface is positive, defining the direction of fields E_i.

may be neglected [67]. As will be shown later, this assumption holds well for the materials considered in this study. An extension of this approach, taking into account lateral effects and elastic properties of bilayers, has been discussed by Turik and Radchenko [94]. The extension of the model to include these additional effects leads to extra terms in the final equations but does not modify qualitatively the main conclusions of the work. We next assume that the external faces of the bilayer are connected to a charge amplifier, under short-circuit (virtual ground) conditions. If the piezoelectric coefficients of the two layers are different, a net charge will appear at the interface between the two layers, Fig. 4.20. This charge will give rise to an electric field E_i and associated charge density (polarization), $\varepsilon_i E_i$, in each layer, where $\varepsilon_i E_i$ is the dielectric permittivity of layer i. The total charge response of layer i is thus given by $D_i = \varepsilon_i E_i + d_i \Pi$. Using Poisson's condition $\partial^2 V_i / \partial x^2 = 0$, where V_i are electric potentials, $E_i = -\partial V_i / \partial x$, and the following boundary conditions: $V_1(x = 0) = 0$, $V_2(x = l) = 0$, and $V_1(a) = V_2(a)$, and $V_1(a) = V_2(a)$; the fields E_i may be calculated as a function of pressure Π as:

$$E_1 = v_2(d_2 - d_1)\Pi/(\varepsilon_1 v_2 + \varepsilon_2 v_1), \quad E_2 = -E_1 v_1 / v_2, \tag{4.41}$$

where v_i is the volume fraction of layer i.

Under the short-circuit conditions described above, the piezoelectrically induced surface-charge density D of the bilayer is related to the pressure Π by $D = d_{\text{tot}}\Pi$, where d_{tot} is the effective piezoelectric coefficient of the bilayer. Since for two materials connected in series $D_1 = D_2 = D$, the effective piezoelectric coefficient d_{tot} of the bilayer can be calculated as:

$$d_{\text{tot}} = (v_1 \varepsilon_2 d_1 + v_2 \varepsilon_1 d_2)/(v_1 \varepsilon_2 + v_2 \varepsilon_1). \tag{4.42}$$

If lateral effects are considered, Eqn. (4.42) would include an extra term dependent on the elastic coefficients of the two materials and their transverse

piezoelectric coefficients. Apart from simplifications used in its derivation, Eqn. (4.42) is generally valid for two piezoelectrics (including nonferroelectrics) arranged in series.

We now consider the case when the pressure is alternating, $\Pi = \Pi_0 \cos(\omega t)$. If the two materials are weakly conducting, we assume that the conductivity, σ, can be introduced [95] through the complex permittivity, $\varepsilon_i = \varepsilon_i' - \mathrm{i}\sigma_i/\omega$. For simplicity, ε_i' will be sometimes written as ε_i and it will be clear from the context to which variable the symbol refers. Replacing the complex ε_i in Eqn. (4.2), d_{tot} also becomes complex and one obtains

$$d_{\mathrm{tot}} = d_\infty + \frac{\Delta d}{1+\tau^2\omega^2} - \frac{\mathrm{i}\omega\tau\Delta d}{1+\tau^2\omega^2} = d'_{\mathrm{tot}}(\omega) - \mathrm{i}d''_{\mathrm{tot}}(\omega), \tag{4.43}$$

where $\tau = (v_1\varepsilon_2' + v_2\varepsilon_1')/(v_1\sigma_2 + v_2\sigma_1)$ is the relaxation time (the time constant) of the bilayer, $\Delta d = d_0 - d_\infty$ is the relaxation strength, $d_0 = (v_1 d_1\sigma_2 + v_2 d_2\sigma_1)/(v_1\sigma_2 + v_2\sigma_1)$ is the static ($\omega\to 0$) piezoelectric coefficient of the bilayer, and $d_\infty = (v_1 d_1\varepsilon_2' + v_2 d_2\varepsilon_1')/(v_1\varepsilon_2' + v_2\varepsilon_1')$ is the piezoelectric coefficient at $\omega\to\infty$. Expression (4.43) has the same form as piezoelectric relaxation obtained from bistable model, Eqn. (4.25), and rate-dependent displacement of domain walls, Eqn. (4.27). However, its physical origin is different. It is a consequence of the difference in the conductivity and piezoelectric coefficients in the two layers, and is thus similar to the Maxwell–Wagner relaxation for two dielectrics, except that the imaginary term proportional to $1/\omega$ is missing [93]. If $d_1 = d_2$, then $d_0 = d_\infty$ and relaxation does not occur even if the permittivities and conductivities of the two phases are different. Thus, the relaxation has a truly electromechanical origin and is not due solely to the dielectric effect. Owing to the nonzero d''_{tot}, the piezoelectric coefficient is out of phase with the pressure, and the charge versus pressure relationship exhibits a hysteresis. The sign of d''_{tot} is determined by the sign of Δd. For $\Delta d > 0$ ($d_0 > d_\infty$), d'_{tot} decreases with increasing frequency, exhibiting retardation, whereas for $\Delta d < 0$, d'_{tot} increases with the increasing frequency, exhibiting relaxation [96], Fig. 4.21. As commonly done in the literature on relaxation processes [96], we refer to both cases as relaxation. Depending on the sign of Δd, the tangent of the piezoelectric phase angle, $\tan\delta_p = d''_{\mathrm{tot}}/d'_{\mathrm{tot}}$, can be either positive or negative (the longitudinal d'_{tot} in ferroelectric ceramics is always positive). Consequently, the piezoelectric (charge versus pressure) hysteresis can have either a counterclockwise or a clockwise sense of rotation, as illustrated in Fig. 4.21. In other words, the total piezoelectric charge D (material response) may either lag behind or precede the pressure Π (excitation), as already anticipated in Section 4.3. If other mechanisms, besides the conductivity, contribute to the dielectric dispersion [$\varepsilon_i = \varepsilon_i'(\omega) - \mathrm{i}\varepsilon_i''(\omega)$], Eqn. (4.43) must be modified accordingly. An equation similar to (4.43) has been

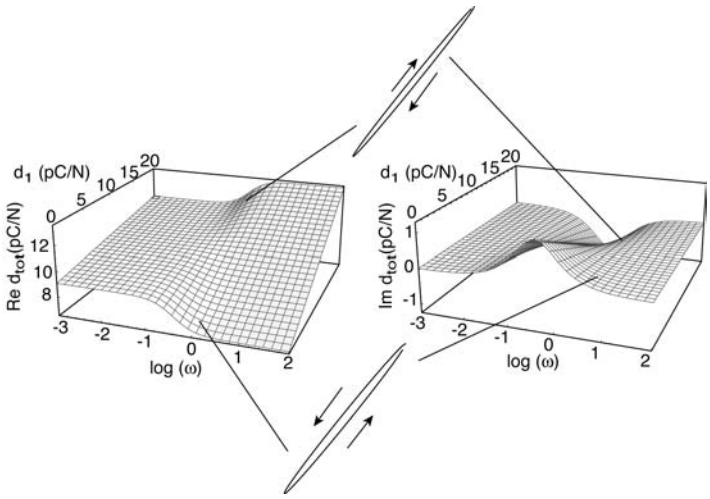

FIGURE 4.21 The piezoelectric retardation and relaxation of a bilayer consisting of two materials with the properties typical for bismuth-titanate-based Aurivillius structures ($d_2 = 10$ pC/N, $\varepsilon_2/\varepsilon_0 = 100$, $\varepsilon_1/\varepsilon_0 = 200$, $\sigma_1 = 10^{-9}$ $(\Omega\text{m})^{-1}$, $\sigma_2 = 10^{-10}$ $(\Omega\text{m})^{-1}$, $V_0 = 0.5$, $\varepsilon_0 = 8.85 \times 10^{-12}$ F/m). The piezoelectric coefficient of phase 1 is varied. Calculations are made using Eqn. (4.43). Hystereses are shown at two selected values of d_1, illustrating the counterclockwise and clockwise rotations.

derived by Ueda *et al*. [95] for a three-phase polymer system consisting of a continuous nonpiezoelectric phase, in which are embedded spherical piezoelectric particles surrounded by a conducting shell.

Let us examine more closely the reasons for the appearance of the negative piezoelectric phase angle and the clockwise hysteresis. The total charge associated with each layer consists of two contributions. The first, purely piezoelectric part $d_i\Pi$, is instantaneous, nonhysteretic (if piezoelectric coefficients d_i are not complex) and is exactly in phase with the pressure. The second part, $\varepsilon_i E_i$, associated with the field E_i, is due to uncompensated piezoelectric charges ($d_1 \neq d_2$) at the interface. In nondispersive materials, depending on the sign of $d_2 - d_1$, one of $\varepsilon_i E_i$ is exactly in phase (0°) and the other exactly in antiphase (180°) with the pressure Π, Eqn. (4.41). Owing to the dielectric permittivity dispersion (e.g. by conductivity), there is an additional phase angle between charges $\varepsilon_i E_i$ and pressure Π leading to the charge versus pressure hysteresis. In the following discussion we consider only the conductivity effects.

Let a pressure Π be applied on the bilayer, as shown in Fig. 4.20. The piezoelectric effect then produces instantaneously charges Q_1 and Q_2 at the

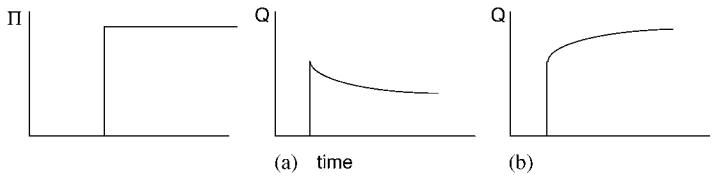

FIGURE 4.22 The time dependence of the pressure Π and the piezoelectric charge Q in the case of (a) relaxation and (b) retardation.

interface, which for the given configuration are of the opposite sign, ($Q_1 > 0$, $Q_2 < 0$, Fig. 4.22). The total charge Q at the interface may be written as $Q = Q_1 + Q_2$. Let us next assume that $|Q_1| > |Q_2|$ (equivalent to $d_1 > d_2$). If the charge decays much faster through material two, $|Q|$ increases with time. If the charge decays faster through material one, $|Q|$ decreases with time. The piezoelectric response exhibits retardation in the former case, and relaxation in the latter case, as shown in Fig. 4.22. The electric fields E_i, and associated charges, $\varepsilon_i E_i$, which are proportional to Q, therefore show the same temporal dependence as Q. For an alternating pressure, $\varepsilon_i E_i$ thus exhibits a phase angle with respect to the pressure. From the discussion above it follows that the sign of the phase angle (retardation or relaxation) must depend on the electrical time constants of the two layers. The component of $\varepsilon_i E_i$, which is out of phase with Π, written here as $(\varepsilon_i E_i)''$, can be calculated using Eqn. (4.41) where ε_i is replaced with complex $\varepsilon_i = \varepsilon_i' - \mathrm{i}\sigma_i/\omega$. One obtains that $(\varepsilon_i E_i)''$ is the same for both layers and is equal to:

$$(\varepsilon_i E_i)'' = \frac{\omega(\tau_2 - \tau_1)(d_2 - d_1)v_1 v_2 \sigma_2 \sigma_1}{(1 + \omega^2\tau^2)(v_2\sigma_1 + v_1\sigma_2)^2}\Pi_0, \tag{4.44}$$

where $\tau_i = \varepsilon_i'/\sigma_i$ is the electrical time constant of the layer i. As expected from the discussion above, $(\varepsilon_i E_i)''$ depends on the electrical time constants of the two layers. Note that the phase angles between $\varepsilon_1 E_1$ and Π and $\varepsilon_2 E_2$ and Π are not equal because the in-phase components of $\varepsilon_i E_i$ are different for the two layers.

Rearrangement of the terms in Eqn. (4.43) leads to the following expression for the imaginary part of the bilayer's piezoelectric coefficient:

$$d''_{\mathrm{tot}} = \frac{\omega\tau(\tau_2 - \tau_1)(d_2 - d_1)v_1 v_2 \sigma_2 \sigma_1}{(1 + \omega^2\tau^2)(v_2\sigma_1 + v_1\sigma_2)(v_2\tau_1\sigma_1 + v_1\tau_2\sigma_2)}. \tag{4.45}$$

It is seen that for a given $d_2 - d_1$, the sign of the piezoelectric phase angle and the sense of the hysteresis rotation are defined by the difference in the electrical time constants of the two layers, τ_2-τ_1. Because the time constants

of the two layers are functions of temperature, the same bilayer may, as a function of temperature, exhibit a positive, a negative or a zero piezoelectric phase angle corresponding, respectively, to a counterclockwise or clockwise hysteresis, Fig. 4.21, or absence of hysteresis. This unusual result does not violate energy conservation since, as discussed in Section 4.3.2, D and Π are not conjugate work variables. In addition, the author has shown numerically that this type of piezoelectric dispersion satisfies Kramers–Kronig relations. This is expected since the causality principle must be obeyed. Those results will be published elsewhere.

As shown by Holland [70] and as outlined in Section 4.3.2, the total energy loss in piezoelectric materials consists of mechanical and electrical contributions, both of which are always positive, and of a coupled piezoelectric term, which may be either positive (energy loss) or negative (partial energy gain). The piezoelectric term is always smaller than the electric and mechanical terms so that the total energy loss, as required by thermodynamics, is positive even when the piezoelectric 'loss' term is negative. Considering the piezoelectric hysteresis, it is helpful to remember that the charge–pressure hysteresis in the piezoelectric effect is only a part of the total material response, which, depending on the boundary conditions, also contains elastic (strain–pressure) and dielectric (charge–electric field) hystereses. In the present case, the total energy loss will, for example, include conductivity losses and elastic losses. We next show that the elastic relaxation and hysteresis are induced in a heterogeneous piezoelectric sample even in the case when only conductivity losses are present in the individual components. This effect is solely due to electromechanical coupling.

Let us consider again the bilayer model presented in Fig. 4.20. Both layers are subjected to the same stress Π. The strain x_i in each component is given by constitutive relations (4.6), where, for simplicity, we again consider longitudinal effects only:

$$x_i = d_i E_i + s_i \Pi. \tag{4.46}$$

As before, subscript i denotes components of the bilayer, and E_i are given by Eqn. (4.41). The total strain x of the bilayer is:

$$x = v_1 x_1 + v_2 x_2. \tag{4.47}$$

After inserting x_i from Eqn. (4.46) and E_i from Eqn. (4.41), x can be written as $x = s_{\text{tot}}\Pi$ where compliance of the bilayer, s_{tot}, is given by:

$$s_{\text{tot}} = v_1 s_1 + v_2 s_2 - \frac{v_1 v_2 (d_1 - d_2)^2}{v_2 \varepsilon_1 + v_1 \varepsilon_2}. \tag{4.48}$$

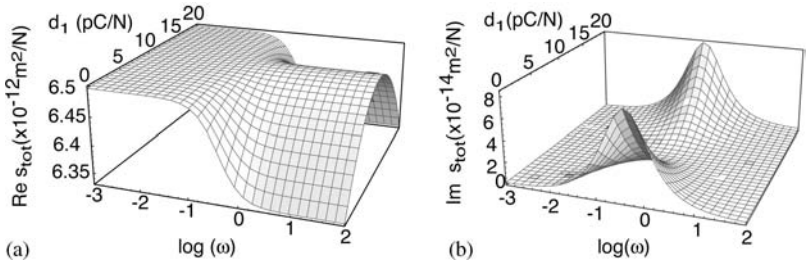

FIGURE 4.23 The retardation and relaxation of elastic compliance of a bilayer consisting of two materials with the properties typical for bismuth-titanate-based Aurivillius structures ($d_2 = 10$ pC/N, $\varepsilon_2/\varepsilon_0 = 100$, $\varepsilon_1/\varepsilon_0 = 200$, $\sigma_1 = 10^{-9}$ $(\Omega\text{m})^{-1}$, $\sigma_2 = 10^{-10}$ $(\Omega\text{m})^{-1}$, $V_0 = 0.5$, $\varepsilon_0 = 8.85 \times 10^{-12}$ F/m, $s_1 = 8 \times 10^{-12}$ m^2/N, $s_2 = 5 \times 10^{-12}$ m^2/N). The piezoelectric coefficient of phase 1 is varied. The plot is generated using Eqn. (4.48) and $\varepsilon_i = \varepsilon_i' - \mathrm{i}\sigma_i/\omega$.

Expression $d_i^2/(\varepsilon_i s_i)$ is the coupling coefficient [79] and in simple geometries, such as the present case, has the meaning of the electromechanical energy conversion factor. Thus, it is always equal to or less than one [79]. This means that s_{tot} is a positive-definite coefficient. If bilayer components are elastically and piezoelectrically perfect, and the only source of dispersion is conductivity in each layer ($\varepsilon_i = \varepsilon_i' - \mathrm{i}\sigma_i/\omega$), one obtains that s_{tot} is dispersive, Fig. 4.23, and that the x–Π relationship is hysteretic. As expected, the elastic phase angle is always positive, i.e. strain lags in phase behind pressure, and the elastic hysteresis of the composite always rotates in a counterclockwise sense. Note that the sample is short-circuited and the electric field across the bilayer is zero; however, the individual layers exhibit counterclockwise dielectric hysteresis D–E due to the conductivity losses. Using relations (B12)–(B17) it is possible to show that g_{tot}, e_{tot} and h_{tot} coefficients of the bilayer are complex, exhibiting either counterclockwise or clockwise hysteresis. It should be mentioned that $\tan\delta_{h\text{tot}}$ is small since, in the first approximation, $\tan\delta_{h\text{tot}} \approx \tan\delta_{\varepsilon\text{tot}} + \tan\delta_{s\text{tot}} - \tan\delta_{d\text{tot}}$, but is nonzero. This last relationship can be derived from Eqn. (B21), by taking all coefficients as complex, and neglecting the quadratic and higher loss terms.

Finally, we point out that the Maxwell–Wagner-like mechanism is not the only process that can lead to piezoelectric relaxation of the bilayer. If components of the bilayer are dielectrically nondispersive, but exhibit dispersion in their elastic properties, the piezoelectric coefficient and permittivity of the bilayer would become dispersive through the electromechanical coupling.

4.3.5 Experimental Evidence of Clockwise Piezoelectric Hysteresis

Despite numerous observations of piezoelectric relaxation with negative and positive phase angles over the past 40 years [63,65,66], mainly made on polymer-based systems, the first explicit discussion and experimental evidence of the clockwise piezoelectric hysteresis has been presented only recently [58,72]. The bilayer model discussed above lends itself perfectly to such a study. Two piezoelectric ceramics with nondispersive piezoelectric properties, and different conductivities and permittivities are chosen [58,72]. Properties of each individual component and of the composite can be measured. From the properties of the components it is possible to calculate the expected responses of the ceramic–ceramic composite and compare them with the experimental results.

The experiments have been performed on $SrBi_4Ti_4O_{15}$ and related ferroelectric ceramics. These materials belong to the family of layered structures or Aurivillius phases. The crystal structure of these materials consists of one or more perovskite layers separated by bismuth oxide sheets, Fig. 4.24. Ferroelectric phases of many of these compounds exhibit orthorhombic structure, with ferroelectric polarization lying parallel to the plane of the layers. The single crystals and grains in ceramics have a tendency to grow in the form of thin plates, with crystal layers parallel to the plane of the platelets, Fig. 4.24. Conductivity of the grains is highest in the plane of the layers while the piezoelectric properties are high along the polarization direction and small or zero in the direction perpendicular to the plane of the layers. Using hot-forging techniques, textured ceramics can be prepared so that the majority of the grains are oriented in the same direction, Fig. 4.24. A bilayer can be formed with two such ceramics, one with grains oriented perpendicularly and the other parallel to the external pressure, Fig. 4.25. For the crystal symmetry of $SrBi_4Ti_4O_{15}$, the piezoelectric properties of the ceramic with grain platelets oriented perpendicular to the pressure will show small (ideally zero) piezoelectric response. The ceramic with grain platelets oriented parallel to the pressure will show a high piezoelectric effect. Regardless of their orientation, the piezoelectric effect of textured ceramics is nondispersive. As expected from the model, such a bilayer exhibits piezoelectric relaxation, Fig. 4.26, with a phase angle [58,72] which, in the case of the bilayer prepared from the hot-forged $SrBi_4Ti_4O_{15}$, ceramics, exhibits clockwise hysteresis over a large temperature range.

In ceramics with random-oriented grains, plate-like grains often form colonies with the same orientation, Fig. 4.27. These colonies and surrounding grains of different orientation form basic bilayer units. Each such unit,

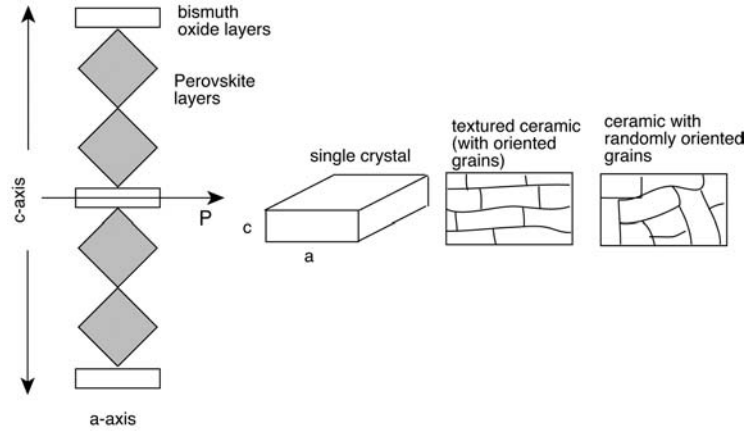

FIGURE 4.24 Schematic presentation of (a) Aurivillius layer structure; (b) single crystals with platelet form; (c) textured ceramics with plate-like grains; (d) ceramics with randomly oriented plate-like grains.

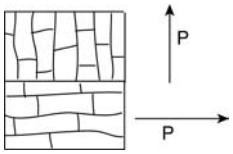

FIGURE 4.25 Schematic presentation of a bilayer formed of two textured $SrBi_4Ti_3O_{15}$ ceramics using a hot-forging technique. The direction of polarization P is indicated for each layer.

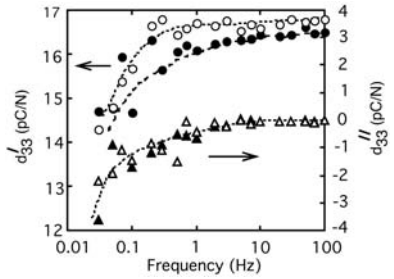

FIGURE 4.26 Real (circles) and imaginary (triangles) components of the piezoelectric d_{33} coefficient of an $SrBi_4Ti_3O_{15}$ bilayer at 190°C. The open symbols represent measured values and the full symbols calculated values. The dashed lines are guides for the eye. (Courtesy of Marlyse Demartin).

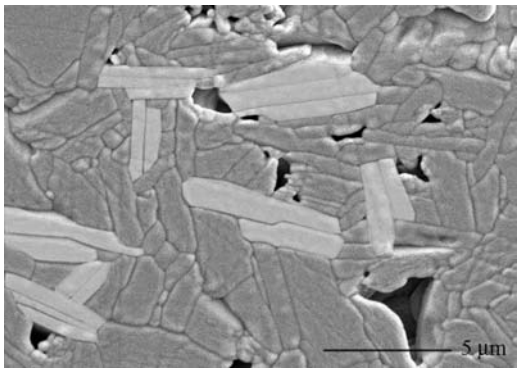

FIGURE 4.27 Microstructure of $SrBi_4Ti_4O_{15}$ ceramic with randomly oriented grains. Occasionally, two or more grains form colonies where all grains exhibit the same orientation. Together with the neighboring grains or colonies with dissimilar orientation, these clusters form local bilayers. (Courtesy of Marlyse Demartin).

and their average over the whole sample, may exhibit Maxwell–Wagner piezoelectric relaxation. As the microstructure of the sample changes (grain size, packing of the grains, density, etc.), samples with nominally the same composition, but prepared in a different way, may exhibit either clockwise, zero or counterclockwise hysteresis, as shown in Fig. 4.28 for $SrBi_4Ti_4O_{15}$ ceramics. A striking example of the piezoelectric relaxation with hysteresis evolving with frequency from clockwise to counterclockwise is shown in Fig. 4.29 for a $Bi_4Ti_3O_{12}$ ceramic [58]. Like $SrBi_4Ti_4O_{15}$, this ceramic is also composed of anisotropic grains which locally form bilayer units.

It is interesting to consider the piezoelectric hysteresis in $AgNa(NO_2)_2$ single crystals, in which piezoelectric relaxation was discussed in the previous section. Even though the authors did not explicitly consider or measure the hysteresis, the data presented give enough information to reconstruct the hysteresis at different frequencies and temperatures. If we express the piezoelectric coefficient as $d_{22} = d'_{22} - id''_{22}$ then the strain is given by [63]:

$$x = |d_{22}|E_0 \sin(\omega t - \delta), \tag{4.49}$$

where δ represents the phase angle between the field and strain. Then, $\tan\delta = d''_{22}/d'_{22}$. An unusual property of this material is that the real part of the piezoelectric coefficient d'_{22} changes the sign with the frequency, Fig. 4.19. At 3 kHz and $-13.5°C$, $d'_{22} < 0$ and $d''_{22} < 0$, giving clockwise hysteresis, Fig. 4.30. Note that this case, when both the real and imaginary

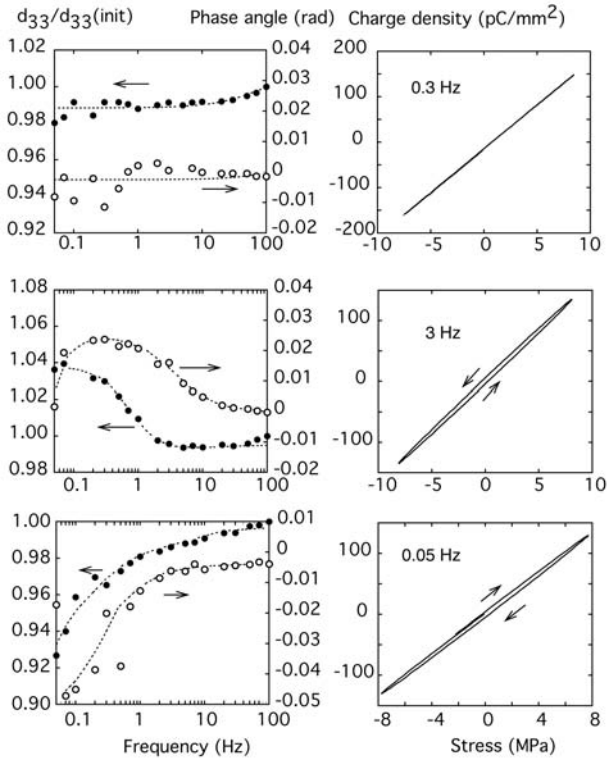

FIGURE 4.28 Left: piezoelectric coefficient and its phase angle as a function of frequency; and right: hysteresis in $SrBi_4Ti_3O_{15}$ ceramics with nominally the same composition but processed under different conditions illustrating the absence of hysteresis, clockwise or counterclockwise. (Courtesy of Cyril Voisard).

components are negative, corresponds to the usual counterclockwise hysteresis when both the real and imaginary components are positive. At 10 kHz and -13.5°C (see Fig. 4.19) $d'_{22} = 0$ and $d''_{22} < 0$. One thus obtains $\delta = -90°$, i.e. the strain advances the field by 90°. This leads to a clockwise hysteresis with its major and minor axes parallel to the coordinate system axes, as shown in Fig. 4.30. Finally, at 20 kHz and -13.5°C, $d'_{22} > 0$ and $d''_{22} < 0$ give clockwise hysteresis, Fig. 4.30. Unfortunately, in their experiments Yamaguchi and Hamano [63] have measured the phase angle and not the hysteresis directly.

In summary, in the case of piezoelectric coefficients, neither the real nor imaginary parts of a piezoelectric coefficient have a definite sign, the sign of the two components may be opposite, and either real or imaginary

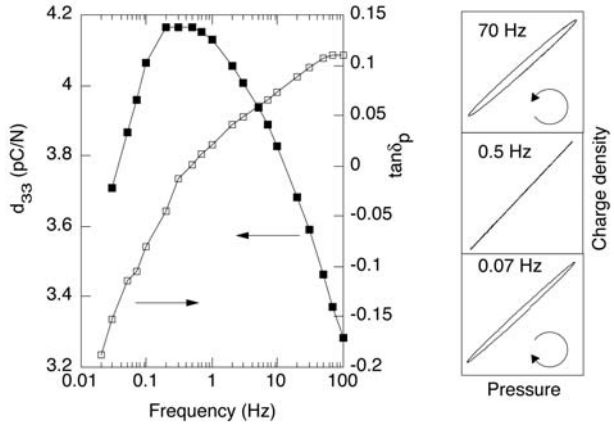

FIGURE 4.29 Piezoelectric coefficient d_{33} and tan δ_p of a single-phase $Bi_4Ti_3O_{12}$ ferroelectric ceramic with highly anisotropic grains, at room temperature as a function of frequency. On the right are shown charge-pressure hysteresis loops at selected frequencies, with a clockwise hysteresis at 0.07 Hz and counterclockwise hysteresis at 70 Hz. (Courtesy of Pedro Duran Martin).

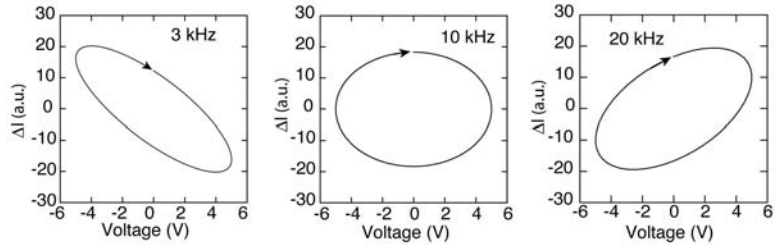

FIGURE 4.30 The piezoelectric hystereses in $AgNa(NO_2)_2$ single crystals calculated from data presented in Fig. 4.19 at −13.5°C.

components may vanish at a given frequency or temperature. Some of the possibilities are summarized in Fig. 4.13. Consequently, the piezoelectric hysteresis may exhibit clockwise hysteresis and hysteresis with its main axes parallel to the coordinate system axes. Such cases are not possible in properties relating the conjugate work variables (e.g. polarization–electric field, elastic strain–stress, or magnetization–magnetic field).

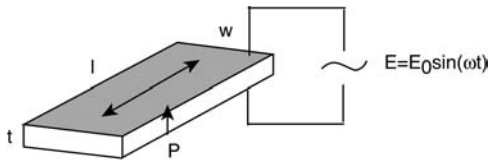

FIGURE 4.31 Piezoelectric resonator in transverse (d_{31}) mode. The gray area indicates symmetrical electroded surfaces, and the double arrow the direction of vibrations. The l, w and t indicate the length, width and the thickness of the sample, and P is the polarization.

4.3.6 REDUCTION OF POWER LOSS DUE TO PIEZOELECTRIC COUPLING

As shown by Holland [70] and discussed in Section 4.3.2, the piezoelectric coupling may lead to a partial reduction of the power loss in a material. In this section we show direct experimental evidence of such power-loss reduction, observed in a piezoelectric resonator.

For completeness, we first briefly outline the derivation [79] of equations governing oscillations of a piezoelectric material subjected to an alternating electric field, $E = E_0 e^{i\omega t}$. At so-called quasi-static conditions (low frequency), the strain x is homogeneous throughout the sample and, in a perfect material, follows the field, $x = dE_0 e^{i\omega t}$ (Eqn. (4.5)). If the rate of change of the field is comparable to the velocity of acoustic waves through the material, the strain is no longer homogeneous, internal stress Π develops in the sample and modifies the piezoelectric strain. If we consider a long ceramics bar, poled along its thickness, Fig. 4.31, the constitutive equations can be written as:

$$x_1 = d_{31}E_3 + s_{11}\Pi_1, \tag{4.50}$$

$$D_3 = \varepsilon_{33}E_3 + d_{31}\Pi_1. \tag{4.51}$$

At acoustical wavelengths the material can be considered as continuous. Newton's law for an elemental volume $\mathrm{d}V$ displaced by distance δ can be written as:

$$\rho \mathrm{d}V \partial^2\delta/\partial t^2 = F, \tag{4.52}$$

where $F = (\partial\Pi_1/\partial x)\mathrm{d}V$ is the force. Since the field E_1 is independent on the coordinate x and since by definition $x_1 = \partial\delta/\partial x$, Eqns (4.50) and (4.52) together give the following wave equation:

$$\frac{\partial^2\delta}{\partial t^2} = \frac{1}{s_{11}^E\rho}\frac{\partial^2\delta}{\partial x^2} = (v^E)^2\frac{\partial^2\delta}{\partial x^2}, \tag{4.53}$$

where v^E is the velocity of the transverse elastic waves in the bar. For simple harmonic motion, $\delta = \delta_0 e^{i\omega t}$ and one obtains from Eqn. (4.53)

$$\delta = [C_1 \sin(\omega x/v) + C_2 \cos(\omega x/v)]e^{i\omega t} \tag{4.54}$$

Using $x_1 = \partial\delta/\partial x$ and Eqn. (4.50), C_1 and C_2 can be calculated from the following boundary conditions: $\Pi_1 = 0$ at $x = 0$, $x = l$. Substituting Eqns. (4.54) and (4.50) into (4.51), the dielectric displacement D_3 can be calculated. The admittance Y of the vibrating bar is obtained from the ratio of the current I and voltage V across the vibrating bar:

$$Y = I/V = \frac{w \int \frac{\partial D_3}{\partial t} dx}{\int E_3 dz}. \tag{4.55}$$

Finally, the admittance of the bar can be expressed as a function of material coefficients d, s and ε:

$$Y = i\frac{\omega w l}{t}\left(\varepsilon_{33}^{\Pi} - \frac{d_{31}^2}{s_{11}^E}\right) + i\frac{2wd_{31}^2}{(\sqrt{\rho s_{11}^E})s_{11}^E t}\tan\frac{\omega l(\sqrt{\rho s_{11}^E})}{2}. \tag{4.56}$$

We see that resonance occurs (admittance becomes infinite) when $\omega = n\pi/(l\sqrt{\rho s_{11}^E})$ where $n = 1, 3, 5 \ldots$. This is the same frequency at which mechanical resonance of an unloaded frictionless bar occurs. The piezoelectric resonance is thus nothing else but a mechanical resonance excited in piezoelectric materials by an electric field that oscillates at the frequency that is identical to the mechanical resonant frequency of the bar. Clearly, this situation is ideal since some sort of mechanical damping and electrical losses are always present. In the presence of losses, purely imaginary admittance $Y = iB$ in Eqn. (4.56), is shown in Fig. 4.32(a), will exhibit a real part, G, called conductance. The full admittance, $Y = G + iB$, is shown in Fig. 4.32(b). Formally, electrical and mechanical losses and their piezoelectric coupling can be introduced by replacing the real s, ε and d in Eqn. (4.56) with complex $s' - is''$, $\varepsilon' - i\varepsilon''$ and $d' - id''$ [40,53,71,97–99]. The power dissipation of a resonator near the resonant frequency can be expressed as [100]:

$$P_d = \frac{1}{2}V_0^2 \mathrm{Re}\, Y, \tag{4.57}$$

where V_0 is the driving-voltage amplitude. Thus, the power dissipation is proportional to the conductance G of the resonator. We see from Fig. 4.32(a) that in an ideal resonator the power dissipation is zero ($G = 0$), whereas in a 'lossy' resonator, due to the piezoelectric coupling, the power

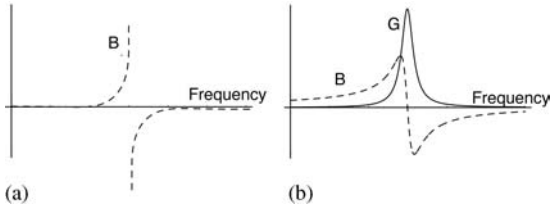

FIGURE 4.32 Admittance of (a) a lossless and (b) a lossy piezoelectric resonator.

dissipation becomes large at resonance (G exhibits a maximum). This can be seen by inserting complex material coefficients into (4.56). One obtains that:

$$G \propto \omega K(\varepsilon'' s, d) + 2d' d'' F_1(\omega, s) - [d'^2 - d''^2] F_2(\omega, s), \tag{4.58}$$

where indexes are dropped out, $K(\varepsilon'' s, d)$ is a function of the material parameters but not of the frequency, and F_1 and F_2 are functions of the frequency and real and imaginary components of the elastic compliance. Over the limited frequency range at resonance, the material coefficients are assumed to be independent of frequency. For a nonpiezoelectric material, $G \propto \omega\varepsilon''$ and G increases [93] with increasing frequency.

In modified lead-titanate ceramics, see Section 4.3.3, the d_{31} coefficient changes its sign with temperature [71]. As in $AgNa(NO_2)_2$, at the temperature where $d'_{31} = 0$, the imaginary part $d''_{31} \neq 0$. When $G(\omega)$ of the bar is measured in the vicinity of the temperature where d'_{31} changes the sign, a minimum is observed in $G(\omega)$, Fig. 4.33. According to Eqn. (4.57), and general description of conductivity-related losses in dielectric materials [93], such a minimum suggests that the part of the total power dissipation that is due to the conductivity, is reduced. This result appears to be the only direct experimental evidence of *reduction* of the power dissipation due to piezoelectric coupling.

4.4 PIEZOELECTRIC AND DIELECTRIC HYSTERESIS IN NONLINEAR SYSTEMS UNDER SUBSWITCHING CONDITIONS

In previous sections we have discussed piezoelectric hysteresis in linear systems, where hysteresis originates from the frequency- and temperature-dependent phase angle between the field and the material response. A large number of heterogeneous systems and composites, ferroelectric ceramics, polymers and single crystals exhibit this type of piezoelectric hysteresis.

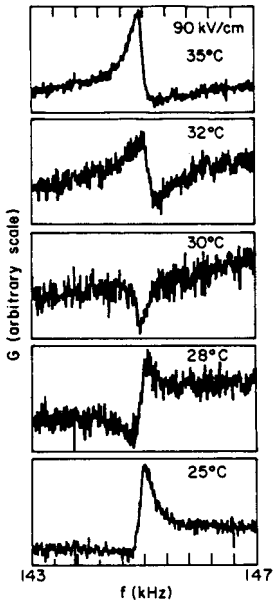

FIGURE 4.33 Conductance $G(\omega)$ of a PSmT ceramic at the temperature range where the real part of the piezoelectric coefficient, $\mathrm{Re}\, d_{31}$, changes sign. Near 30°C, where $\mathrm{Re}\, d_{31} = 0$, $G(\omega)$ exhibits a minimum indicating a small reduction in the power dissipation.

However, the piezoelectric response of some of the most widely used ferroelectric piezoelectrics is more complex. A typical soft $Pb(Zr_{1-x}, Ti_x)O_3$ ceramic exhibits a strong piezoelectric nonlinearity and nonlinear hysteresis, in addition to the frequency-dependent piezoelectric coefficient, Fig. 4.1(b). In this section, we shall see how this type of hysteresis in piezoelectric materials can be described, and will look in some detail into problems associated with the frequency dependence of the nonlinear and hysteresis parameters.

We start the section with a brief description of the $Pb(Zr_{1-x}, Ti_x)O_3$ (PZT) solid solution. PZT belongs to the perovskite family (Section 4.2.3, Fig. 4.4). At room temperature it exhibits ferroelectric tetragonal structure for $x > 0.48$, ferroelectric rhombohedral structure for $x < 0.48$ [28] and a monoclinic structure in a narrow region around $x \approx 0.48$ [101,102]. The narrow region separating the tetragonal and rhombohedral phases is called the morphotropic phase boundary (MPB). The compositions that lie at the MPB exhibit high piezoelectric properties, Fig. 4.34, [103,104]

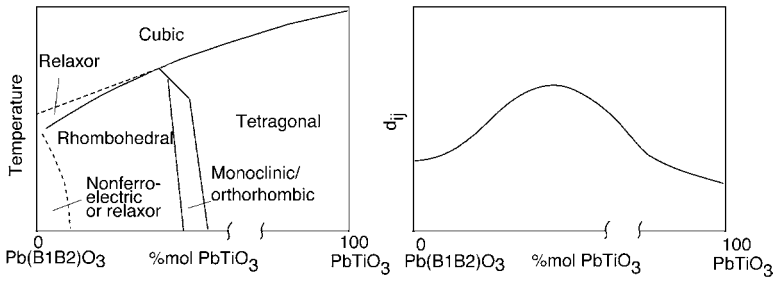

FIGURE 4.34 Schematic representation of (a) the temperature–composition phase diagram of complex solid solutions, such as PZT, and (b) typical dependence of the piezoelectric coefficients on composition. The maximum is observed approximately at the morphotropic phase boundary, in the region where the tetragonal and rhombohedral phases meet via an intermediate monoclinic or orthorhombic phase. The phases indicated by the dashed lines are observed in some materials.

accompanied by dielectric, elastic, and piezoelectric nonlinearity, hysteresis and frequency dispersion of the properties. Typical values of the piezoelectric coefficients in PZT are 100–500 pm/V or pC/N. This is two orders of magnitude higher than in quartz. The PZT material can be made hard or soft (see Section 4.5.2), with various strength of hysteresis and nonlinearity. There are hundreds of other ferroelectric materials and solid solutions [1,28], however, the qualitative description given below has a rather general validity.

Furthermore, we shall draw a parallel between dielectric and piezoelectric response. As shown in Section 4.4.4, at week fields, which are mainly of interest in this section, the strain and polarization response are dominated by the movement of ferroelastic domain walls. This means that the dielectric (polarization–field) and piezoelectric (strain–field) hystereses are governed by the same mechanisms. By comparing the two types of hysteresis it is possible to obtain information on the actual hysteresis process operating in a material.

4.4.1 DESCRIPTION OF THE PIEZOELECTRIC AND DIELECTRIC HYSTERESES AND NONLINEARITY

Rayleigh Hysteresis and Higher Harmonics Response

The simplest type of the piezoelectric hysteresis and nonlinearity observed in polycrystalline ferroelectrics is shown in Fig. 4.35, for a soft PZT

ceramic.[1] At weak fields the direct piezoelectric coefficient is nearly a linear function of the driving-field amplitude and the associated hysteresis exhibits sharp ends indicating the fact that the hysteresis is nonlinear and that its origin is more complex than in systems discussed before in Section 4.3, where the hysteresis is simply a consequence of the phase angle between the driving field (input) and the material's response (output). The hysteresis evolves with the field in such a way that its tip follows the curve of the charge density maximum, Fig. 4.35. This type of nonlinear piezoelectric behavior has been observed in a number of ferroelectric ceramics, Fig. 4.36. At larger fields, the coefficient curves either upward [105–107] or downward and may exhibit a field independent region at very weak fields (see Section 4.4.3). As we shall see below, the key feature of this type of electromechanical response is that the hysteresis and nonlinearity are closely related; in ideal cases, one property (hysteresis or nonlinearity) can be quantitatively predicted once the other property (nonlinearity or hysteresis) is known. A similar type of hysteresis has been observed for the dielectric properties of ferroelectric materials [108–111].

In the regime where the piezoelectric or dielectric coefficient is approximately a linear function of the driving-field amplitude, the piezoelectric or dielectric nonlinearity and hysteresis can be well described [57,112] by the Rayleigh equations, well known from the field of magnetics [75,113]. In the case of piezoelectric or dielectric response, the Rayleigh equations are written as:

$$R(F) = (m_{\text{init}} + \alpha_m F_0)F \pm \alpha_m (F_0^2 - F^2)/2, \tag{4.59}$$

$$R(F_0) = (m_{\text{init}} + \alpha_m F_0)F_0,$$

$$m(F_0) = m_{\text{init}} + \alpha_m F_0, \tag{4.60}$$

where the material coefficient $m = \varepsilon$ or d, the general driving field $F = \Pi$ or E, the general material response $R = D$ or x, F_0 and R_0 are corresponding amplitudes, α_m is the Rayleigh coefficient for the dielectric polarization, converse or direct piezoelectric effect, and m_{init} is the zero-field value of the permittivity, converse or direct piezoelectric coefficient. In the rest of the text, index m in α_m will often be omitted for simplicity. Equation (4.59) describes the hysteresis, with the sign '+' corresponding to the descending, and the sign '−' to the ascending fields. The knowledge of $m(F_0)$ then

[1] All measurements of the direct piezoelectric effect discussed in this chapter were performed under compressive bias stress and dynamic stress whose amplitude is at least half of that of the compressive bias. For convenience of presentation, the hystereses are presented centered with respect to both the dynamic stress and charge density axes.

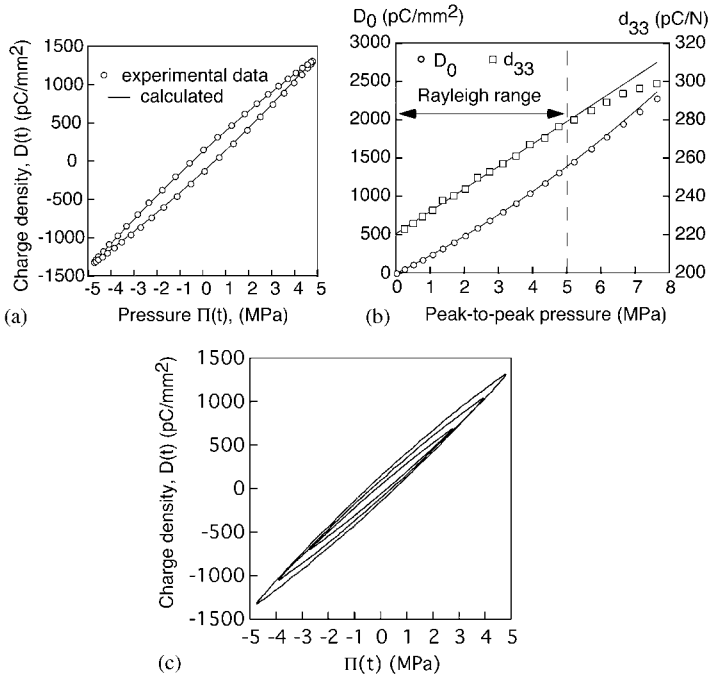

FIGURE 4.35 (a) Charge density–pressure hysteresis, (b) field dependence of the charge density and d_{33}, and (c) evolution of the hysteresis with increasing field amplitude, in a soft PZT ceramic. In (a) and (b) circles and squares represent experimental points, and the solid lines are obtained using Rayleigh relations (4.59) and (4.60).

allows calculations of $R(F_0)$ and vice versa, as demonstrated in Fig. 4.35 for the direct piezoelectric and in Fig. 4.37 for the converse effect. Therefore, the hysteresis and nonlinearity have their origin in the same physical process. As we shall see later, this is not always the case: a process that contributes to the coefficient nonlinearity may not necessarily be hysteretic. Furthermore, the term 'quasi-Rayleigh behavior' will be used whenever the hysteresis and nonlinearity are closely related in the above sense (one can be calculated from the other), even if the behavior predicted by Eqn. (4.60) is not satisfied, i.e. it is more complex than linear (see Section 4.4.3). The reasons and justification for this rather loose employment of the terms will become apparent later on in this section.

While the original discovery of the Rayleigh law in magnetics was empirical [114], several theoretical models have been subsequently developed

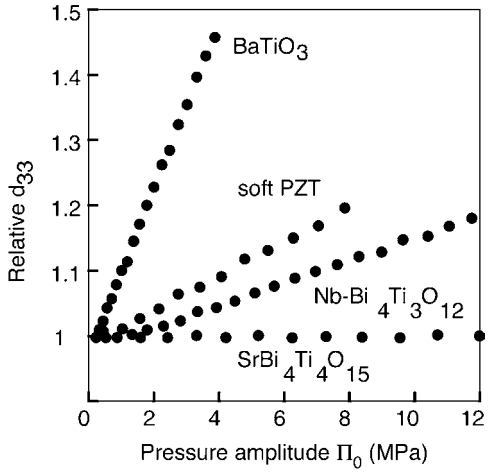

FIGURE 4.36 Field dependence of the longitudinal piezoelectric coefficients in four ferroelectric ceramic materials. In each case (except in $SrBi_4Ti_4O_{15}$ where the response is anhysteretic) the charge–force hysteresis has the shape illustrated in Fig. 4.35(c).

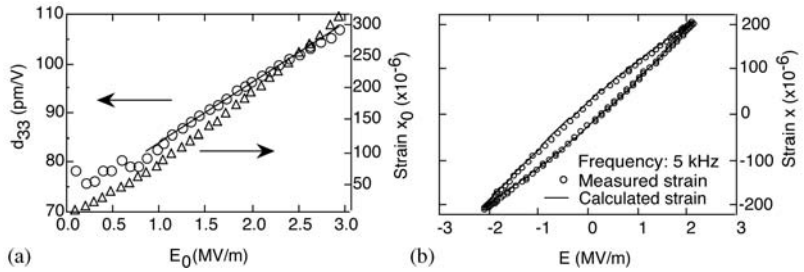

FIGURE 4.37 (a) Field dependence of the strain and d_{33}, and (b) strain–electric field hysteresis in a PZT thin film. In (a) and (b) circles and triangles represent experimental points and solid lines are obtained using Rayleigh relations (4.59) and (4.60). (Courtesy David V. Taylor).

with the specific purpose to deriving these relations [114–116]. Those early physical models, the formal description by Preisach [114] (Section 4.4.3) and some very recent results [117,118] have all shown that the Rayleigh behavior in magnetics is intimately linked to the disorder in the system. By simplifying the problem considerably, one can say that the Rayleigh behavior is obtained when domain walls move in the form of small Barkhausen jumps in a medium with randomly distributed pinning centers, Fig. 4.38.

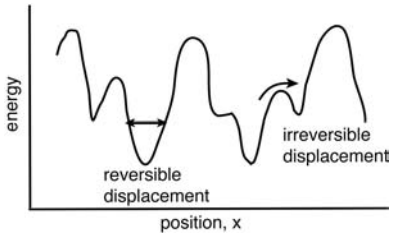

FIGURE 4.38 Energy profile for a domain wall moving in a medium with random pinning centers. For details see [115,116,122].

Following these different approaches, one can easily see that a similar theoretical framework can be used for the description of the displacement of domain walls in any ferroic medium (ferromagnetic, ferroelectric, ferroelastic), or, even more generally, for the displacement of other types of interfaces. The Rayleigh law is thus used to describe the ferroelectric [119–122] and piezoelectric hysteresis [57], usually assuming that the underlying mechanism is the displacement of domain walls. It is tempting to speculate that in ferroelectric compositions close to the morphotropic phase boundary, where free energies of neighboring phases are close to each other, the interfaces between different phases can be moved by external fields and contribute to the properties in a similar way as the moving domain walls [59]. At present, there is no direct evidence that this interphase boundary displacement is actually happening.

We next investigate properties of the Rayleigh relations by examining, in some detail, Eqn. (4.59) for the hysteresis. If $F = F_0 \sin(\omega t)$, then development of Eqn. (4.59) into Fourier series gives:

$$R(F) = (m_{\text{init}} + \alpha F_0)F_0 \sin(\omega t) - \frac{4\alpha F_0^2}{3\pi}\cos(\omega t) - \frac{4\alpha F_0^2}{3\pi}\left[\frac{1}{5}\cos(3\omega t) - \frac{1}{35}\cos(5\omega t) + \ldots\right]. \tag{4.61}$$

There are several remarkable properties of Eqn. (4.61). The first is that only odd harmonics are present. This is a property of nonlinear functions that exhibit so-called half-wave symmetry, $R(t + T/2) = -R(t)$, where t is the time and T the period of the driving field [123]. The second property is that only cosine terms appear in the Fourier series. For a sinusoidal driving field, cosine terms indicate phase lag, implying that in a Rayleigh system all nonlinear contributions are hysteretic. This should not be entirely unexpected if one remembers that the Rayleigh equations describe the response of a system in which displacement of domain walls in the form

of Barkhausen jumps is controlled by a random distribution of the pinning centers. Equation (4.61) thus reflects the fact that every domain-wall displacement is at the same time hysteretic and nonlinear. This property becomes clearer when described in the framework of the Preiscah formalism (Section 4.4.3). An alternative way of stating the same fact is by looking at the phase angle of higher harmonics. Expansion of a nonlinear function into Fourier series may be written as:

$$R(t) = \sum [R'_n \sin(\omega t) + R''_n \cos(n\omega t)], \tag{4.62}$$

where n is the number of the harmonic, and R'_n and R''_n are the expansion coefficients. The phase angle δ_n of the nth harmonic, which, in analogy with the discussion of complex material coefficients in Section 4.3, is defined by $R_n(t) = \sqrt{(R'_n)^2 + (R''_n)^2}\sin(n\omega t - \delta_n)$, can be calculated as:

$$\delta_n = -\arctan(R''_n/R'_n). \tag{4.63}$$

Since for a Rayleigh system and for $n > 1$ all $R'_n = 0$ (Eqn. (4.61)), it follows that the phase angle of all higher harmonics is $\pm 90°$. Finally, the third important property of Eqn. (4.61) is that all hysteretic and nonlinear terms are quadratic functions of the driving-field amplitude.

The above analysis thus identifies a fingerprint of the Rayleigh behavior that can be verified experimentally. Let us illustrate this on some examples and see how analysis of the nonlinearity and hysteresis can be used to detect different processes that take place in a ferroelectric. Figure 4.39(a) shows the dielectric permittivity of a 1.44 μm thick PZT thin film with Zr/Ti ratio 45/55 and [111] preferential orientation as a function of the amplitude of the driving electric field. As-prepared, aged film was first subjected to fields of increasing amplitude, up to ~4.5 MV/m (first branch of the measurement cycle). The field amplitude was then decreased (second branch) to zero and then increased again (third branch). The permittivity is a strong function of the field, and it is evident that the film changes its response between the first and the subsequent branches of the measurement cycle. Once the response of the film has stabilized (second and third branches), the permittivity can be well described by Eqn. (4.61). The parameters $\varepsilon_{\text{init}}$ and α derived from the field dependence of the permittivity are used to predict the D–E hysteresis, Fig. 4.39(b), giving a good agreement between the experimental and calculated values. Furthermore, the third harmonic of the dielectric displacement is proportional to $E_0^{2.2}$, Fig. 4.39(c), close to what is predicted by Eqn. (4.61). Finally, during the second and the third branches, the value of the phase angle of the third harmonic, Fig. 4.39(d), is close to 90°, again as predicted by Eqn. (4.61). In the

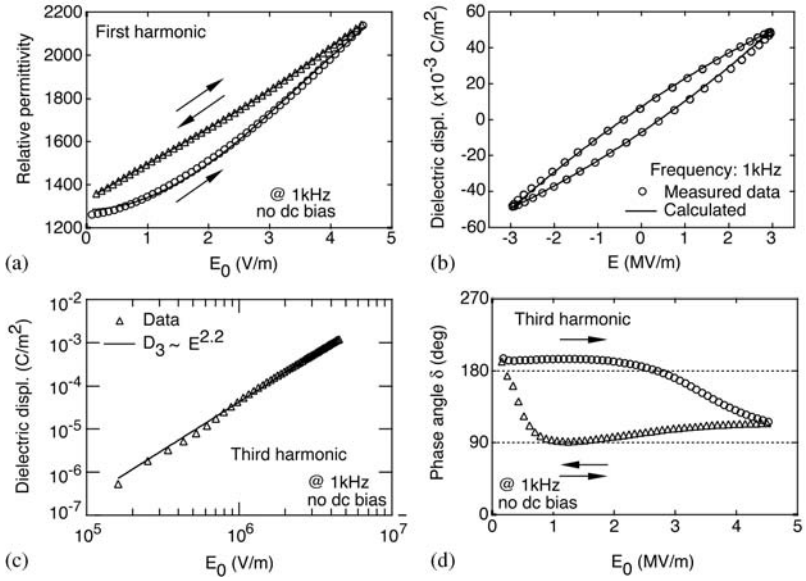

FIGURE 4.39 Dielectric permittivity for increasing and decreasing field amplitudes. (a) The bottom curve is measured during the first increasing branch of the first field cycle. After the first cycle, the increasing and decreasing branches coincide; (b) polarization–field hysteresis; (c) amplitude of the third harmonic of polarization versus field amplitude; and (d) phase angle (represented here as 180-δ_3) of the third harmonic for increasing and decreasing field amplitudes (see (a)). The measurements were made on a PZT thin film, as explained in the text. (Courtesy David V. Taylor).

following paragraph we shall try to show how small discrepancies from the behavior predicted by Eqn. (4.61) may be used to detect the presence of different types of nonlinear processes and domain-wall pinning mechanisms taking place in the material. It is clear that, in the absence of a more rigorous theoretical treatment, such a discussion may be only qualitative.

The difference in the permittivity behavior (the first harmonic response) between the first and the subsequent branches of the field cycle indicates that the film changes its state during the first measurement. This is reflected in the behavior of the phase angle of the third harmonic – it is zero at the beginning of the first branch and then switches to $\approx 90°$ at high fields. During the subsequent cycles, the phase angle is $\approx 90°$, except at weak fields, indicating the existence of a threshold field for the nonlinear contributions. If we assume that the origin of the hysteresis and nonlinearity is in the field-induced displacement of domain walls, the behavior of the

films can be tentatively explained in the following way. The as-prepared, aged films contain defect centers that strongly pin domain walls (see Section 4.5.2). When the field is first applied, the domain walls' movement is reversible (nonhysteretic) but nonlinear. This may happen if the domain walls move under the field away from the pinning centers, but return to them due to strong restoring forces once the field is removed. This is seen in the presence of the third harmonic, whose angle is zero. Once the field is strong enough to depin the domain walls, they start moving in a hysteretic, nonlinear way, in the form of Barkhausen pulses, and contribute to polarization in a way predicted by the Rayleigh equations: the phase angle of the third harmonic becomes $\approx 90°$, meaning that most of the nonlinear contributions to the third harmonic are hysteretic.

Another consequence of the nonlinear, nonhysteretic (reversible) movement of the domain walls is that, in a general case, the amplitude of the third harmonic material response is expected to be proportional to $a_3E_0^3 + a_5E_0^5 + \ldots$ [124,125], whereas in the Rayleigh case only a term proportional to E_0^2 appears in the expansion. Small deviations from the behavior predicted by the Rayleigh equations may thus be due to residual, strongly pinned domain walls that move in a reversible nonlinear fashion. The threshold field for the third harmonic phase angle suggests that the energy profile for domain walls is not perfectly random (see Section 4.5.2) and does not contain shallow minima that would allow domain-wall contributions at very weak fields.

To test these hypotheses, the as-prepared, aged films were subjected to a thermal treatment to release domain walls from the pinning centers. If polarization is then measured immediately, without waiting for the film to age and the charged defects to pin the wall again (Section 4.5.2), the third harmonic switches to 90° at much weaker fields (Fig. 4.40) than in an aged film (Fig. 4.39(d)), consistent with the assumption that most of the domain walls will be depinned by the thermal treatment. We shall return to this result in Section 4.5.2.

Similar results are obtained for the piezoelectric strain–electric field relationship, Fig. 4.41. Depending on the film state (degree of aging), preparation condition, texture, thickness, and other parameters, the discrepancy from the ideal Rayleigh behavior is found in different degrees. For example, the exponent of the third harmonic field dependence is found to vary between 1.9 and 2.6 [126]. Perhaps the most interesting feature is the appearance of the second harmonic in the polarization response, which is absent in Eqn. (4.61). The second harmonic is probably a consequence of the asymmetry in the material induced by internal bias field that renders the Rayleigh loop asymmetric (see Section 4.4.3). The internal field (i.e. the poling of the film) may be a consequence of the measuring process itself

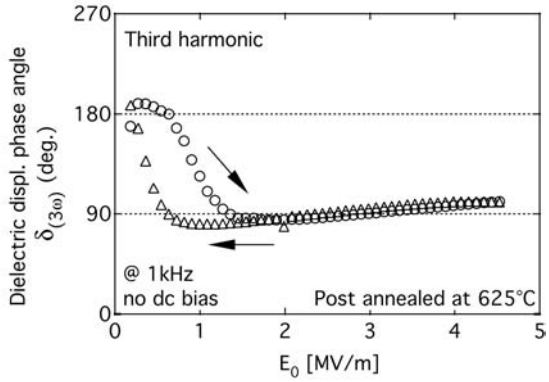

FIGURE 4.40 Phase angle (represented here as 180-δ_3) of the third harmonic of polarization response for increasing and decreasing field amplitudes in an annealed PZT film. Compare with (d) in Fig. 4.39. (Courtesy David V. Taylor).

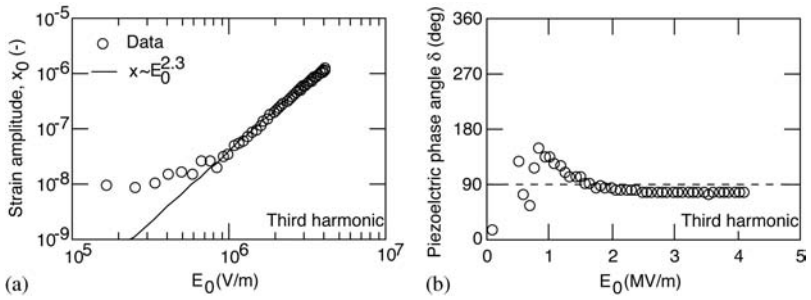

FIGURE 4.41 (a) Amplitude of the third harmonic of the strain as a function of the field amplitude, and (b) phase angle (represented here as 180-δ_3) of the third harmonic of the strain as a function of the field amplitude. The measurements were made on a PZT thin film [126]. (Courtesy David V. Taylor).

[124], which, as shown in Fig. 4.39(a), changes the nonlinear characteristics of the film. It can be easily shown that the second harmonic will appear if the α coefficient in Eqn. (4.59) is not equal for increasing and decreasing fields (the hysteresis is asymmetrical).

In the absence of a more rigorous theoretical treatment, we see that the above approach can lead to interesting hints on the hysteretic and nonlinear processes taking place in ferroelectric materials. It should be emphasized, however, that the nonlinear and hysteresis parameters need to be analyzed in their entirety. The linear dependence of the permittivity on the electric field amplitude (the Rayleigh relation (4.60)) has, for

example, been observed in relaxor-ferroelectric $Pb(Mg_{1/3}Nb_{2/3})O_3$, but with the phase angle of the third harmonic equal to 180° and not to 90°. In this case, therefore, the nonlinear component is not hysteretic in higher harmonics, as required by the Rayleigh equations, and one has to invoke a different model to explain the nonlinearity. The following procedure may be proposed to establish whether a hysteretic, nonlinear material behaves indeed as a Rayleigh system: (i) the material coefficient (piezoelectric coefficient, permittivity) should be a linear function of the field amplitude, (ii) the total hysteresis can be predicted from the nonlinear parameters of the coefficient nonlinearity, (iii) the amplitude of all harmonics is a quadratic function of the field, (iv) the phase angle of the third harmonic is 90°, (v) the fifth harmonic has the phase angle of −90°, (vi) the ratio of the amplitude of the first and the third harmonic should be five, and so on.

It can be concluded from the above discussion that pure Rayleigh behavior is difficult to find in a real material. Other processes can operate concurrently with it, and the randomness of the energy landscape required for the true Rayleigh behavior may never exist. The Rayleigh system is thus an approximation, and should be treated as such. Its opposite is an ordered system exhibiting nonlinear, but nonhysteretic behavior (see Section 4.5). In such a system the phase angle of all harmonics is 0° or 180°. It is thus tempting to think of a departure from the Rayleigh behavior as a measure of order in the system. A more rigorous theoretical treatment [117,118] is obviously needed to make a definite and general claim along these lines. As already mentioned, we shall rather arbitrarily call any nonlinear hysteretic system in which the hysteresis can be calculated from the parameters describing the nonlinearity (and vice versa) a 'quasi-Rayleigh system'.

At high driving-field amplitudes, $m(F_0)$ is no longer a linear function of the field amplitude, Fig. 4.35(a). We shall discuss a formal description of such cases in Section 4.4.3. For the present purposes it is sufficient to say that the corresponding hysteresis can be well approximated, Fig. 4.42, by the modified Rayleigh equation:

$$\begin{aligned} m(F_0) &= m_{\text{init}} + \alpha F_0 + \beta F_0^2 + \gamma F_0^3 + \ldots = m_{\text{init}} + \alpha' F_0, \\ \alpha'(F_0) &= \alpha + \beta F_0 + \gamma F_0^2 + \ldots, \\ R(F_0) &= (m_{\text{init}} + \alpha' F_0) \pm \frac{\alpha'}{2}(F_0^2 - F^2). \end{aligned} \tag{4.64}$$

Cubic and higher-order terms can be added if necessary to the hysteretic part of Eqn. (4.64).

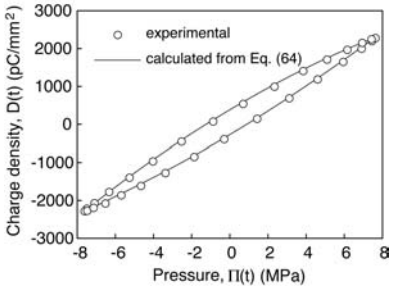

FIGURE 4.42 Charge density–pressure hysteresis (circles) measured in the pressure range where the Rayleigh relations (4.59)–(4.60) are no longer valid. The hysteresis can still be calculated (solid line) from the field dependence of the polarization using Eqn. (4.64).

Hysteresis Losses in Rayleigh-Like Systems

We next analyze the 'losses' associated with the Rayleigh loop. The total energy dissipation per unit volume associated with the hysteresis is given by its area A, which in the case of the Rayleigh loop can be calculated from Eqn. (4.59):

$$A_R = \int_{\text{cycle}} R\mathrm{d}F = \frac{4\alpha_m F_0^3}{3}. \tag{4.65}$$

Note that A_R does not possess energy units in the case of mixed pairs of piezoelectrically related variables, e.g. (D, Π) and (x, E), but does in the case of dielectric (D, E) and mechanical (x, Π) variables. If areas of experimentally measured hystereses, A_{exp}, are compared with those predicted by Eqn. (4.65) for a pure Rayleigh process, it is often found [57,127] that $A_{\text{exp}} > A_R$ over the field range where the Rayleigh relation (4.60) holds. This is illustrated in Fig. 4.43(a), which shows, for the same sample used to generate the data shown in Fig. 4.35, the areas of experimental hystereses, the areas predicted by Eqn. (4.65), and their difference. For the particular case of hysteresis shown in Fig. 4.35, the difference $A_{\text{exp}} - A_R$ is about 14 per cent. The log–log plot of A_{exp} and A_{exp}-A_R versus Π_0 (Fig. 4.43(b)) shows that $A_{\text{exp}} \propto \Pi_0^{2.7}$ and $A_{\text{exp}} - A_R \propto \Pi_0^2$, while from Eqn. (4.65) we see that $A_R \propto \Pi_0^3$. Since $\Pi_0^{2.7}$ can be obtained from the sum $b\Pi_0^3 + c\Pi_0^2$, this indicates the presence of a non-Rayleigh hysteretic mechanism that is a quadratic function of the field amplitude. For a linear system, in which

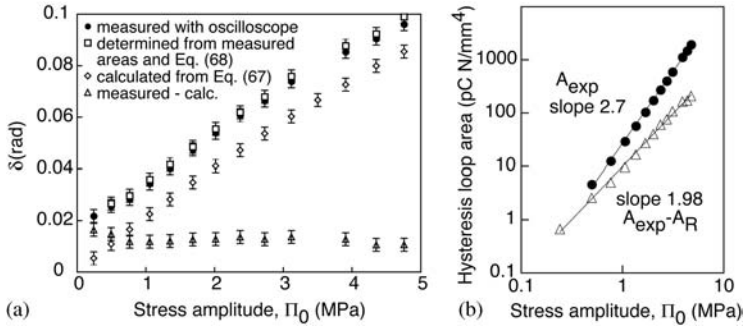

FIGURE 4.43 (a) The piezoelectric phase angle δ for a soft PZT ceramic measured by an oscilloscope (full circles), determined from the areas of experimental loops and Eqn. (4.68) (squares), and calculated from the Rayleigh parameters and Eqn. (4.67) (diamonds). The difference between the experimental and calculated phase angles is shown by the triangles. The error bars are equal to 0.005 rad. (b) The area of experimental loops, A_{exp}, and the difference of A_{exp} and the area of Rayleigh loops, A_R, as a function of the driving-field amplitude. A_{exp} corresponds to full circles in (a), A_R corresponds to diamonds in (a) and $A_{\text{exp}} - A_R$ corresponds to triangles in (a). Solid lines are linear fits on the double-logarithmic scales. Slopes of the fitted lines are indicated for each curve.

$F = F_0 \sin(\omega t)$ and $R = R_0 \sin(\omega t - \delta)$, the surface of the R–F hysteresis is:

$$A_{\text{lin}} = \int_{\text{cycle}} R\mathrm{d}F = \pi R_0 F_0 \sin\delta = \pi m'' F_0^2, \tag{4.66}$$

where m'' is the imaginary component of the generalized susceptibility. We thus see that the area of the total measured nonlinear hysteresis can be separated into the sum of the Rayleigh term, $A_R \propto F_0^3$, Eqn. (4.65), and the linear term, $A_{\text{lin}} \propto F_0^2$, Eqn. (4.66).

Alternatively, we can compare the phase angles of the ideal Rayleigh and experimental hystereses. Because of the orthogonality of sinusoidal functions, only the fundamental harmonic in Eqn. (4.61) will contribute to the integral in (4.65). The area of the Rayleigh hysteresis thus becomes $A_R = \pi R_0 F_0 \sin\delta_R$, the same as in the linear case, where δ_R now signifies the field-dependent phase angle between the driving field and the fundamental harmonic. Therefore, the expected phase angle of the Rayleigh expression (4.61) can be obtained from (4.65) as:

$$\delta_R \approx \sin\delta_R = \frac{A_R}{\pi R_0 F_0} = \frac{4\alpha_m F_0}{3\pi m}, \tag{4.67}$$

and the phase angle associated with the measured hysteresis as:

$$\delta_{\text{exp}} \approx \frac{A_{\text{exp}}}{\pi R_0 F_0}. \tag{4.68}$$

One obtains that $\delta_{\text{exp}} - \delta_R \approx$ constant, as is indeed observed experimentally, see Fig. 4.43. This is again consistent with the presence of a linear, hysteretic piezoelectric response, which operates in the background of the dominating nonlinear Rayleigh behavior.

An ideal Rayleigh hysteresis is a rate-independent, zero-temperature approximation [75]. We have seen, however, in Section 4.3 that the thermally activated piezoelectric relaxation in linear systems may lead to strong frequency dependence of the material complex coefficients. Thus, a linear relaxation process operating simultaneously with a nonlinear Rayleigh process is expected to lead to the frequency-dependent parameters of the Rayleigh hysteresis. Such a case is discussed in the next section.

4.4.2 FREQUENCY DEPENDENCE OF THE PIEZOELECTRIC COEFFICIENTS

Figure 4.44(a) and (c) show the direct longitudinal piezoelectric coefficient d_{33} of a soft PZT and the permittivity ε_{33} of a PZT thin film as a function of frequency at room temperature. At each frequency the nonlinear behavior can be described well by the Rayleigh relations, (4.59)–(4.60), but, as seen from Fig. 4.44(b) and (d), the nonlinear parameters m_{init} and α_m are now frequency dependent. The phase angle and the area of the R–F hystereses first increase and then become smaller as the frequency is increased, atleast over the examined frequency range, as shown in Fig. 4.45 for the piezoelectric charge–force hysteresis in a PZT ceramic.

It is possible [128] to effectively separate the linear, frequency-dependent contribution to the measured hysteresis from the Rayleigh, rate-independent contribution, by assuming the presence of a viscous process that can be described by a Debye-like equation (4.24):

$$d^* = d_\infty + \frac{\Delta d}{1 + \mathrm{i}\omega\gamma\Delta d}, \tag{4.69}$$

where γ represents apparent piezoelectric 'viscosity'. Assuming that the Rayleigh and viscous processes are independent, the total piezoelectric charge density can be described by:

$$D = (d_{\text{init}} + \Delta d + \alpha\Pi_0)\Pi \pm \frac{\alpha}{2}(\Pi_0^2 - \Pi^2) + \gamma\Delta d\frac{\partial D}{\partial t}. \tag{4.70}$$

Equation (4.70) is obtained by assuming that the Rayleigh term, Eqn. (4.59), is equal to the equilibrium term of the rate dependent equation

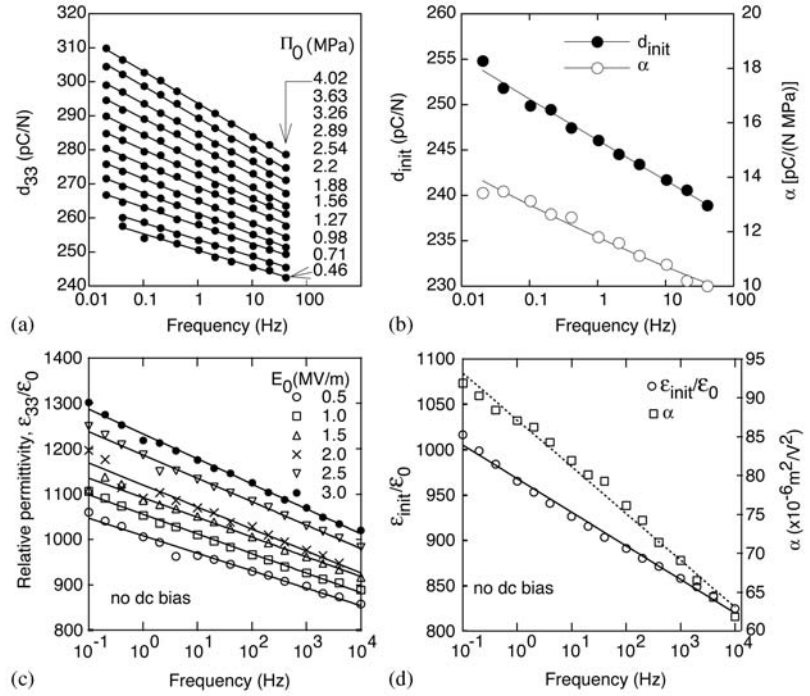

FIGURE 4.44 Frequency dependence of (a) the direct piezoelectric coefficient d_{33} for different pressure amplitudes, and (b) d_{init} and α_d in a soft PZT ceramic. Frequency dependence of (c) permittivity ε_{33} for different electric-field amplitudes, and (d) $\varepsilon_{\text{init}}$ and α_ε for a PZT thin film. (Thin film data courtesy of David V. Taylor).

(e.g. (4.21) or (4.26)). Note that in the general case α needs to be replaced by the field-dependent α', as indicated by Eqn. (4.64). It follows from Eqn. (4.69) that $\tan\delta_{\text{lin}} = \omega\gamma\Delta d$, so that the Rayleigh parameter α (or α') and $\tan\delta_{\text{lin}}$ can both be determined by fitting an experimental hysteresis with Eqn. (4.70). If the hysteresis fit is made using the purely rate-independent quasi-Rayleigh equation (4.64), one should obtain larger apparent α' because the hysteresis contains the viscous contribution. This is indeed observed, as shown in Fig. 4.46 for the direct piezoelectric effect in a PZT sample, which compares α's calculated by fitting experimental hysteresis using Eqns. (4.64) and (4.70). The α' evaluated by using corrected Eqn. (4.70) is in excellent agreement with the α' determined from $d(\Pi_0)$. Finally, the δ_{lin} calculated by fitting the experimental hystereses with (4.70) is in good agreement, Fig. 4.46(d), with the

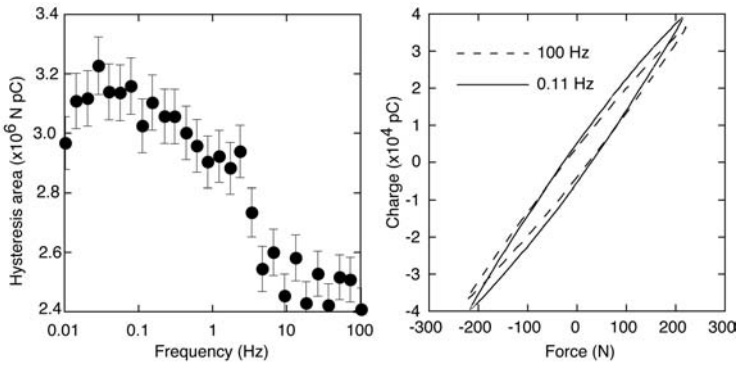

FIGURE 4.45 Left: area of the charge density–pressure hysteresis of a soft PZT ceramic as a function of the driving-field frequency, and right: example of hystereses at two frequencies.

phase angle obtained by determining $\delta_{\text{exp}} - \delta_R$, as explained earlier in Section 4.4.1.2.

Even though it may be useful from the practical point of view, the above approach for hysteresis separation is clearly too simplified. Equation (4.69) is limited to cases exhibiting the simplest Debye-type frequency dispersion. Strongly nonlinear ferroelectric systems, however, tend to exhibit a broad dispersion in the dielectric and piezoelectric properties, as shown in Fig. 4.44. Before developing a unified description of the frequency dispersion and nonlinearity, it is necessary to have a clear physical picture of the processes that lead to the broad frequency dependence of the electromechanical response. The difficulty here does not lie only in the theoretical modeling, but in having reliable experimental data on which to base or verify the theoretical model. We shall illustrate these difficulties below in a few examples.

Figure 4.44(a) and (c) suggest that, over the examined frequency range, the permittivity ε and the piezoelectric coefficient d decrease linearly with $\log(\omega)$. This behavior is even more apparent in Fig. 4.47, where $\varepsilon \propto \log(1/\omega)$ over six orders of magnitude. Several models [129,130] treating the dynamics of interfaces (e.g. domain walls, dislocations) in random/disordered systems have obtained frequency dependence of the susceptibility in the form $[\ln(1/\omega\tau_{\text{eff}})]^{\theta}$, where the exponent θ is related to the roughness of the energy potential. That approach has been applied to interpret experimental results in ferroelectric materials [57,131–134]. It turns out that, while the real component of the generalized susceptibility may appear to follow the linear-logarithmic dependence, the behavior of the imaginary

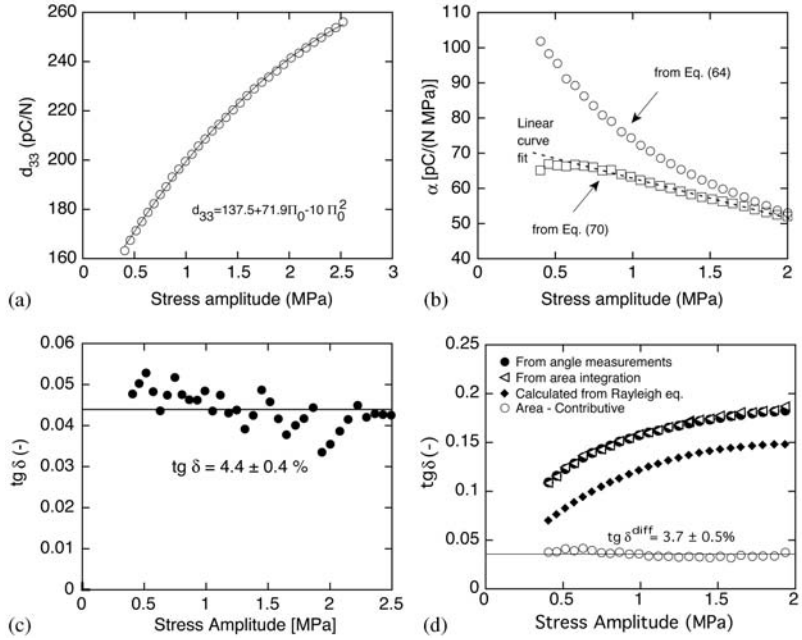

FIGURE 4.46 (a) d_{33} as a function of the pressure amplitude; (b) α calculated by fitting experimental hysteresis using modified Rayleigh equation (4.64) and its correction (4.70), which includes rate-dependent contributions; (c) tangent of the piezoelectric phase angle determined by fitting hystereses at different driving fields with Eqn. (4.70); (d) calculation of the phase angle from the experimental loops and from a purely Rayleigh relationship. The phase angles in (c) and the difference shown in (d) are, within experimental error, equal. (Courtesy Gilles Robert).

component is not always consistent with this behavior. For a system with a broad distribution of relaxation times, the real and imaginary components of the permittivity should be approximately related by [69]:

$$m'' \approx -\frac{\pi}{2}\frac{\partial m'}{\partial \ln \omega}. \tag{4.71}$$

For $\theta \approx 1$, which is the case observed for $m = d$, ε in PZT ceramics and films (Fig. 4.44), it follows from $m' \propto [\ln(1/\omega\tau_{\text{eff}})]$ that $m'' \approx$ const. As we shall see below, the experimentally determined m'' are in many cases frequency dependent. Unfortunately, the exact $m''(\omega)$ function for a given process is not always easy to verify experimentally in ferroelectric materials, since several dispersive mechanisms may operate simultaneously and their separation becomes difficult. In dielectrics, such additional

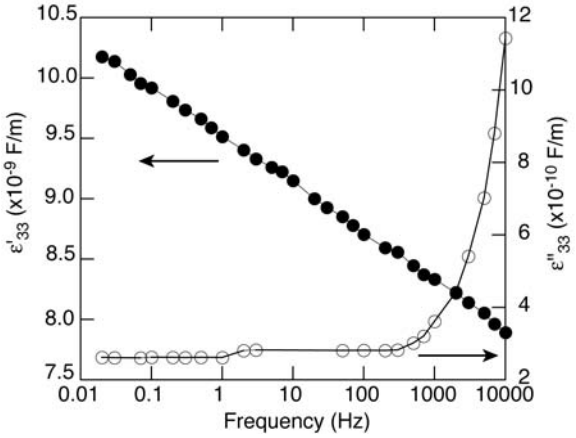

FIGURE 4.47 Complex dielectric permittivity of a PZT thin film suggesting logarithmic frequency dependence over six orders of magnitude. The increase of the imaginary part at high frequencies is an experimental artifact. (Courtesy Bharadwaja Srowthi).

contributions include conductivity for which $\varepsilon'' = \sigma/(\omega\varepsilon_0)$, the piezoelectric resonances, other, e.g. Debye-like, dispersive processes [132,133], and possibly inductive resonances (see Fig. 4.47). A specific dispersion mechanism can often be observed only over a limited frequency range, and becomes distorted at the high and low limits where other process take over, so that it becomes difficult to conclude whether $m'' \approx$ const holds (see Fig. 4.47). This behavior can sometimes be masked by competing mechanisms and elaborate schemes need to be used for their separation [133]. Alternatively, the logarithmic frequency dependence can be obtained by assuming an exponentially broad distribution of the waiting times [26,135].

Another model that can lead, over a limited frequency range, to an apparent linear-log dispersion of the generalized susceptibility is based on the power law $m \propto 1/\omega^{\beta}$ with $\beta << 1$. This behavior can be derived phenomenologically in the following way [132,136]. Let us consider, for simplicity only, the contribution of 180° domain walls to the dielectric polarization of a ferroelectric. Assume that under the action of an external field $E(t)$, the domain wall displaces by $\Delta l(t)$. The contribution of the moving domain wall to the polarization is then:

$$\Delta P(t) = (2P_S/d)\Delta l(t), \tag{4.72}$$

where d is the average width of a domain that, depending on its orientation, carries polarization $\pm P_s$. If the velocity v of the domain wall is a linear

function of the field, $\partial\Delta l(t)/\partial t = \mu E$, and the field $E = E_0 e^{i\omega t}$ is sinusoidal, one obtains from (4.72) the following rate-dependent equation:

$$\frac{\partial \Delta P(t)}{\partial t} = \frac{2P_s}{d}\frac{\partial \Delta l(t)}{\partial t} = \mu E_0 e^{i\omega t}. \tag{4.73}$$

This is equivalent to assuming that the force per unit domain-wall area exerted by external field is $2P_sE(t)$ [136,137] and that in the general equation of the balanced forces:

$$m\frac{\partial^2 \Delta l}{\partial t^2} + k\Delta l + \eta\frac{\partial \Delta l}{\partial t} = 2P_sE(t) \tag{4.74}$$

the first, inertial term, and the second, restoring-force term, can be neglected. The domain wall thus moves in an irreversible manner, by hopping from one pinning center to another, not unlike the conduction process.

The solution of the reduced equation (4.74) or (4.73) is:

$$\Delta P(t) = \frac{2P_S\mu}{(i\omega)d}E, \tag{4.75}$$

which gives for the permittivity:

$$\varepsilon(\omega) = \varepsilon_\infty + \frac{2P_S\mu}{(i\omega)d} = \varepsilon_\infty + \frac{\varepsilon_\infty}{i\omega\tau_{\text{eff}}}, \tag{4.76}$$

where ε_∞ represents instantaneous dielectric permittivity, and effective relaxation time τ_{eff} is the time necessary for the domain-wall contribution to be equal to the instantaneous polarization, $\Delta P(t) = \varepsilon_\infty E$. As in the case of the Debye relaxation (Section 4.3.1), one introduces phenomenologically [132] exponent $\beta < 1$ into Eqn. (4.76) leading to:

$$\varepsilon(\omega) = \varepsilon_\infty + \frac{\varepsilon_\infty}{i\,(\omega\tau_{\text{eff}})^\beta}. \tag{4.77}$$

Equation (4.77) possesses particular properties that can be verified experimentally. Before discussing these in some detail, we briefly mention some limitations of Eqn. (4.74). The first limitation is clearly related to the choice of the field dependence of the domain-wall velocity $v(E) = \mu f(E)$. The data available in the literature suggest that $f(E)$ varies from $f(E) = E$, for displacement of 180° domain walls [137], to $f(E) = \exp(-\delta/E)$ for 90° domain walls in $BaTiO_3$ [138] and tetragonal PZT [139]. However, since $f(E)$ needs to be modified, as suggested by Kleemann *et al.* [132], to take into account polydispersivity, it is possible that for very small β, the different $f(E)$ will

give similar frequency dependences. The second comment is on the fact that Eqn. (4.75) suggests that the domain-wall contribution leads to singularity at low frequencies. This result is nonphysical, since any dissipation mechanism should reduce to zero in the static case, i.e. for a constant field [69]. Equations (4.75)–(4.76) thus represent a 'high' frequency limit of a more complex behavior [82,84]. Indeed, at least in the case of piezoelectric relaxation, a maximum in the imaginary part of $d(\omega)$ is observed at low frequencies. Equation (4.77) has recently been derived by Fedorenko, Mueller, and Stepanow [140], considering stochastic motion of domain walls.

Some of the properties of Eqn. (4.76) are given below. By separating the real and imaginary parts, and taking for the material coefficient the most general case ($m = m' - \mathrm{i}m'' = d, \varepsilon, s$) one obtains:

$$m'(\omega) = m_\infty + \frac{m_\infty \cos(\frac{\beta\pi}{2})}{(\omega\tau_{\text{eff}})^\beta}, \tag{4.78}$$

$$m''(\omega) = \frac{m_\infty \sin(\frac{\beta\pi}{2})}{(\omega\tau_{\text{eff}})^\beta}. \tag{4.79}$$

It follows from Eqns. (4.78)–(4.79) that $m' - m_\infty$ and m'' should have the same slope β when presented as a function of $\log(\omega)$. Likewise, the slope of the Cole–Cole plot ($m''(\omega)$ *v*ersus $m'(\omega) - m_\infty$) is now frequency independent and is equal to $\tan(\beta\pi/2)$. Neglecting the behavior at very low frequencies, where another functional dependence will need to be used to bring $m''(\omega \to 0) = 0$, and any other processes that may control the response at high frequencies, we make the following assumptions: (i) the field-dependent mechanism described by the Rayleigh equation (4.61) is the high-frequency limit of the purely rate-dependent process described by (4.78)–(4.79); and (ii) the rate-dependent and rate-independent losses couple, i.e. they are not simply additive. Taking into account assumptions (i) and (ii), and keeping only the first harmonic term in Eqn. (4.61), we obtain the following expression for the complex coefficients:

$$m'(F_0, \omega) = m_{\text{init}} + \alpha_m F_0 + \frac{m_i^R \cos\left(\beta\frac{\pi}{2}\right)}{(\omega\tau)^\beta}, \tag{4.80}$$

$$m''(F_0, \omega) = \frac{4\alpha F_0}{3\pi} + \frac{m_i^R \sin\left(\beta\frac{\pi}{2}\right) \times f(F)}{(\omega\tau)^\beta}, \tag{4.81}$$

where $m_i^R = m_{\text{init}} + \alpha F_0$, and $f(F)$ is the field-dependent factor that describes the coupling of the frequency-dependent and rate-independent

losses. Clearly, it should hold that $f(F) \to 1$ as $F_0 \to 0$. In addition, from Eqns (4.80)–(4.81), one expects that the plot of $m''(\omega) - 4\alpha_m F_0/3\pi$ versus $m'(\omega) - (m_i + \alpha_m F_0)$ should give a straight line with slope $\tan\left(\beta\pi/2\right) \times f(F)$. Both conditions hold fairly well for the permittivity in PZT thin films and the longitudinal piezoelectric coefficient in ceramics. Figure 4.48, for example, illustrates the validity of the linear relationship for the Cole–Cole plots ($m''(\omega)$ versus $m'(\omega)$), which must now include field-dependent terms. The value of β is very small, below 0.1, indicating why over the examined frequency range the frequency dependence can be equally well described by $\ln(1/\omega)$ and $1/\omega^\beta$ behavior. Note that Eqns (4.80)–(4.81) account for the frequency dependence of the measured (apparent) Rayleigh parameters (Fig. 4.44) and the field dependence of the power-law parameters (not shown). For example, rearrangement of terms in Eqns (4.80)–(4.81) gives:

$$\begin{aligned} m'(F_0, \omega) &= m_i + \alpha_m F_0 + \frac{m_i^R \cos\left(\beta\frac{\pi}{2}\right)}{(\omega\tau)^\beta} \\ &= m_i \left[1 + \frac{\cos\left(\beta\frac{\pi}{2}\right)}{(\omega\tau)^\beta}\right] + \alpha_m \left[1 + \frac{\cos\left(\beta\frac{\pi}{2}\right)}{(\omega\tau)^\beta}\right] F_0 \\ &= m_i^{\text{meas}}(\omega) + \alpha_m^{\text{meas}}(\omega) F_0, \end{aligned} \tag{4.82}$$

where now $m_i^{\text{meas}}(\omega) \propto 1/\omega^\beta$ and $\alpha_m^{\text{meas}}(\omega) \propto 1/\omega^\beta$, as seen in Fig. 4.44. It should be noted that a similar grouping of terms may be made assuming the linear-log behavior [57,131].

Measurements of a complex piezoelectric coefficient at ultralow frequencies is particularly challenging. We present in Fig. 4.49 the piezoelectric phase angle of a PZT ceramic with a broad frequency dispersion (power-like or logarithmic) and of a PSmT ceramic with a quasi-Debye dispersion (Section 4.3.3). We see that both materials present a peak that clearly differs in broadness and strength. Thus, in the case of PZT, it is difficult to conclude which type of behavior is involved (power, logarithmic above the peak, or a broad Debye-type) without covering a significantly higher frequency range (many orders of magnitude). It has been suggested by Metzler and Klafter [84] that the power-law dependence $1/\omega^\beta$ is simply a medium-to-low frequency approximation of the Davidson–Cole extension of the Debye-type relaxation (Section 4.3.3). They further suggest that all types of modified (polydispersive) relaxations can be described by a generalization of the classical exponential relaxation based on the fractional Fokker–Planck equation. In this sense [75], it is thus not surprising that the Rayleigh behavior, typical for disordered systems, is accompanied

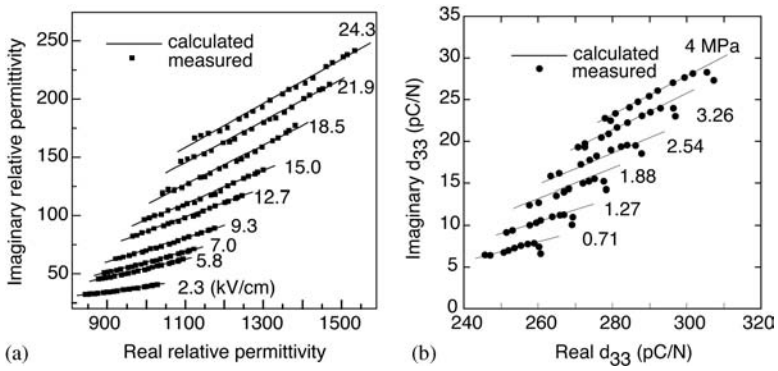

FIGURE 4.48 Cole–Cole plots for (a) the complex permittivity, and (b) the direct piezoelectric coefficient, both of which apparently exhibit the power-law dependence on the driving-field frequency. The permittivity was measured on a PZT thin film and the piezoelectric data on a soft PZT ceramic. (Thin-film data courtesy of Bharadwaja Srowthi).

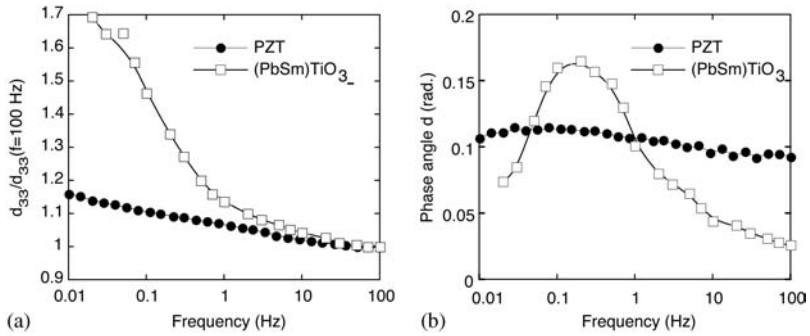

FIGURE 4.49 (a) Relative direct longitudinal d_{33} piezoelectric coefficient, and (b) its phase angle as a function of frequency for a soft PZT ceramic and the modified lead-titanate (PSmT) sample.

by a dynamic, rate-dependent process characterized by a highly stretched exponential function.

Finally, we discuss the temperature dependence of the Rayleigh-like hysteresis, which, as we have seen, is modified by rate-dependent processes. Figure 4.50 shows the hysteresis and nonlinearity for the permittivity in a thin PZT film. Both the hysteresis and nonlinearity become smaller with decreasing temperature. For a quasi-Rayleigh process this is equivalent to having an $\alpha(T)$ that decreases with decreasing temperature.

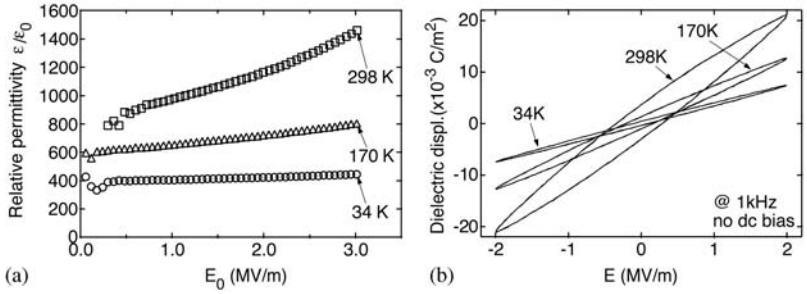

FIGURE 4.50 (a) Field dependence of the relative dielectric permittivity, and (b) hystereses, at different temperatures, for a PZT thin film [126]. (Courtesy David V. Taylor).

This change of the hysteresis may indicate evolution of the potential energy profile for domain walls with temperature. For example, it is known that the domain-wall width increases [21] and, therefore, the pinning force becomes weaker [141] with increasing temperature.

4.4.3 PREISACH APPROACH: PREISACH DISTRIBUTIONS AND EFFECTS OF STATIC FIELDS ON NONLINEARITY

The first formal attempt to interpret the Rayleigh relations was developed by Preisach [114]. As discussed elsewhere in this book and in other references [10,75] this approach has eventually become one of the most powerful tools to describe hysteretic phenomena in general. The Preisach model was first applied to ferroelectric materials by Turik in the 1960s [119–121]. In this section we shall show how this approach can be used to obtain analytical expressions of piezoelectric nonlinearity and hysteresis in cases when the Rayleigh description is insufficient (the field dependence of the piezoelectric coefficient is nonlinear, Eqn. (4.64)), and to describe the effects of bias fields on piezoelectric nonlinearity and hysteresis.

In the Preisach approach, which we shall briefly present for the sake of completeness, it is assumed that a hysteretic system contains a collection of simple bistable units (e.g. a domain wall in a pinning field) where each unit is characterized by two parameters: a bias (or internal) field (F_i) and a coercive field (F_c). Each state of the unit is assumed to contribute to the total response R by the same amount $\pm R_0$ (see Fig. 4.51).

The bias field can take any value from $-\infty$ to $+\infty$, while the coercive field is defined as positive. The half-plane of possible values for F_i and F_c is called the Preisach plane. In a given system, the bistable units exhibit a statistical distribution of these parameters that can be characterized by the

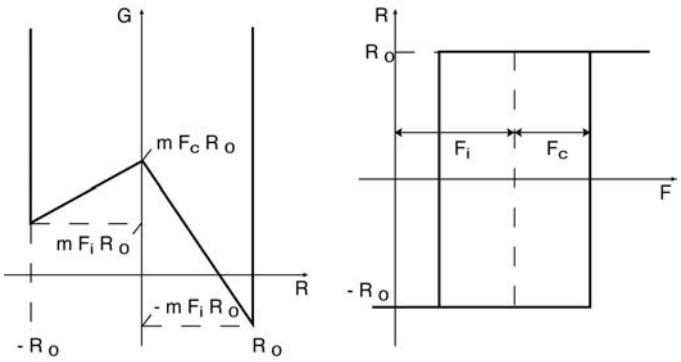

FIGURE 4.51 (left) Energy profile, and (right) square hysteresis of an elementary bistable unit (from [75]). m is a generalized susceptibility.

distribution function $f(F_i, F_c)$ defining the density of bistable units in the plane. $f(F_i, F_c)$ obeys the following normalization condition:

$$\int_0^{\infty} \int_{-\infty}^{+\infty} f(F_i, F_c) \mathrm{d}F_i \mathrm{d}F_c = 1. \tag{4.83}$$

The Preisach description holds only for a definite class of hysteretic processes. It has been proven that the agreement of a given experimental hysteretic system with this formalism is verified if and only if it exhibits so-called wiping-out and congruency properties [10,75]. Both are considered to be valid in ferroelectric materials [4,5].

The Preisach formalism is implemented as follows: let us consider the Preisach plane for zero external field. It can be divided into three regions (Fig. 4.52): region a, where $F_i > F_c$, hence a negative zero-field state ($-R_0$); region b, where $F_c > |F_i|$, hence an indefinite zero-field state, which depends on history; and region c, where $F_i < -F_c$, hence a positive zero-field state ($+R_0$).

Once an external field, F, is applied, it acts in the same way as a homogeneous bias field. The b-region cone, $F_i = F \pm F_c$, is thus moved upward or downward accordingly and units crossing the limits between the regions are, if necessary, switched to the stable state. Thus, for increasing fields, the cone is shifted up and all bistable units where $F_i + F_c < F$ are switched to a positive state. For decreasing fields, the cone is shifted down and all the units where $F_i - F_c > F$ are switched to a negative state contributing by $\pm 2R_0$ to the total response. Clearly, this contribution will depend on the number of switched units that are characterized by the distribution function, $f(F_i, F_c)$. The Rayleigh case corresponds to a uniform

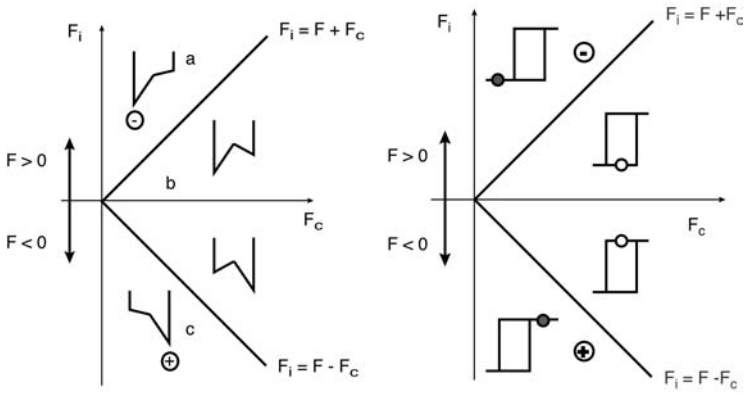

FIGURE 4.52 State of the bistable units as a function of their position on the Preisach plane at zero applied field (from [75]).

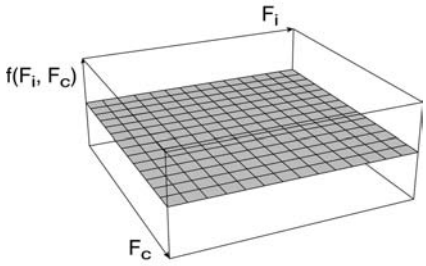

FIGURE 4.53 Flat Preisach distribution function corresponding to the Rayleigh relations.

distribution function, Fig. 4.53, and associated contributions only depend on the swept area of the Preisach plane [75].

The nonlinear part of the total response may be calculated in the following way [142]. For an alternating field with amplitude F_0 and offset $F_=$ (e.g. $F = F_= + F_0 \sin(\omega t)$) the total nonlinear contributions are proportional to the integral of the distribution function over the large triangle Δ defined by the vertices $(0; F_= + F_0)$, $(0; F_= - F_0)$ and $(F_0; F_=)$. The hysteresis equation can be obtained from the field-dependent integrals of the distribution function over the growing gray regions (as shown in Fig. 4.54) taking into account the sign of the applied field derivative F (i.e. considering increasing or decreasing F). In the case of a uniform distribution $f = \text{const}$ (the Rayleigh case), the nonlinear contribution to the response R is proportional to the area A of the large triangle, $A_\Delta = F_0^2$, which thus gives the linear

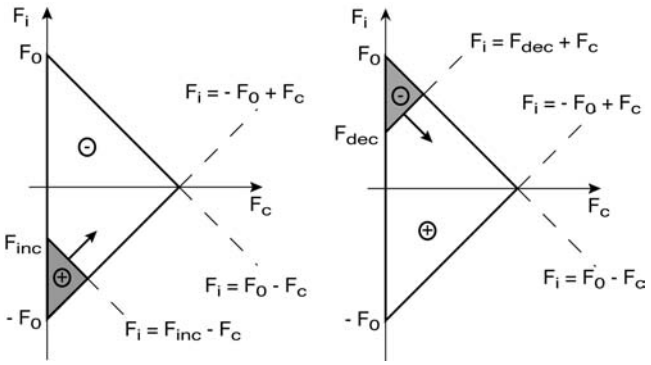

FIGURE 4.54 Schematic view of the switched bistable units for an alternating external field without bias ($F_{=} = 0$). F_{inc} and F_{dec} stand for increasing and decreasing applied field F.

dependence of the general susceptibility ($m = R/F_0$) on the amplitude of the applied field.

For arbitrary fields, the nonlinear response can be obtained only when the state of the units situated in the metastable cone (region b of Fig. 4.52) is known. This is not the case when the initial state is obtained directly from a temperature-dependent phase transition from the paraelectric phase. However, if the sample has been prepared by applying some known field profile, $F(t)$, after the bistable units have appeared on cooling from the paraelectric phase, the state line, $b(F_c)$, representing the field history of the sample, can be defined (see Fig. 4.55).

Turik [119–121] used this formalism to analyze the nonlinear dielectric behavior of $BaTiO_3$. He treated F_i as an effective field applied on a given domain, created by surrounding domains and free charges in the ferroelectric, and F_c as the field at which polarization of the isolated domain switches, without considering long-range electrostatic influence. Assuming that the applied external electric field is homogeneous inside the ceramic, it is then possible to introduce a function of the statistical distribution of domains according to their coercive and internal field $f(F_i, F_c)$. At weak fields (at small F_i and F_c), $f(F_i, F_c)$ may be expanded in a MacLaurin series, which is symmetrical with respect to F_i [119]:

$$f(F_i, F_c) = f_0 + gF_c + hF_c^2 + kF_i^2 + \cdots . \tag{4.84}$$

At high fields, Eqn. (4.84) may be considered as an approximation. In the case of ferroelectrics, the distribution function $f(F_i, F_c)$ may change with time at large fields (as depolarization occurs, for example), and from

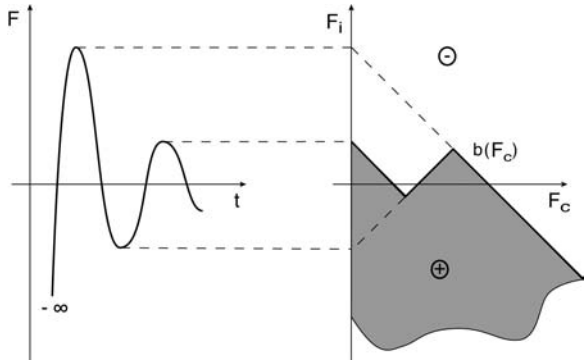

FIGURE 4.55 Definition of the state line $b(F_c)$ as a function of the field history since the application of a negative infinite field and subsequent series of local-field extrema (from [75]).

experiments one can determine $f(F_i, F_c)$ not in its initial state but at its settled state, which depends on the amplitude of the alternating voltage. At weak fields, typically in the Rayleigh range, where $f(F_i, F_c) \approx f_0$, such problems do not arise, and $f(F_i, F_c)$ permits description of both the initial and the final state of the ceramic. Assuming that the distribution function described in Eqn. (4.84) is valid for the dielectric and piezoelectric effects, it is possible to obtain expressions for the descending and ascending branches of the dielectric or piezoelectric hysteresis. Some examples of how this is done as well as the limitations of function (4.84) will be discussed later in this section.

In the case when an external bias field $F_=$ and an alternating field with amplitude F_0 are applied simultaneously on a ferroelectric ceramic along the direction of remnant polarization, the region of the Preisach plane within which reorientation of 180° and/or non-180° domains causes an irreversible contribution to the general susceptibility has a triangular shape, as shown in Fig. 4.56. This region is called the 'working range' area. An increase in F_0 leads to an increase of the 'working range', and causes a monotonous increase in contributions of local domain switching to the general susceptibility.

In the case of the piezoelectric effect in tetragonal materials where only 90° domain walls contribute to the response, and to reduce the problem to the scalar form of the Preisach formalism, we assume that two-thirds of the total number of domains can switch in the direction of the applied field (the equivalent of 90° domain-wall movement). Then, according to Fig. 4.56, the following result for the increasing (R^+) and decreasing (R^-)

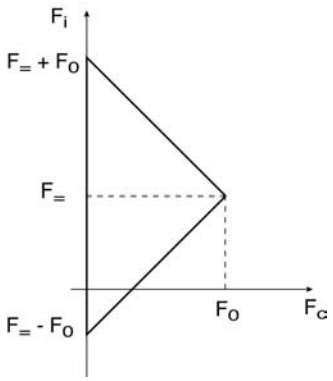

FIGURE 4.56 Portion of the Preisach plane reoriented by a field of amplitude F_0 and offset (bias) $F_=$.

branches of the hysteresis can be derived (see above and [119,143]) using the totally switched-down state as the reference:

$$R^-(F) = R_m - \frac{4R_0}{3}\int_0^{(F_=+F_0-F)/2}\int_{F+F_c}^{F_=+F_0-F_c} f(F_i, F_c)\mathrm{d}F_i\mathrm{d}F_c, \tag{4.85}$$

$$R^+(F) = \frac{4R_0}{3}\int_0^{(-F_=+F_0+F)/2}\int_{F_=-F_0+F_c}^{F-F_c} f(F_i, F_c)\mathrm{d}F_i\mathrm{d}F_c, \tag{4.86}$$

with

$$R_m(F) = \frac{4R_0}{3}\int_0^{F_0}\int_{F_=-F_0+F_c}^{F_=+F_0-F_c} f(F_i, F_c)\mathrm{d}F_i\mathrm{d}F_c. \tag{4.87}$$

R_m corresponds to the total nonlinear contribution, which depends on the amplitude of the alternating pressure F_0 applied simultaneously with the constant bias field $F_=$. The above formulas are valid for any distribution function, for instance, they describe effectively the observed Rayleigh hysteresis in the case of lead zirconate titanate for $f(F_i, F_c) = f_0$. With the help of Eqns (4.85)–(4.87), it is possible to determine the equation of the final hysteresis corresponding to the distribution function $f(F_i, F_c)$. For the distribution function $f(F_i, F_c)$ of Eqn. (4.84), the R_m is given by:

$$R_m = \frac{4R_0}{3}F_0^2\left(f_0 + \frac{g}{3}F_0 + \frac{1}{6}(h+k)F_0^2 + kF_=^2 + \cdots\right), \tag{4.88}$$

which finally corresponds to the following contribution to the piezoelectric coefficient:

$$\Delta d_{33}(F_0, F_=) = \frac{R_m}{2F_0} = \frac{2R_0}{3}F_0\left[f_0 + \frac{g}{3}F_0 + \frac{1}{6}(h+k)F_0^2 + kF_=^2 + \ldots\right]. \tag{4.89}$$

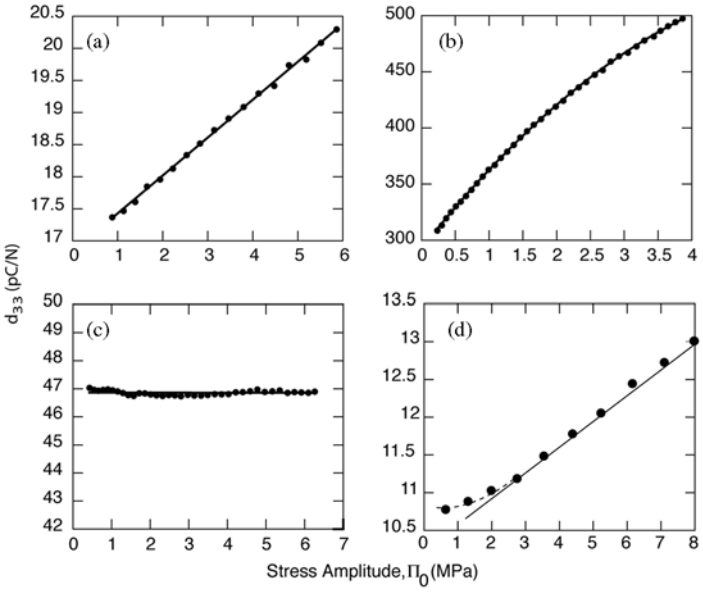

FIGURE 4.57 Various types of d_{33} dependences on the amplitude of the applied stress: (a) Nb-doped $Bi_4Ti_3O_{12}$, (b) $Pb(Zr_{0.53}, Ti_{0.47})O_3$, (c) Sm-doped $PbTiO_3$ (PSmT), and (d) $0.95Bi_4Ti_3O_{12}$-$0.05Bi_3TiNbO_9$ ceramics. Dots represent experimental data, solid lines stand for Preisach-based fittings and the dashed line in (d) was plotted to guide the eye along experimental values. (Courtesy Gilles Robert).

We next examine several typical experimental examples of the nonlinearity of the direct piezoelectric coefficient and discuss it in terms of the formalism developed above by using, in particular, Eqns (4.84) and (4.89). Hence, stress Π and charge displacement D will be equivalent to the field F and response R, respectively. Note that for direct piezoelectric measurements the sample is always in compression and hence the applied bias stress $\Pi_=$ is always greater than the applied amplitude Π_0; the swept area is thus situated in one quadrant only of the Preisach plane (as shown in Fig. 4.56).

The dependence of the piezoelectric coefficient on the field amplitude, $d_{33}(\Pi_0)$, manifests itself qualitatively differently for piezoelectrics with different ease of domain-wall motion. Various types of experimentally observed dependences are illustrated in Fig. 4.57.

In the first approximation, the distribution of domains with respect to Π_c and Π_i may be considered as uniform, i.e. $f(F_i, F_c) \approx f_0$. In this case

no noticeable deviation of $d_{33}(\Pi_0)$ from the linear dependence would be observed over a limited driving-field range. This yields the Rayleigh law valid in the case of small stress amplitudes or for materials containing very homogeneously distributed defects, as shown for $Bi_4Ti_3O_{12}$ in Fig. 4.57(a).

In materials with high piezoelectric properties, such as soft PZT and relaxor–ferroelectric ceramics, the defects appear not to be uniformly distributed. In these materials, Π_c and Π_i are small, i.e. the mobile domain walls are concentrated near the origin of the Preisach coordinate system. As Π_0 increases, regions with lower distribution densities are involved in the reorientation process. The associated distribution function is then given by:

$$f(\Pi_i, \Pi_c) \approx f_0 + g\Pi_c + \cdots < f_0(g < 0), \tag{4.90}$$

leading to a decrease in the rate of increase of d_{33} with Π_0. The field dependence of the piezoelectric coefficient thus becomes nonlinear, deviating more and more from the Rayleigh law, as illustrated in Fig. 4.57(b) for lead zirconate titanate at the morphotropic phase boundary. Note that if the distribution function is given by the two explicitly written terms in Eqn. (4.90), a quadratic dependence of the piezoelectric coefficient is expected from Eqn. (4.89). Indeed, the fitted second-order polynomial in Fig. 4.57(b) shows very good agreement with the experimental data.

This deviation from the linear dependence of $d_{33}(\Pi_0)$ can even lead to a quasi-saturation of the nonlinear contribution (see Fig. 4.58) as the swept area reaches Preisach plane regions where the number of contributing units goes to zero. This saturation can be reached both in very soft materials where most of the domain walls are situated close to the origin of the Preisach plane and in hard materials where very few domains may be mobile with the exception of some units close to the origin (the case illustrated in Fig. 4.58). If higher driving fields are considered, additional terms need to be added to Eqn. (4.84). Some very hard ceramics may be characterized with an almost complete absence of mobile domains in the region of small Π_i and Π_c. This leads to the absence of or to a very weak $d_{33}(\Pi_0)$ dependence as shown in Fig. 4.57(c) for samarium-doped lead titanate.

The threshold field, i.e. the quasi-constant $d_{33}(\Pi_0)$ at small Π_0, can be interpreted in the Preisach formalism as a depletion of moving domain walls close to the $(0; \Pi_=)$ point of the Preisach plane leading to no extrinsic contributions at low Π_0. The threshold field can then be seen as the stress corresponding to the presence of mobile domain walls having Π_c or Π_i close to the value of the applied field. In this case the distribution function may look like:

$$f(\Pi_i, \Pi_c) = g\Pi_c + \cdots (\mathrm{g} > 0). \tag{4.91}$$

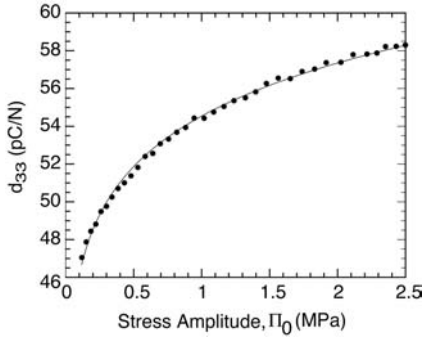

FIGURE 4.58 Dependence of d_{33} on amplitude of the applied stress for $Pb(Zr_{0.40}, Ti_{0.60})O_3$ ceramic. (Courtesy Gilles Robert).

The corresponding $d_{33}(\Pi_0)$ dependence may be close to what is displayed in Fig. 4.57(d) for $0.95Bi_4Ti_3O_{12}$-$0.05Bi_3TiNbO_9$. Clearly, description of a material exhibiting a threshold field accompanied by subsequent quadratic behavior of the piezoelectric coefficient would require more terms in the expansion of Eqn. (4.84).

The developed Preisach formalism can also be applied to describe the dependence of the piezoelectric coefficient on bias stress $d_{33}(\Pi_=)$. First of all, it should be noted that the triangular 'working range' in Fig. 4.56 displaces to the region of larger internal stresses Π_i as $\Pi_=$ increases. This requires the use of a larger number of terms in the expansion of Eqn. (4.84). Only the minimal number of terms that takes into account dependence of the electromechanical hysteresis loop and piezoelectric coefficient on Π_i is indicated in Eqn. (4.84). A typical bias stress dependence of the piezoelectric nonlinearity in tetragonal lead zirconate titanate is shown in Fig. 4.59.

For a qualitative interpretation of $d_{33}(\Pi_0, \Pi_=)$ dependence presented in Fig. 4.59, it is sufficient to assume that in Eqn. (4.89) coefficient $k < 0$, i.e. the number of mobile domain walls decreases as $\Pi_=$ increases. This means that an increase in $\Pi_=$ displaces the 'working range' in regions of the Preisach plane where there are less switchable units per swept area. In such a simple case, the $d_{33}(\Pi_0)$ dependence is preserved, and relative decrease of d_{33} with $\Pi_=$ is proportional to Π_0. The data displayed in Fig. 4.59 indeed show this decrease of nonlinear contributions to d_{33} with increasing bias stress $\Pi_=$. However, the comparison of the theoretical results presented in Eqns (4.84) and (4.89) with experimental data from Fig. 4.59 shows that, for a quantitative description (especially the saturating behavior at low bias stress), it is necessary to increase the number of terms in the

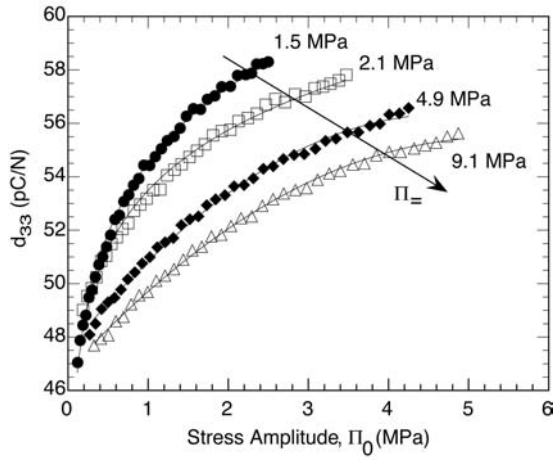

FIGURE 4.59 Dependence of the nonlinear behavior of the piezoelectric d_{33} coefficient for $Pb(Zr_{0.40}, Ti_{0.60})O_3$ on bias stress $\Pi_=$. Note that there is no depoling of the sample as $\Pi_=$ is changed. (Courtesy Gilles Robert).

expansion $f(\Pi_i, \Pi_c)$ or to invoke a more rigorous method of determining $f(\Pi_i, \Pi_c)$ from the piezoelectric hysteresis loop. This quantitative point is treated below, closely following the discussion presented in [144–146], where additional details may be found.

In practice, a commonly observed nonlinearity of the piezoelectric coefficient nonlinearity is of the quadratic type illustrated in Fig. 4.60 (see, e.g. [57,105,107]). Hence, in the following, the emphasis will be put on the description of such nonlinearity and associated hysteresis loops. The Preisach distribution function that yields a quadratic dependence on the field amplitude is given by Eqn. (4.90). However, this function can only be considered as a local approximation, as any distribution function valid for the whole Preisach plane has to satisfy the normalization criteria (4.83), which is not the case for Eqn. (4.90). It is, perhaps, instructive to follow the reasoning [144,146] behind developing an expression for the Preisach distribution, the field dependence of the piezoelectric coefficient and associated hysteresis for this particular case of the quadratic field dependence of the direct longitudinal piezoelectric coefficient, which can then be generalized for more complex cases and general susceptibilities.

Thus, looking for the quadratic field dependence of d_{33} in the form:

$$d_{33}(\Pi_0) = d_{\text{init}} + \alpha\Pi_0 + \beta\Pi_0^2, \tag{4.92}$$

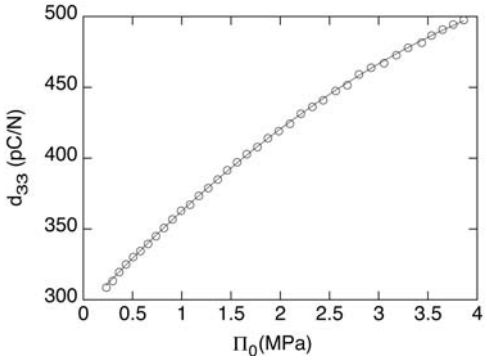

FIGURE 4.60 Dependence of d_{33} piezoelectric coefficient on stress amplitude, Π_0 for a rhombohedral PZT. The solid line represents a quadratic fit to the data points. (Courtesy Gilles Robert).

and using the method described above to compute the domain-wall contribution Δd_{33}, Eqn. (4.89), to the piezoelectric coefficient, it was found that the following distribution function is adequate:

$$f(\Pi_i, \Pi_c) = f_0 + g\Pi_c + k\,|\Pi_i|. \tag{4.93}$$

This distribution function is presented in Fig. 4.61 for negative values of g and k parameters necessary to comply with the normalization criteria. This nonanalytical form can be seen as a first-order linear approximation of any distribution function symmetrical with respect to internal field. The quadratic dependence on internal field was not chosen in Eqn. (4.93) because the nonlinearity associated with such an expression leads to cubic-field dependence of the piezoelectric coefficient.

The corresponding contribution to the piezoelectric response for a purely alternative field (bias field, $\Pi_= = 0$) is given by:

$$\Delta d_{33}(\Pi_0) \propto f_0\Pi_0 + \frac{1}{3}(g+k)\Pi_0^2, \tag{4.94}$$

and by:

$$\Delta d_{33}(\Pi_0, \Pi_=) \propto (f_0 + k\Pi_=)\Pi_0 + \frac{1}{3}g\Pi_0^2, \tag{4.95}$$

in the presence of a strong bias field $\Pi_= > \Pi_0$, which is always the case in direct piezoelectric measurements. The fact that the second-order nonlinear coefficient is independent of bias field may be used to validate the proposed expression. Details of the experimental procedure can be found in [144,145].

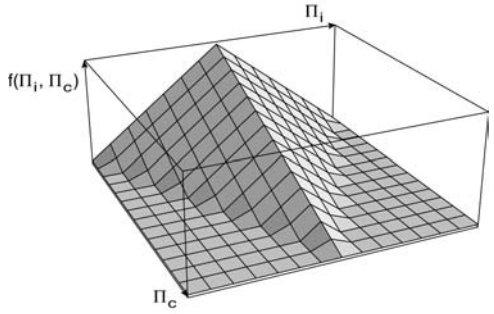

FIGURE 4.61 Roof-like distribution function based on Eqn. (4.93). The maximum of this distribution is situated at the Preisach plane origin. Intersections of the distribution function with F_i and F_c axes correspond to $\pm f_0/k$ and $-f_0/g$, respectively. (Courtesy Gilles Robert).

Typical dependence of $d_{33}(\Pi_0)$ on the bias stress $\Pi_=$ is shown in Fig. 4.62. The obtained curves exhibit a quadratic behavior typical for measurements at high stress amplitudes. After fitting these curves with Eqn. (4.92), the intrinsic and reversible contributions are found to be independent of $\Pi_=$ with $d_0 \approx 139$ pC/N. The nonlinear parameters α and β are plotted in Fig. 4.63 as a function the bias stress.

The dependence of α on the bias stress is close to linear as expected from Eqn. (4.95). However, note that the verification is valid only for the limited range of tested bias stresses (from 3 to 4 MPa), outside this range the distribution function may very well have another shape than what is proposed. In particular, observations of threshold fields and diverging behavior of the piezoelectric coefficient in converse measurements [105] might indicate the existence of a depression (and not a maximum as in our expression) close to the origin of the Preisach plane. Concerning the nonlinear parameter β, Fig. 4.63(b) shows that it is clearly not independent of bias stress, contrary to what would be expected from Eqn. (4.95). This means that the proposed distribution function in Eqn. (4.93) is not accurate enough for the description of the effective bistable unit distribution. Actually, the quadratic nonlinear parameter, β, depends almost linearly on the bias stress. Hence, the formula of the proposed distribution function has to be refined in order to reflect this bias stress dependence. Therefore, an extension consisting of a crossed nonanalytical term may be considered:

$$f(\Pi_i, \Pi_c) = f_0 + g\Pi_c + k\,|\Pi_i| + j\Pi_c\,|\Pi_i|. \tag{4.96}$$

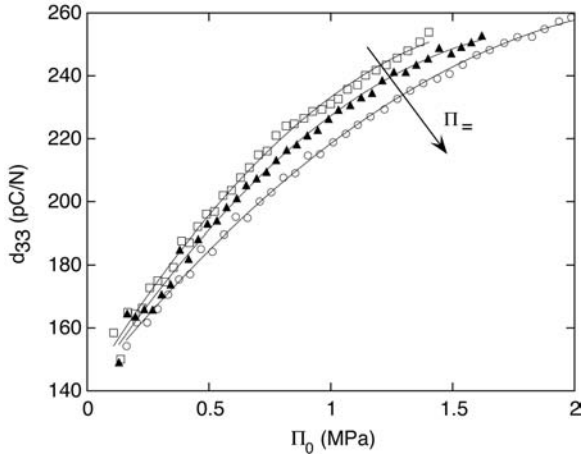

FIGURE 4.62 Dependence of the nonlinearity of the piezoelectric coefficient, d_{33}, on bias stress, $\Pi_{=}$, for a rhombohedral PZT 60/40 ceramic at high stress amplitudes, Π_0. The solid lines were obtained by fitting the experimental points with Eqn. (4.92). The arrow indicates growing values of bias stress in absolute value. (Courtesy Gilles Robert).

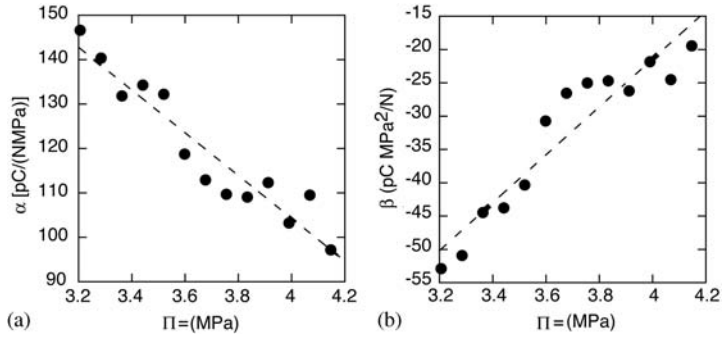

FIGURE 4.63 (a) Bias stress, $\Pi_{=}$, dependence of the nonlinear parameter, α, for the PZT 60/40 in Fig. 4.62. (b) Bias stress, $\Pi_{=}$, dependence of the quadratic nonlinear parameter, β, for the PZT 60/40. The dashed lines represent linear fits to the experimental data points. (Courtesy Gilles Robert).

Its associated piezoelectric stress dependence for $\Pi_{=} > \Pi_0$ is given by:

$$\Delta d_{33} \propto (f_0 + k\Pi_{=})\Pi_0 + \frac{1}{3}(g + j\Pi_{=})\Pi_0^2. \tag{4.97}$$

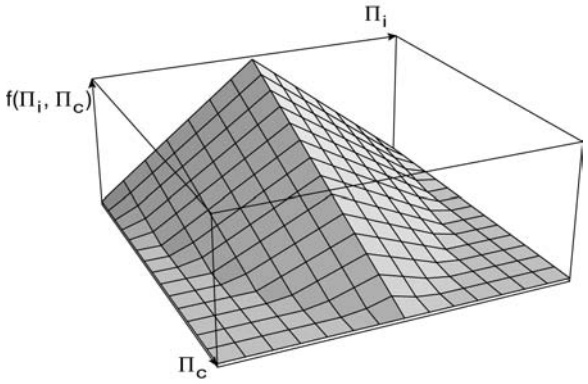

FIGURE 4.64 Schematic view of the corrected roof-like distribution with the extra $\Pi_i - \Pi_c$ coupled term. The maximum of this distribution is situated at the Preisach plane origin. Note that the introduced coupled term causes a curving of both side planes. Intersections of the distribution functions with Π_i and Π_c correspond to $\pm f_0/k$ and $-f_0/g$, respectively. (Courtesy Gilles Robert).

Equation (4.97) correctly accounts for the experimentally observed bias stress dependences of the nonlinear parameters α and β. The crossed term $j\Pi_c\,|\Pi_i|$ expresses accurately the dependence on bias stress of the β coefficient without interfering with the other stress dependences. The proposed distribution function (4.96) can be fully characterized with the data presented in Fig. 4.63. The dependence of α on the bias stress will yield effective f_0 and k, while the dependence of β on bias stress will lead to the effective g and j parameters. The sign of the j coefficient being clearly positive, as may be concluded from Fig. 4.63(b), the distribution function can be plotted considering negative g and k, as shown in Fig. 4.64. This corrected roof-like distribution exhibits an intermediate topography between the original shape (Fig. 4.61) and a conical distribution. Moreover, it is physically more probable as there is no reason for assuming linear traces in the $f(\Pi_i, \Pi_c) = 0$. The maximum of this distribution is situated at the Preisach plane origin. Note that the introduced coupled term causes a curving of both side planes.

The distribution-function parameters were extracted above from the bias stress dependence of the nonlinear piezoelectric coefficient. There is another way to obtain those parameters since, in the Preisach formalism, the loop expression is associated with the distribution function. If fitting the experimental hysteresis with such an expression is possible, it should give the corresponding distribution function parameters. The equation of

the loop corresponding to the corrected roof distribution-function (Eqn. (4.96)) was calculated using Eqns (4.85)–(4.87), resulting in the following expression for the loop:

$$
\begin{aligned}
D = {} & \frac{-k\Pi_0^3}{4} - \frac{j\Pi_0^4}{24} + \left(d_0 + f_0\Pi_0 + k\Pi_=\Pi_0 + \frac{g\Pi_0^2}{4} - \frac{j\Pi_=\Pi_0^2}{4} \right) \Pi + \frac{k\Pi_0}{4}\Pi^2 \\
& + \left(\frac{g}{12} + \frac{j\Pi_=}{12} \right) \Pi^3 - \frac{j}{24}\Pi^4 \\
& \pm \Bigg[\frac{f_0\Pi_0^2}{2} + \frac{k\Pi_=\Pi_0^2}{2} + \frac{g\Pi_0^3}{4} + \frac{j\Pi_=\Pi_0^3}{4} + \left(\frac{k\Pi_0^2}{4} + \frac{j\Pi_0^3}{12} \right) \Pi \\
& - \left(\frac{f_0}{2} + \frac{k\Pi_=}{2} + \frac{g\Pi_0}{4} + \frac{j\Pi_=\Pi_0}{4} \right) \Pi^2 - \left(\frac{k}{4} + \frac{j\Pi_0}{12} \right) \Pi^3 \frac{f_0\Pi_0^2}{2} + \frac{k\Pi_=\Pi_0^2}{2} \\
& + \frac{g\Pi_0^3}{4} + \frac{j\Pi_=\Pi_0^3}{4} \left(\frac{k\Pi_0^2}{4} + \frac{j\Pi_0^3}{12} \right) \Pi - \left(\frac{f_0}{2} + \frac{k\Pi_=}{2} + \frac{g\Pi_0}{4} + \frac{j\Pi_=\Pi_0}{4} \right) \\
& \Pi^2 - \left(\frac{k}{4} + \frac{j\Pi_0}{12} \right) \Pi^3 \Bigg], \qquad (4.98)
\end{aligned}
$$

where $+$ stands for the decreasing and $-$ for the increasing field. A typical hysteresis fitted with this function with the addition of the rate-dependent term (Section 4.4.1.2) is presented in Fig. 4.65. As usual, the hysteresis is plotted taking that the field is equal to $\Pi = \Pi_0 \sin(\omega t)$, whereas the actual driving field is always compressive $\Pi = \Pi_= + \Pi_0 \sin(\omega t)(\Pi_= > \Pi_0)$.

The agreement of the experimental and calculated loop is very good. The same parameters can be used to generate the $d_{33}(\Pi_0)$ for a given bias stress, and, as shown in [144], excellent agreement is again found. Quantitatively, the fitted parameters vary slightly with the stress level, especially at low Π_0, because of the decreasing nonlinear character of the loops. For high enough amplitudes (i.e. $\Pi_0 > 0.8$ MPa), their values were somewhat dispersed but can be considered to be constant, as discussed in detail in [144].

Note that the asymmetrical shape of the loop (observable by the different points at which the loop crosses the axes) is very well described by the model. This asymmetry and related even harmonics in the Fourier expansion of Eqn. (4.98), appear naturally in the model, that is, their description does not require special assumptions as are sometimes made in the literature [59]. As discussed earlier in this section, a true Rayleigh loop, which corresponds to a perfectly random potential, contains only odd harmonics, all of which are out of phase with the driving field. The loop given by Eqn. (4.98) contains 1st, 2nd, 3rd, 4th,6th, 8th, ... harmonics in phase with the

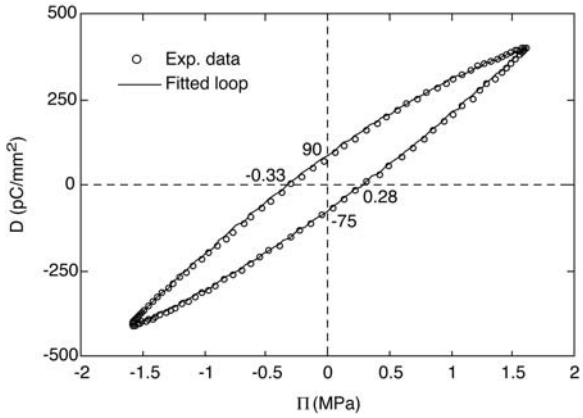

FIGURE 4.65 Example of charge density–pressure hystersis loop for the PZT 60/40 sample, fitted with Eqn. (4.98) and a viscous term. Values of D and Π where the loop intersects the axes are indicated to illustrate asymmetry of the loop. (Courtesy Gilles Robert).

sinusoidal driving field (i.e. $\sin(n\omega t)$ terms), and 1st, 2nd, 3rd, 4th, 5th, 7th, 9th ... harmonics out-of-phase with the field ($\cos(n\omega t)$ terms). Nevertheless, the hysteresis and nonlinearity can be considered as quasi-Rayleigh, since the nonlinearity can be calculated from the hysteresis and vice versa.

4.4.4 REDUCTION OF PIEZOELECTRIC HYSTERESIS IN FERROELECTRIC MATERIALS

Dielectric, ferroelectric, piezoelectric and elastic hystereses are undesired in nearly all applications. The control of electromechanical hystereses is thus of a considerable practical, but also fundamental, interest, because it can be used as a rather sensitive verification tool for theoretical models of hysteresis. The methods for hysteresis reduction include modification of the ferroelectric material with suitable dopants, choice of the driving signal, domain-structure engineering, and control of the response using open or closed loop control.

Hysteresis and nonlinearity in ferroelectric materials can be efficiently reduced by suitable chemical and microstructural modifications of the material. Electromechanical hysteresis in ferroelectrics is mostly caused by the irreversible displacement of domain walls. Thus, an intervention aimed at reducing the hysteresis is usually focused on inhibiting domain-wall motion. Because the domain walls in ferroelectrics are relatively thin (Section 4.2.4), they can be pinned by point (atomic) defects or charged species

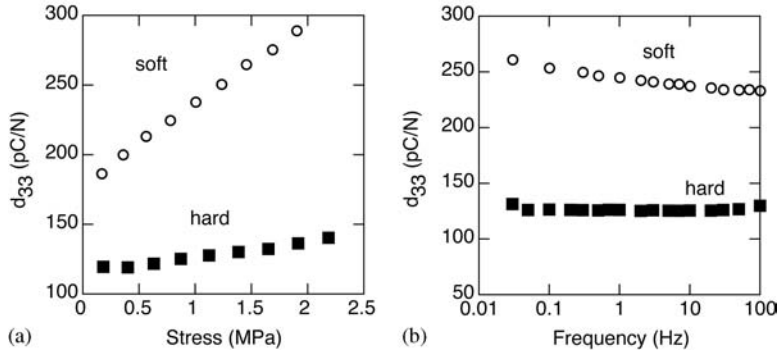

FIGURE 4.66 Left: the pressure, and right: frequency dependence, of d_{33} in a hard $(Pb(Zr_{0.58}Ti_{0.42})_{0.99}Fe_{0.01}O_{3-0.005})$ and a soft $(Pb_{0.99}(Zr_{0.58}Ti_{0.42})_{0.99}Nb_{0.01}O_3)$ ceramic. (Courtesy Maxim Morozov and Grégory Tornare).

such as electrons, which may diffuse into charged domain walls [147–152]. Other pinning mechanisms are associated with the fields created inside grains by electrical [153] and/or elastic dipole defects [154]. Movement of domain walls can also be inhibited by imperfections at the grain boundaries, and dislocations, or could be related to the grain-size-induced internal stresses [39,155,156].

The best-known method for hysteresis control in ferroelectric materials is by chemically modifying a material to render it 'soft' or 'hard'. These terms, borrowed, like the term ferroelectricity itself, from the field of magnetics, have not the same physical origin as their ferromagnetic counterparts. In ferroelectrics, the same base material, PZT, can be made either hard or soft by adding suitable dopants in concentrations on the order of 1%at. In perovskite materials, in general, the donor dopants (e.g. Nb^{+5} on (Zr,Ti) sites) lead to so-called 'soft' materials (high compliance, permittivity and piezoelectric coefficients) accompanied by strong hysteresis and nonlinearity, Fig. 4.66. Acceptor dopants (e.g. Fe^{+3} on (Zr,Ti) sites) lead to 'hard' materials with low values of coefficients but reduced hysteresis, nonlinearity and frequency dispersion, Fig. 4.66. The soft and hard PZT are the best-known examples of how materials engineering may be used in reducing the electromechanical hysteresis [28]. Effects of softening and hardening on ferroelectric hystersis and nonlinearity will be discussed in more detail in Section 4.5. Interestingly, while the origins of hardening are reasonably well understood, the reasons why PZT becomes soft with respect to the pure composition are not well understood, even after more than 50 years of intensive studies of this material [44].

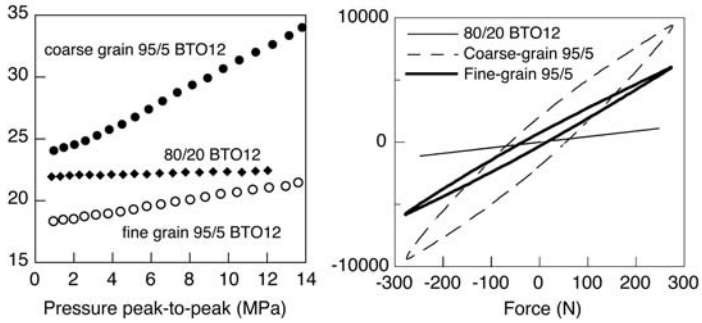

FIGURE 4.67 Left: longitudinal direct piezoelectric d_{33} coefficient for coarse-grained $(Bi_4Ti_3O_{12})_{0.95}(Bi_3TiNbO_9)_{0.05}$ (filled circles), fine-grained $(Bi_4Ti_3O_{12})_{0.95}(Bi_3TiNbO_9)_{0.05}$ (empty circles), and $(Bi_4Ti_3O_{12})_{0.80}(Bi_3TiNbO_9)_{0.20}$ ceramics (diamonds). Right: the charge versus pressure hysteresis for coarse-grained $(Bi_4Ti_3O_{12})_{0.95}(Bi_3TiNbO_9)_{0.05}$ (broken line), fine-grained $(Bi_4Ti_3O_{12})_{0.95}(Bi_3TiNbO_9)_{0.05}$ (thick line), and $(Bi_4Ti_3O_{12})_{0.80}(Bi_3TiNbO_9)_{0.20}$ ceramics (thin line). For figure clarity, the charge for $(Bi_4Ti_3O_{12})_{0.80}(Bi_3TiNbO_9)_{0.20}$ is reduced by a factor of five. (Courtesy Fan Chu).

It is widely accepted that the hardening and hysteresis inhibition in acceptor-doped PZT is related to apparent internal electric fields created by the presence of electrical dipoles. It has been suggested recently that in layer-structure ferroelectrics, the piezoelectric hysteresis may be reduced, Fig. 4.67, by introducing elastic defects into the crystal structures in the form of stacking faults [154].

Hystereses shown in Figs 4.1(b) and 4.2 relate piezoelectrically induced charge and pressure, and strain and electric field. If one chooses other sets of variables, hysteretic response may, in general, change. Figure 4.68(a) shows hysteretic transverse strain (corresponds to d_{31} coefficient) in a soft PZT ceramic as a function of the subswitching field. When the same data are plotted as a function of polarization, which was measured as a function of the field under the same conditions as the strain, one obtains a nonhysteretic response. The strain–field relationship is related to the d coefficient (Eqn. (4.4)), whereas the strain–polarization relationship is related to the g coefficient, Eqn. (B16). Since $d = \varepsilon^{\Pi} g$ (Eqn. (4.B18)), it follows that the hysteresis in the piezoelectric strain–field response (d coefficient) has its origin in processes that contribute to both the strain and the polarization. This is the case, for example, when non-180° domain walls move at weak fields [157]. Their displacement will contribute to both the permittivity and the strain. Under alternating fields, the displacement of 180° walls contributes directly only to the polarization, not to the piezoelectric strain

(except through the poling process). The important assumption here is that in poled ceramics the residual 180° domain walls are too few and do not contribute significantly to the material response. Thus, any hysteresis from the moving non-180° domain walls in the polarization–field relationship will reflect itself in the strain–field relationship, and consequently, the strain–polarization relation will be anhysteretic. The hysteresis at switching fields may be explained by the additional contribution from the switching of 180° domain walls, which are now created and removed periodically during the switching cycle. In this case, the strain–polarization relationship becomes hysteretic, Fig. 4.68(b), since the polarization is controlled by two hysteretic mechanisms, one (180° domain-wall displacement) that contributes only to the polarization and the other (non-180° domain-wall displacement) that affects strain and polarization, whereas the strain is still controlled only by displacement of non-180° walls.

The fact that the strain–polarization relationship is nonhysteretic at weak fields has been exploited in piezoelectric actuators. However, the charge drive is much more complex to realize than the field drive [54], and this way of minimizing the piezoelectric hysteresis is not widely used.

The third approach for hysteresis and nonlinearity control is by engineering the domain structure in such a way that the only domains present are those whose displacement does not contribute to the strain. This method has been recently successfully used in obtaining exceptionally large, hysteresis-free piezoelectric response in complex relaxor–ferroelectric solid solutions (e.g. $Pb(Mn_{1/3}Nb_{2/3})O_3$-$PbTiO_3$, $Pb(Zn_{1/3}Nb_{2/3})O_3$-$PbTiO_3$). It has been recognized recently that many perovskite crystals exhibit enhanced piezoelectric properties when measured along nonpolar directions [104,158–163]. In a tetragonal ferroelectric perovskite, the spontaneous polarization is oriented along the [001] direction, whereas in a rhombohedral crystal it lies along the [111] cubic direction, Fig. 4.4. If certain conditions are satisfied [164], the largest longitudinal piezoelectric response is observed approximately along the [111] cubic direction in tetragonal crystals, and along the [001] pseudocubic direction in rhombohedral crystals, Fig. 4.69(a). The reason for this enhancement of the piezoelectric response along nonpolar directions is that the large shear piezoelectric coefficient contributes to all transverse and longitudinal coefficients when measured along a general, nonpolar direction. The large shear piezoelectric effect is closely related to the presence of phase transitions in the crystal [165]. Since it is usually difficult to cut a monodomain crystal along a nonpolar direction and preserve its monodomain state, crystals are poled after cutting. When a crystal, cut along a nonpolar direction, is poled, it necessarily develops multidomain structures, so-called 'engineered domain states'. In the particular case of the tetragonal and

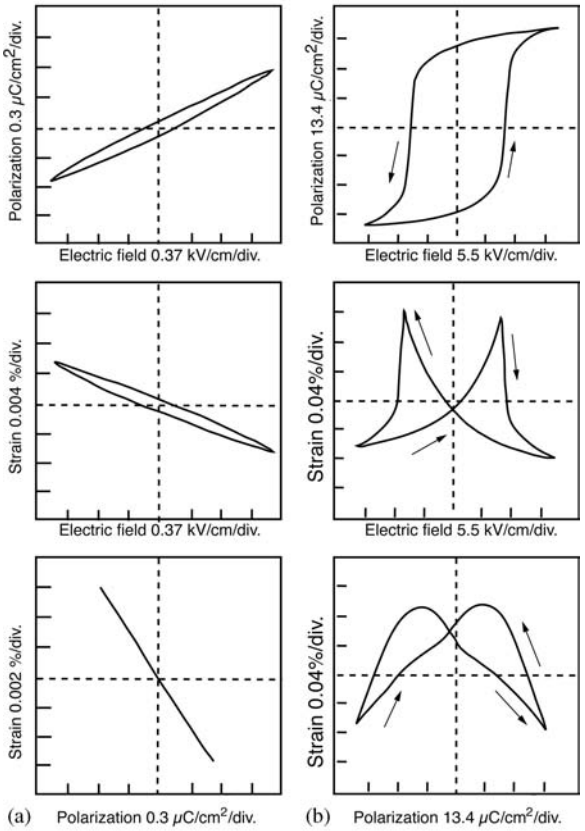

FIGURE 4.68 Polarization–electric field, strain–electric field, and strain–polarization hystereses in a soft PZT ceramic at (a) weak, and (b) switching fields. (From [59] (with kind permissions of L.E. Cross and Susann Brailey of the American Institute of Physics)).

rhombohedral perovskite crystals cut and poled along [111] and [001] pseudocubic axes, the domain structure has the configuration shown in Fig. 4.69(b). The domain walls are ferroelastic but their switching will not contribute to the strain, since, in this configuration, their displacement (reversal) preserves the shape of the crystal. Indeed, the strain–electric field relationship for such a domain structure is anhysteretic, Fig. 4.70, and, in the case of the relaxor–ferroelectrics, the generated strain is several times larger than in classical PZT-based materials.

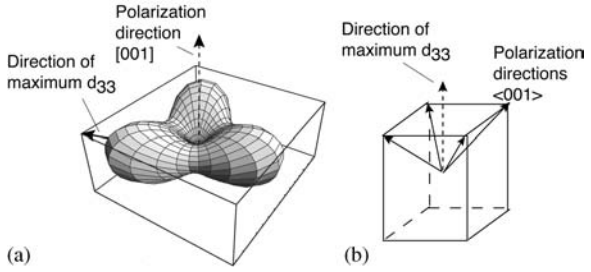

FIGURE 4.69 (a) Dependence of the longitudinal d_{33} piezoelectric coefficient on crystal orientation for a crystal belonging to point group $3m$, such as rhombohedral $Pb(Zn_{1/2}Nb_{2/3})O_3$-$PbTiO_3$. (b) The four domain states in such a crystal poled along pseudocubic [001] direction.

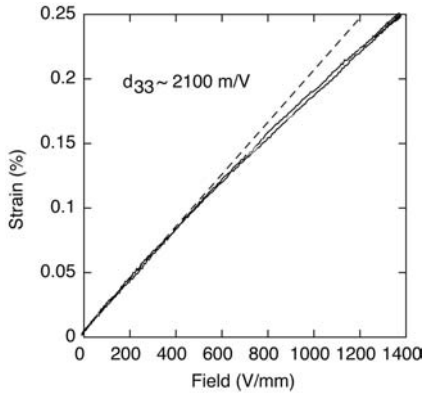

FIGURE 4.70 Nonhysteretic longitudinal piezoelectric strain measured at 0.1 Hz in a 0.67 $Pb(Mg_{1/2}Nb_{2/3})O_3 - 0.33PbTiO_3$ crystal poled along the pseudocubic [001] direction. (Courtesy Matthew Davis).

The hysteresis reduction can also be realized by adjusting the input of the piezoelectric actuator by open (without feedback) or closed (with feedback) loop control of the input signal. In the open-loop case, a model of the actuator's input–output relation is assumed. To obtain the desired linear and nonhysteretic output, the actuator's controller maintains an inverse map of the uncorrected output, as shown schematically in Fig. 4.71.

The new input signal is calculated from the model. Using this approach, an impressive improvement of the actuator output could be obtained by simultaneously controlling creep and hysteresis [166]. It is interesting to note that, since in principle the hysteresis phenomena can

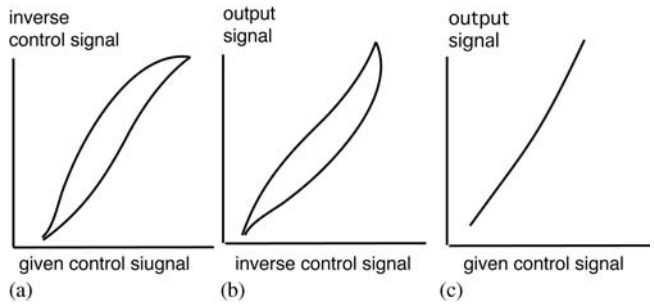

FIGURE 4.71 Inverse control process for piezoelectric actuator after Janocha and Kuhnen [167]: (a) inverse control signal x versus the given control signal y; (b) output signal y versus the inverse control signal x; (c) output signal y versus the given control signal y.

be mathematically reduced to a limited number of classes, a mathematical model can always be found to describe a particular case of the hysteresis. This means that, over a limited range of fields or frequencies, even a physically inaccurate model can give a quantitatively satisfactory description of the actuator output.

The closed-loop systems include one or more sensors that measure the actual output of the actuator. The signal from the sensors is analyzed and input adjusted using an appropriate model to give the desired output. Systems with a feedback circuit give, in general, better control of the actuator output with a smaller error between expected and actual response than systems without feedback. The open-loop systems have an additional disadvantage because they have to be calibrated for aging in the actuator, whereas the closed-loop systems will self-adjust. In both closed- and open-loop cases the number of calculations to achieve an optimal result may be large (sometimes in thousands) [4,5], somewhat limiting these 'smart' systems to operation at a maximum of several hundred Hz to low kHz ranges. A typical application is in piezoelectric scanners for atomic force microscopes [167].

4.5 FERROELECTRIC HYSTERESIS

The ferroelectric (polarization–electric field) hysteresis, Fig. 4.6, is a defining property of ferroelectric materials (Section 4.2.3). In the last fifteen years it has become a subject of intensive studies due to potential applications of ferroelectric thin films in nonvolatile memories [168]. In ferroelectric

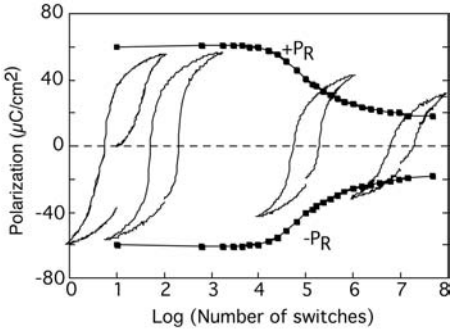

FIGURE 4.72 Illustration of polarization fatigue in a PZT thin film. (Courtesy Enrico L. Colla).

memories the information is stored as positive or negative remanent polarization state. Thus, the most widely studied characteristics of ferroelectric hysteresis were those of interest for this particular application: the value of the switchable polarization (the difference between the positive and negative remanent polarization, $P_R - (-P_R)$), dependence of the coercive field E_c on sample thickness, decrease of remanent or switchable polarization with number of switching cycles (so-called polarization fatigue, Fig. 4.72), polarization imprint, endurance, and retention. The processes that control hysteresis properties and its switching characteristics are still not well understood, partly because the switching involves many mechanisms and depends on the nature of the ferroelectric material itself, types of electrodes used, thickness of the ferroelectric, temperature, field profile, number of field cycles, and many other parameters [168–171]. For example, fatigue characteristics of ferroelectric films of PZT can be greatly improved by choosing a different type of electrode [172].

The very process of switching has been for many years considered mostly in the framework of the Kolgomorov–Avrami–Ishibashi (KAI) model [173,174]. In this model, the switching is controlled by the nucleation and growth of reversed domains, Fig. 4.73. The model has been experimentally successfully verified in single crystals. Only recently [26] has it been shown that this model cannot explain switching in ferroelectric thin films ($< 1\mu$m thick), where it was found that the switching is controlled primarily by the nucleation of reversed domains. The difference between the two cases is that in the KAI model the switching current as a function of time can be well fitted with a function that develops within one or two time decades; in thin films, the switching current evolves over a much broader time interval [175], basically indicating independent switching of many

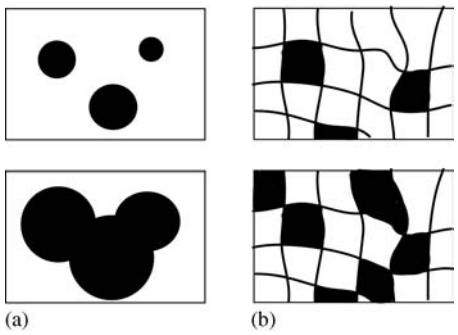

FIGURE 4.73 Schematic representation of switching process: (a) Kolgomorov–Avrami–Ishibashi model of nucleation and sideways motion of domains with oppositely oriented polarization, and (b) switching controlled by nucleation at many regions with broadly dispersed nucleation probabilities. (After [26]).

regions of the film, with different nucleation probabilities [26], Fig. 4.73(b). Interestingly, the latter mechanism reduces to KAI at low temperatures [176]. It thus appears that in polycrystalline materials the hystereses at both switching and subswitching fields (see Section 4.4.1) are controlled by processes that evolve over extremely broad time scales. Even though the physical origins of the weak field (e.g. Rayleigh-like) and switching hystereses are different, these results suggest an important role of disorder in the origins of the hysteresis in ferroelectric materials.

We shall illustrate on a few selected samples how the study of ferroelectric hysteresis (under both switching and subswitching fields) can be an important source of information on the various processes and conditions present in a ferroelectric material.

4.5.1 TILTED HYSTERESIS

The tilt of the loops, Fig. 4.74, can be explained by the presence of a dielectric layer on the top of the ferroelectric [177,178]. This layer, which has a lower dielectric constant than the ferroelectric material, separates the bound charges that are due to the ferroelectric polarization from the compensating charges on the electrodes. Because of the incompletely compensated polarization charge, a field, called the depolarizing field, will develop across the ferroelectric, even if the top and bottom electrodes are shorted.

The depolarizing field is given by $E_d = -Pd/(\varepsilon_d t)$ where d and ε_d are the thickness and permittivity of the dielectric layer, and P and t are the polarization and thickness of the ferroelectric layer [177]. It can be shown

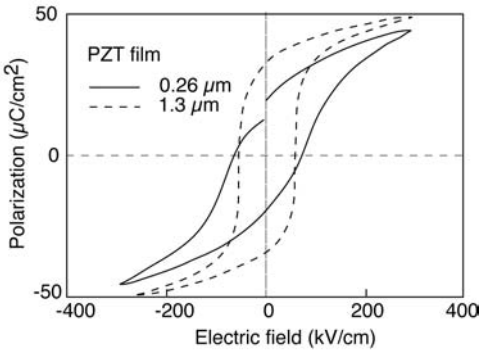

FIGURE 4.74 Comparison of ferroelectric hysteresis loops for two (111)-oriented sol-gel $Pb(Zr_{0.45}Ti_{0.55})O_3$ thin films with different thicknesses. The tilted loop (solid line) is observed in the thinner film that contains a dielectric pyrochlore layer. (Film data: courtesy of D.V. Taylor).

that for $d << t$, the total field E_f across the ferroelectric is given by [177–180]:

$$E_f = E - \frac{Pd}{\varepsilon_d t}, \tag{4.99}$$

where E is the applied field. The tilt of the loop, defined here as the slope of the measured loop at coercive field E_c, may be found from (4.99) as:

$$\left(\frac{\partial E}{\partial P}\right)_{E_C} - \left(\frac{\partial E_f}{\partial P}\right)_{E_C} = \frac{d}{\varepsilon_d t}. \tag{4.100}$$

Since, for the perfectly square loop of the ferroelectric layer, $(\partial P/\partial E_f)_{E_C} \rightarrow \infty$, it follows that the slope of the measured loop $(\partial E/\partial P)_{E_C}$ is equal to $d/(\varepsilon_d t)$, i.e. the loop becomes more tilted as the d/t ratio increases. The tilt of the loops can thus be taken as an indication of the presence of a low dielectric-constant ('passive') layer in series with the ferroelectric.

4.5.2 HYSTERESIS AND NONLINEARITY IN HARD AND SOFT FERROELECTRICS

As already briefly discussed in Section 4.4.4, the concepts of hardening and softening in ferroelectric materials are not well understood. On a descriptive level, the hard materials possess lower susceptibilities (d, ε, s), conductivity and nonlinearity, while the opposite is the case for the soft compositions [28]. Hardening and softening may be achieved by doping

the same base materials, e.g. PZT, by suitable dopants. As illustrated in Fig. 4.75, it is possible to continuously change the character of the material from hard to soft by changing the concentration and nature of the dopants. In practice, commercial soft and hard materials are not produced from the same base composition, so their differences cannot be attributed solely to the presence of the dopants, but also to the crystal structure, value of the transition temperature, and other parameters.

When a ferroelectric is doped with an acceptor dopant (a lower valence than the host atom, e.g. Fe^{+3} or Fe^{+2} on Ti^{+4} sites in PZT or $BaTiO_3$), a positively charged oxygen vacancy, V_O^{+2}, is created, which neutralizes the effective negative charge introduced by the acceptor dopant, Fe_{Ti}^{-1} or Fe_{Ti}^{-2}, Fig. 4.76(a). The number of oxygen vacancies depends on the acceptor charge. In soft materials, replacement of Ti^{+4} with donors, such as Nb^{+5}, brings in additional electrons or creates lead vacancies, V_{Pb}^{-2}, as the charge-compensating defect. The electric dipoles are thus created between the aliovalent substition and the associated vacancy [153,181]. Because of the difference in size among the host and atoms and dopants on one side and oxygen anions and empty oxygen sites on the other side, these dipoles will at the same time behave as elastic dipoles. For simplicity, in the rest of the text we shall mainly be concerned with the electrical nature of the defects.

At present, the most widely accepted explanation of the hardening mechanism in ferroelectric ceramics is the following [153,181]. In the cubic phase, the dipoles in a ceramic are randomly oriented. In a regular perovskite, in which oxygen octahedra are not tilted, the dipoles within an individual grain may lie along any one of the six equivalent ⟨100⟩ directions that are defined by the positions of Ti and O ions (see Fig. 4.4). When the sample is cooled through the paralelectric–ferroelectric phase transition, the onset of spontaneous polarization and strain will tend to reorient defect dipoles along the polarization direction, Fig. 4.77, in order to reduce their potential energy.[2] The polarization direction on each side of a domain wall is fixed by the presence of defects, and the walls become more difficult to move [1,153]. Thus the ceramic becomes hard for both the large (global switching) and weak (subswitching) fields.

Preferential orientation of the defect dipoles is seen experimentally as the presence of an effective internal bias field in the sample. If the ceramic is polarized at a high temperature (but below T_c), and by fields sufficiently high to reorient dipoles and domains, the whole hysteresis loop, when measured by an alternating external field applied along the

[2] It is arbitrarily chosen that the dipoles are oriented in the same sense as the ferroelectric polarization of the neighboring unit cells.

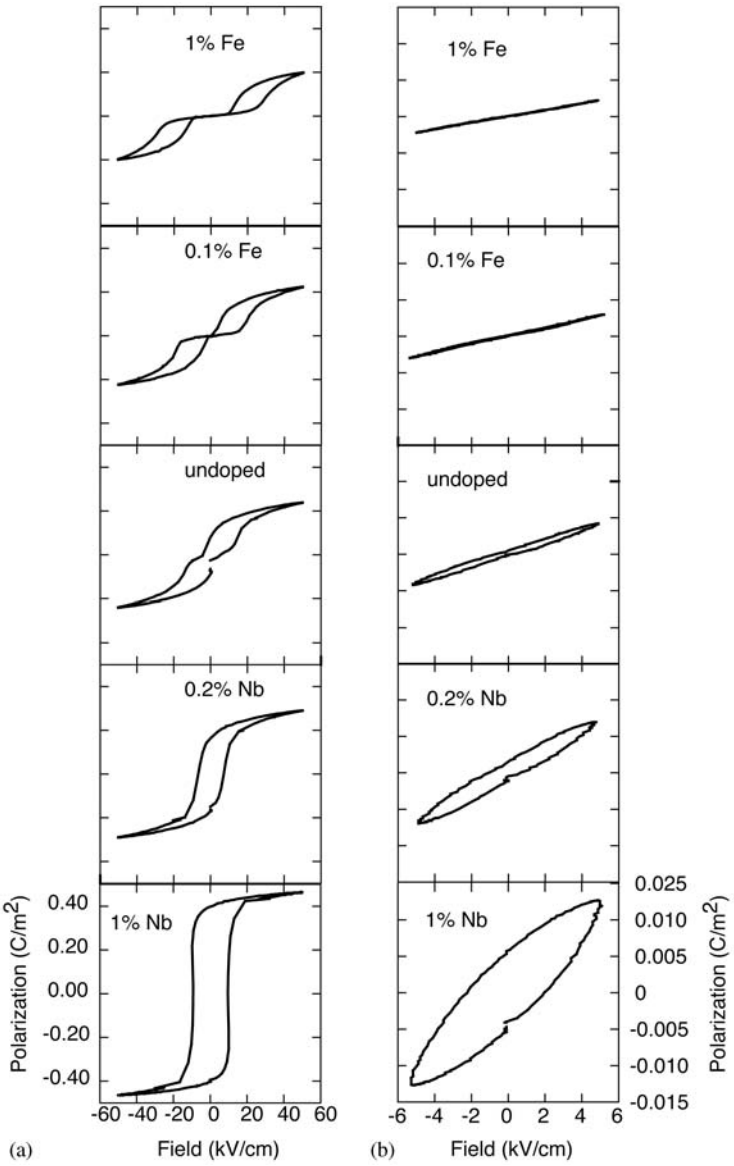

FIGURE 4.75 Polarization–electric field loops at (a) switching, and (b) subswitching fields, for rhombohedral $Pb(Zr_{0.58}Ti_{0.42})O_3$ ceramics with different concentrations of Fe and Nb dopants. Hardness decreases and softness of ceramics increases from the top to the bottom. Vertical scales for all loops are the same and are indicated for the sample with highest Nb concentration. (Courtesy Maxim Morozov).

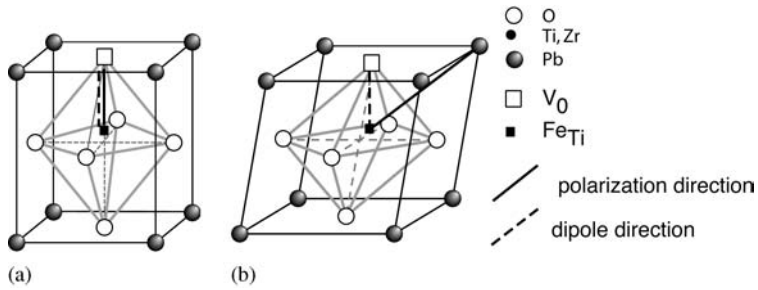

FIGURE 4.76 Illustration of defect dipoles created by an acceptor dopant in (a) tetragonal, and (b) rhombohedral unit cell of a perovskite crystal.

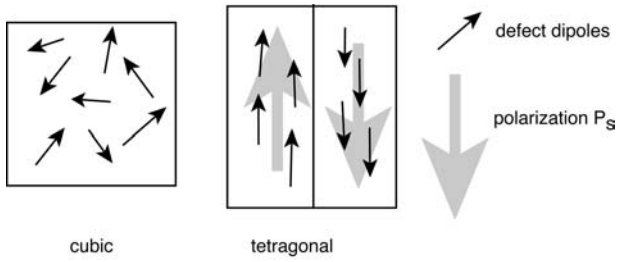

FIGURE 4.77 Schematic representation of defect dipoles in the paraelectric cubic and the ferroelectric tetragonal phases of a perovskite crystal. For simplicity only 180° walls are indicated. Defect dipoles are presented by small black arrows, and polarization within domains with large gray arrows. The defect dipoles will align with polarization, and the sense of orientation is taken arbitrarily to be the same as that of polarization within the domain.

polar axis, appears to be shifted along the field axis, Fig. 4.78 (left). This shift reveals the presence of an apparent internal (bias) field that originates from the alignment of the dipoles (or another mechanism, see later in this section) along the macroscopic polarization direction. In unpoled ceramics, orientation of dipoles along each side of every domain wall will lead to so-called constricted or pinched loops, Fig. 4.78 (right). The pinching appears because some domains contain dipoles oriented along the positive and some along the negative directions of the measuring field; one can think of a pinched loop to be composed of two partial loops, one with a negative and the other with a positive internal field. Both biased and pinched loops have been studied in detail in single crystals of triglycine sulphate (TGS) doped with alanine, where microscopic mechanisms of the pinching are now rather well understood [1].

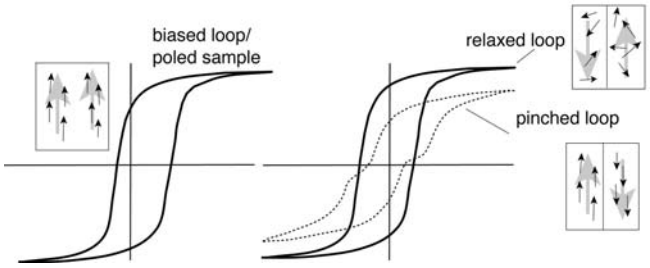

FIGURE 4.78 Hysteresis loops in hard rhombohedral PZT ceramics. Left: a loop with internal bias; right: symmetrical field relaxed loop and a pinched loop in aged material. After [154]. Arrows are identified in Fig. 4.77.

Pinched loops can be relaxed in two ways: (i) by cycling the ceramic hundreds of times with switching fields, Fig. 4.78 (right), or (ii) by heating the sample over the transition temperature where dipoles will necessarily be disordered, and then quenching the sample to room temperature, Fig. 4.79. After quenching, the aging process starts immediately and after some time the loop becomes pinched again. The dipole reorientation process evolves over many time decades following logarithmic law [153].

The dynamics of dipole reorientation in Fe-doped perovskites has been studied by electron paramagnetic resonance (EPR) [150–152] giving direct evidence that they reorient under external fields. Ordering of dipoles within one domain during aging is not seen by this technique, since it takes signals from all dipoles from a very large number of randomly oriented grains and domains where, on average, the dipoles are oriented randomly along all permissible crystallographic directions. The evidence of microscopic ordering is, however, seen in the loop pinching, which is a macroscopic property.

It is important to note that alignment of defect dipoles is not the only mechanism that can cause hardening and apparent internal fields. Diffusion of defects into charged or strained domain walls can lead to domain-wall pinning and hardening while a concentration of defects at grain boundaries can lead to internal fields and pinched loops [147,149,153,182,183]. Recently, some authors have directly questioned the possibility that the small amounts of dopants used (typically, on the level of one per cent) could in fact explain the large coercive fields and the aging process in hard materials [184]. However, the direct evidence of dipole reorientation presented by EPR experiments clearly shows that reorientation of dipoles does occur under external fields. On the other hand, the macroscopically observed loop pinching and depinching give a clear indication

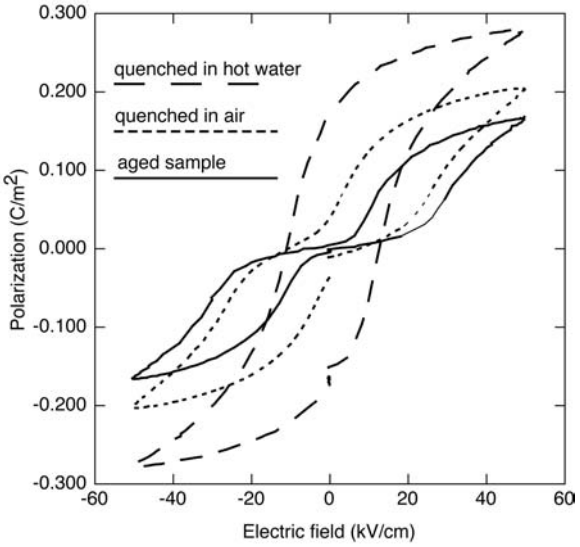

FIGURE 4.79 Aged and thermally relaxed hysteresis loops of $Pb(Zr_{0.58}Ti_{0.42})O_3$ with one per cent Fe. Different degrees of thermal relaxation are achieved by quenching samples from above T_c into media with different thermal conductivities. Measurements were made once the samples reached room temperature. (Courtesy Maxim Morozov).

that some kind of order–disorder process takes place in hard materials and that it is related to the hardening mechanisms. We shall thus base the rest of the discussion on these experimental facts, without necessarily invoking a specific microscopic mechanism of hardening.

Lets us first see how a pinched loop can be described by using the Preisach approach [185]. We assume that there are two populations of domain walls, one in which the polarization is fixed by some type of defect along the negative and the other along the positive direction of the applied field. This is equivalent to assuming the presence of two well-defined populations of Preiscah units, one dispersed around a negative and the other around a positive bias field, E_i, in the Preisach plane. If, for simplicity, we also assume that the Preisach distribution is constant as a function of the coercive field E_c up to some arbitrary value E^*, and becomes zero above this value, we can easily construct a polynomial of, for example, fourth order that gives the Preisach distribution $f(E_i, E_c)$ shown in Fig. 4.80(a). Following the procedure in Section 4.4.3, the associated hysteresis can be derived. As expected, and shown in Fig. 4.80(b), this type of double-peak

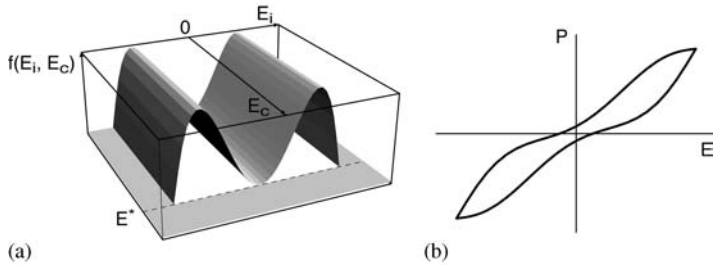

FIGURE 4.80 (a) Plot of the proposed polynomial Preisach distribution function for a ferroelectric material containing defect dipoles oriented along two preferred directions. (b) The hysteresis loop calculated from the Preisach distribution in (a). (Courtesy Gilles Robert).

distribution exhibits pinched hysteresis. Clearly, one can assume a physically more realistic Preisach distribution (e.g. double Gaussian) or derive $f(E_i, E_c)$ from the hysteresis-loop shapes.

Another approach to describe hard materials is to assume an appropriate energy profile for the domain walls. Robels and Arlt [181] have proposed a V-shaped potential that is valid for an infinitely thin wall, where the force exerted by aligned dipoles on both sides of the domain wall does not change with the distance from the wall, Fig. 4.81(a) except by abruptly changing its sign at the wall position. When a wall changes its position by Δl, defects in this region do not reorient immediately, and thus the free energy of a wall increases by $\Delta G = \Delta n(t) A \left|\Delta l\right| \Delta W_e$, where A is the surface of the wall, $\Delta n(t)$ is the concentration of dipoles in the shifted region, and ΔW_e is the energy associated with a defect oriented against the polarization (estimated to be 30 meV). By considering only displacements of domain walls that are smaller than the domain-wall thickness, the clamping force F_{cl} exerted on domain walls by the surrounding aligned dipoles can be modified in the wall region by a force that linearly changes with the wall displacement. In other words, the nonanalitical V-potential is replaced by a parabolic potential so that $F_{\mathrm{cl}} \propto n(t)\Delta l$, Fig. 4.81(b). As the sample ages, $n(t)$ increases as more dipoles become aligned with polarization on each side of the domain wall. The corresponding clamping-force constant then changes with time in proportion to the number of aligned defects, $k_{\mathrm{cl}} \propto n(t)$, which is equivalent to changing the slope of the potential. An additional force on domain walls in Robels and Arlt's model comes from a restoring force on the moving domain walls, which is present even in the absence of defects (Section 4.3.1). The energy potential associated with this restoring force is also assumed to be parabolic, with a force constant

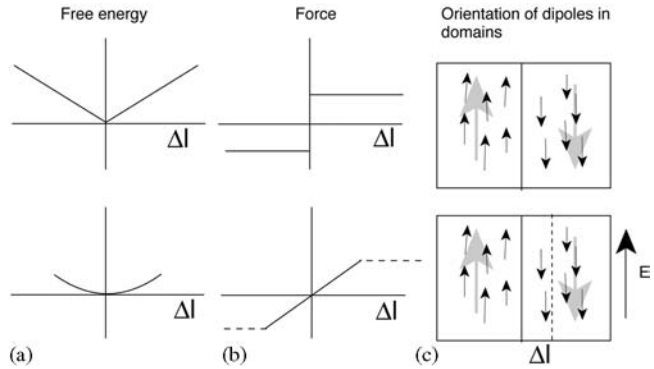

FIGURE 4.81 (a) Free energy, and (b) corresponding force for 'V' (top) and parabolic (bottom) potentials. In (c) repartition of defect dipoles (small black arrows) and polarization (large gray arrows) in the absence (top) and upon application (bottom) of an external field. Δl designates displacement of the wall. In the displaced region, the dipoles and polarization are misaligned. (After [187]).

k. The total force constant in this model is therefore $k_{\text{tot}} = k + k_{\text{cl}}(t)$ and it evolves with time as $n(t)$, leading to a steeper potential, i.e. the domain walls become more difficult to move and the material becomes harder, as the sample ages. Note that within this model the energy potential between aged and relaxed (disordered) ceramics differs only quantitatively, i.e. in the number of aligned dipoles.

While qualitatively explaining the aging process and hardening with time, the model does not take into account nonlinearity of the polarization or hysteresis that are observed at subswitching fields. The nonlinear effects can be included [186] by keeping the original V-shape potential that describes the movement of domain walls beyond the wall region. To account for the linear, reversible movement of the domain walls in the wall region, the sharp V-potential is smeared[3] at the origin, Fig. 4.82(a). As in the original model, an additional restoring force characterized by the force constant k and a parabolic potential may be added to describe the movement of the walls when the concentration of ordered dipoles approaches zero. Finally, the free energy of the wall is modified by the presence of an external field E. If a simple one-dimensional case is considered, the energy change per unit domain-wall area caused by displacement of a domain wall by a distance x (equal to Δl in Robles and Arlt's model) is given by $-2P_S Ex$. In this very simplified case, the free energy of a domain wall in a

[3]Smearing of Robels and Arlt's V-potential was proposed by A.K. Tagantsev.

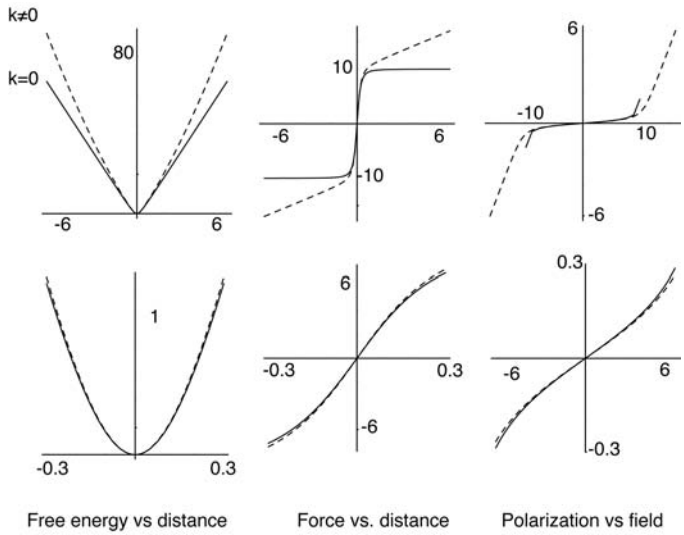

FIGURE 4.82 Modified V-potential for a domain wall, the force acting on the wall, and the polarization caused by the domain-wall displacement in a hard material. Top: at a large distance from the domain-wall position at rest. Bottom: in the smeared region. The numbers (whose values are chosen arbitrarily) on the axes are included to indicate order of magnitude and enable comparison of effects at large distances and in the smeared region. Dashed lines indicate the case $k \neq 0$ in Eqn. (4.101).

very hard material is given by:

$$\Delta G = \frac{1}{2}kx^2 + k_{\mathrm{cl}}\left(\sqrt{x^2 + x_0^2} - x_0\right) - 2P_S E x, \tag{4.101}$$

where k describes the steepness of the additional harmonic potential and can be neglected for small displacements; k_{cl} describes the steepness of the modified V potential, and x_0 defines the width of the smearing region of the V potential around $x = 0$. As in the original model, k_{cl} can be related to the time-dependent concentration of the aligned defects. The equilibrium position of the wall is obtained from the stability condition:

$$\partial \Delta G / \partial x = 0 \tag{4.102}$$

Since the polarization change is proportional to the domain-wall displacement [47], $\Delta P \propto P_s x$, the solution of Eqn. (4.102) gives both $x(E)$ and $\Delta P(E) \propto x(E)$. In this model, the contribution of the dipolar reorientation

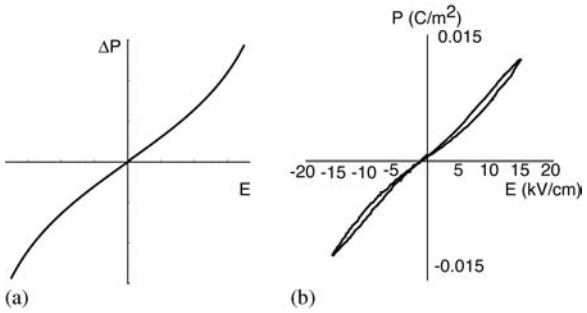

FIGURE 4.83 (a) Solution of Eqn. (4.102) in the smeared region and its comparison with (b), an actual polarization–field curve measured in a hard PZT ceramic. (Experimental data courtesy of Maxim Morozov).

to the polarization change is neglected. Equation (4.102) can be solved analytically [186], and one of its solutions is shown in Fig. 4.83, together with an experimental polarization of a hard rhombohedral PZT sample measured at a subswitching field.

The nonhysteretic, nonlinear behavior predicted by Eqn. (4.101) and shown in Fig. 4.83(a), is only an approximation. Even in very hard ceramics, a small pinched hysteresis is evident below macroscopical subswitching fields, Fig. 4.83(b). In addition, a strong double hysteresis occurs at very large (global switching) fields, Fig. 4.75. The hysteresis at subswitching fields may be introduced in the model by assuming that the V-potential is not smooth but contains local minima, Fig. 4.84(a), that may be due to the distribution of coercive and internal fields associated with inhomogeneous distribution and imperfect alignment of defect centers. The strong hysteresis that appears at very large fields is due to global ferroelectric switching of the sample, Fig. 4.85. The global switching is still controlled by the presence of the internal fields as seen from the comparison of the maximum polarization achieved in a double loop with remanent polarization achieved in thermally relaxed loops, Fig. 4.79. Polarization in the aged double loop is half of that in the thermally relaxed loop, suggesting that only part of the aged sample switches in each field direction.

The strong double loop obtained under switching conditions can be formally represented by deep local minima on each side of the modified V-potential, as shown in Fig. 4.85. This presentation is formally similar to the description of the double ferroelectric loops sometimes observed in ferroelectric materials above the paraelectric phase-transition temperature [14] or in antiferroelectric materials [1].

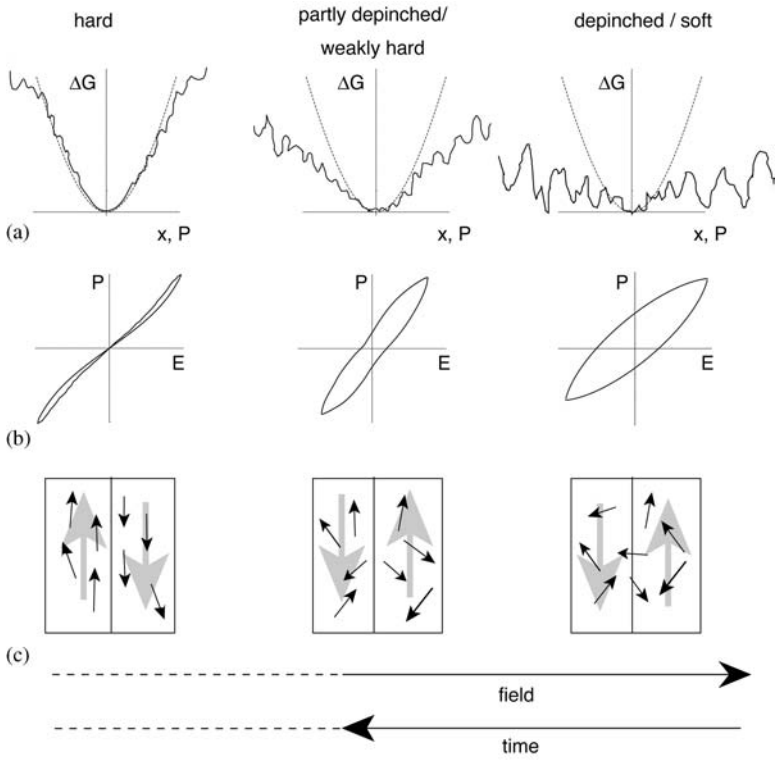

FIGURE 4.84 Potential of a domain wall for (left) a very hard, (middle) a partially depinched or weakly hard material, and (right) a relaxed field, thermally relaxed field or soft sample. V-potential in the smeared region with introduced roughness is given by the dashed line. (a) Energy profile of the domain wall; (b) polarization–field hysteresis; (c) schematic representation of ordering of defect centers within domains. Compare with Figs 4.82 and 4.83 and with Fig. 4.85 for switching fields. Experiments have shown transition from (middle) to (right) after relaxing with the field, and from (right) to (middle) after aging. Compare with Fig. 4.86.

In very hard materials the pinched hysteresis persists up to high fields. In some cases, the loop cannot be completely relaxed even after a large number of field cycles (> 300); however, the depinching can always be achieved by thermal relaxation. In less hard materials, only weak pinching is sometimes observed, Fig. 4.84. The corresponding energy profile can be qualitatively described by decreasing the steepness of the disordered V-potential, Fig. 4.84. Such weakly pinched hystereses can be easily

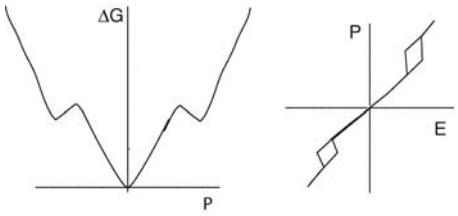

FIGURE 4.85 Illustration of the free-energy profile and associated hysteresis for an unpoled hard ferroelectric, such as PZT, with internal bias field. In contrast to Figs 4.81, 4.82, and 4.84, only global switching of the ferroelectric is considered and any local roughness of the potential can be neglected on this scale. Only formally, this description is analogous to that of double loops in ferroelectrics above the ferroelectric–paraelectric phase-transition temperature or in antiferroelectric materials. See [1,14].

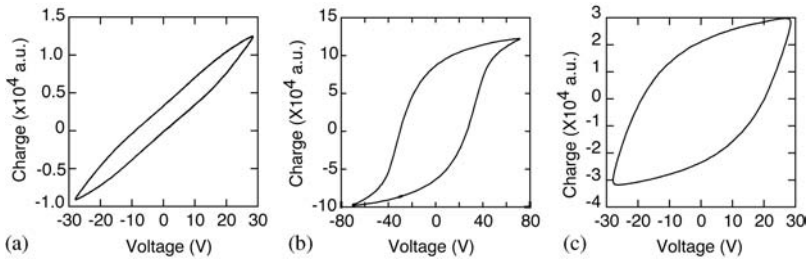

FIGURE 4.86 (a) Polarization–field hysteresis measured in a well-aged PZT thick film. (b) Switching hysteresis used to relax film in (a). (c) The polarization–field hysteresis measured under the same conditions as in (a) after field relaxation. (Courtesy Juliette Müller).

relaxed by strong fields, as illustrated in Fig. 4.86. After field relaxation, the energy profile of the domain wall should resemble the one in Fig. 4.38, typical for materials with Rayleigh-type behavior, and is shown in Fig. 4.84(c), together with the relaxed subswitching loop. When the field is removed, the dipoles will start realigning, slowly building up the internal field. Ordering of defects restores the sharpness of the V-potential, and after a sufficient aging time, the pinched hysteresis appears. The time and field thus have opposite effects on the energy profile of domain walls, as illustrated schematically in Fig. 4.84.

It has been indicated in Section 4.4.1 that the Rayleigh behavior in a material is closely linked to disorder. Macroscopic, experimentally observable characteristics of a disordered system are hysteresis and nonlinearity, which in Rayleigh-like systems are closely linked. In an ideal Rayleigh

system, every nonlinear movement is hysteretic, as seen by the fact that the phase angle of *all* harmonics is exactly out of phase with respect to the driving field ($\delta_n = 90°$). This property of Rayleigh systems offers a convenient, although not absolute and rigorous, way to investigate evolution of the free-energy profile suggested by the qualitative model discussed above. Before presenting experimental results, let us first examine what are the expected properties of the polarization response described by Eqn. (4.101). It is possible, just from the form of the V-potential and polarization in Fig. 4.82, to state the following: (i) for a sinusoidal driving field, $\Delta P(t)$ will be a function with a half-wave symmetry (Section 4.4.1) [123]. That means that, ideally, only odd harmonics will be present in expansion of $\Delta P(t)$ into Fourier series; (ii) since in the absence of the field the free energy profile (4.101) is symmetrical with the distance x, and since it has no local minima, and rate-dependent processes are neglected, the fundamental and all higher harmonics of the polarization will, ideally, exhibit a zero phase angle with respect to the driving field (Section 4.5.1, Eqns (4.62)–(4.63)). Since, as discussed above, the real potential cannot be ideally smooth, the phase angle cannot be exactly zero. However, as long as the nonlinear component coming from the displacement of the walls in the dominating V-potential is much stronger than the nonlinearity due to small irreversible displacements, the phase angle of the higher harmonics should be close to zero (see Eqns (4.62)–(4.63)). These properties and their analog for a Rayleigh-like system are experimentally verifiable macroscopic properties.

We next look at the field and time dependence of the phase angle of the third harmonic, δ_3, for the polarization response of a tetraganal PZT thick film, in which the hardening is induced by a small amount of Fe impurities present in the starting powders used to prepare the samples. Thus, the material is not too hard. An aged sample should exhibit $\delta_3 \approx 0°$, which, according to the above analysis, should ideally correspond to a hard material with aligned defects. Figure 4.87(a) shows $\delta_3(E)$ for such a sample in a well-aged state. The corresponding hysteresis is illustrated in Fig. 4.86(a). The hysteresis is slightly pinched, indicating a small number of ordered dipoles, which explains the nonzero value of $\delta_3(E)$.

After the sample is cycled with a strong field, Fig. 4.86(b), the weak-field hysteresis becomes depinched, Fig. 4.86(c), and $\delta_3(E)$ becomes close to 90°, Fig 4.87(b), in agreement with disordering of the pinning centers and removal of the internal bias field. The effect of aging is shown in Fig. 4.87(c) and (d), where it is seen that $\delta_3(E)$ slowly decreases with time toward zero. One should note that in all cases shown in Fig. 4.87, the measuring subswitching field may itself affect alignment of the defect

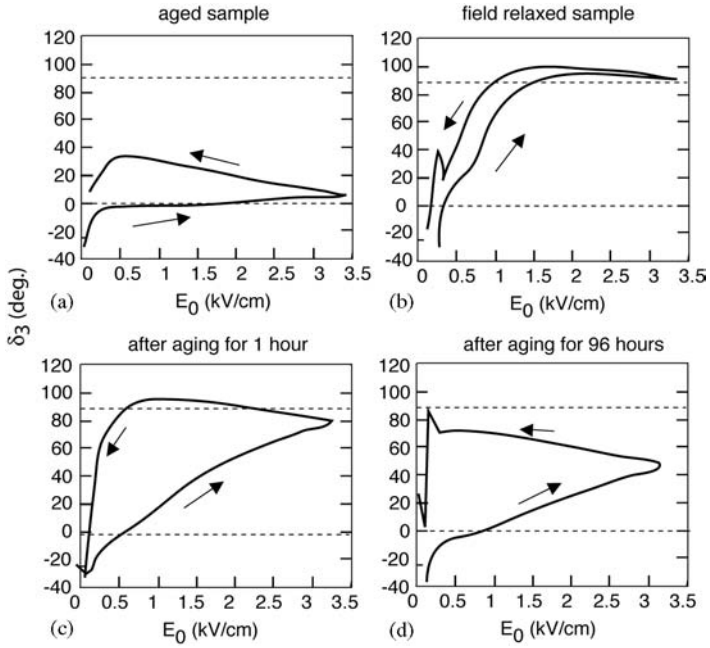

FIGURE 4.87 The phase angle of the third harmonic of polarization, δ_3, for a 15μm thick screen-printed PZT film: (a) well-aged film; (b) immediately after relaxation with a switching field; (c) after aging the relaxed film for one hour; (d) after aging the relaxed film for four days. Arrows show the direction (increasing or decreasing) of the field amplitude. (Courtesy Juliette Müller).

centers. This is clearly shown in Fig. 4.88 that displays evolution of $\delta_3(E)$ in a ceramic sample during three field cycles, possibly suggesting that the roughness of the V-potential changes during measurements and with time. The competing effects of time and field *during* the measurements should thus be taken into account when interpreting the data. One can conclude that the main points of the very qualitative model presented above for hard materials are in good agreement with the results of this simple experiment.

The mechanisms of softening of the elastic, dielectric and piezoelectric properties in soft materials are presently not understood, even on a simple phenomenological level. Soft materials also contain electric and elastic dipoles, consisting of, for example, charged V_{Pb}-Nb_{Ti} pairs. Depending on the concentration of the donor dopant, the charge balance can also be achieved with free electrons [28]. Considering presumably weak mobility

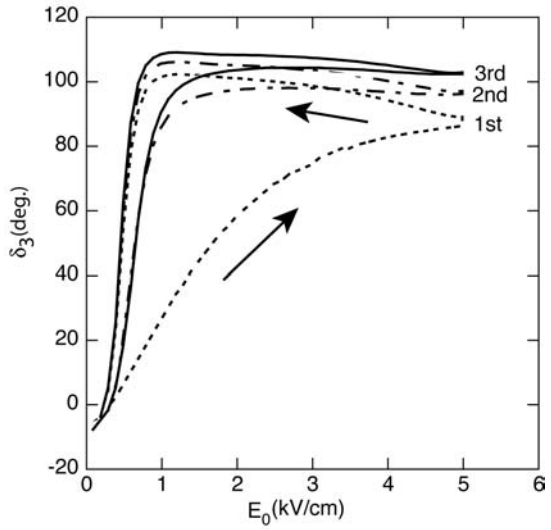

FIGURE 4.88 Effect of field cycling on the phase angle of the third harmonic polarization response, $\delta_3(E_0)$, in a 0.58/0.42 PZT ceramic doped with 0.1 per cent Fe. (Courtesy Maxim Morozov).

of heavy Pb ions, it is perhaps understandable why V_{Pb}-Nb_{Ti} defects in soft materials cannot align with polarization as easily as Fe_{Ti}-V_O pairs. However, why the presence of V_{Pb}-Nb_{Ti} dipoles should lead to softening of the properties with respect to a pure material is presently not understood. It is not unlikely that the softening may be caused by processes unrelated to the presence of defect dipoles. The hysteresis in soft materials can be successfully described at all subswitching fields by the quasi-Rayleigh relations, as discussed in detail in Section 4.4.

APPENDIX A. TENSOR NOTATION

In Voigt convention, a pair of indices $ii = 11, 22, 33$ is replaced with the single index $m = 1, 2, 3$, respectively, and the mixed pairs of indices (which represent shear components of strain and stress tensors) $ij = 23$ or 32, 13 or 31, 12 or 21 are written as $m = 4, 5, 6$, respectively. In all tensor relationships, summation over repeated indices is assumed. Tensor indices are defined with respect to an orthogonal coordinate system, so that, for example, P_3 represents the component of electric polarization along the z-direction of an (x, y, z) orthogonal coordinate system. Axes of the

coordinate system are oriented either along crystallographic axes of a crystal, or with the z-axis along the polarization direction of a ceramic.

APPENDIX B. THERMODYNAMIC DERIVATION OF THE PIEZOELECTRIC EFFECT AND PIEZOELECTRIC CONSTITUTIVE EQUATIONS

The coupling between the thermal, elastic and electrical parameters of a material can be introduced formally using a thermodynamic approach. The results are equations of state that give relations between material parameters measured under different experimental conditions. These relations are essential for modeling and understanding the response of piezoelectric and pyroelectric devices. The approach is outlined below and a more detailed discussion can be found in [1,11,14].

It follows from the first and second law of thermodynamics that the reversible change $\mathrm{d}U$ in the internal energy U of an elastic dielectric that is subjected to a small change of strain $\mathrm{d}x$, electric displacement $\mathrm{d}D$, and entropy $\mathrm{d}S$, is given by:

$$\mathrm{d}U = T\mathrm{d}S + \Pi_{ij}\mathrm{d}x_{ij} + E_i\mathrm{d}D_i, \tag{B.1}$$

where T is the temperature of the material. Since, in most experimental situations, one works under isothermal conditions, and uses electric field and stress as independent variables, it is useful to change the set of independent variables from (S, x, D) to (T, Π, E). To change the independent variables from the original set to the other we perform a Legendre transformation of U by adding expression $-TS - \Pi_x - ED$ to U. The resulting free-energy function:

$$G = U - TS - \Pi_{ij}x_{ij} - E_iD_i \tag{B.2}$$

is known as the Gibbs free energy. The differential of G gives, together with (4.16):

$$\mathrm{d}G = -S\mathrm{d}T - x_{ij}\mathrm{d}\Pi_{ij} - D_i\mathrm{d}E_i. \tag{B.3}$$

From Eqn. (B.3) one obtains:

$$S = -\left(\frac{\partial G}{\partial T}\right)_{\Pi,E}, x_{ij} = -\left(\frac{\partial G}{\partial \Pi_{ij}}\right)_{T,E}, D_i = -\left(\frac{\partial G}{\partial E_i}\right)_{T,\Pi} \tag{B.4}$$

where the subscripts indicate variables kept constant. The total differentials of S, Π and D can be written as:

$$\underset{\text{heat capacity}}{\mathrm{d}S = \left(\frac{\partial S}{\partial T}\right)_{\Pi,E}} \mathrm{d}T + \underset{\text{piezocaloric effect}}{\left(\frac{\partial S}{\partial \Pi_{ij}}\right)_{T,E}} \mathrm{d}\Pi_{ij} + \underset{\text{electrocaloric effect}}{\left(\frac{\partial S}{\partial E_i}\right)_{T,\Pi}} \mathrm{d}E_i, \tag{B.5}$$

$$\underset{\text{thermal expansion}}{\mathrm{d}x_{ij} = \left(\frac{\partial x_{ij}}{\partial T}\right)_{\Pi,E}} \mathrm{d}T + \underset{\text{elastic compliance}}{\left(\frac{\partial x_{ij}}{\partial \Pi_{kl}}\right)_{T,E}} \mathrm{d}\sigma_{ij} + \underset{\text{converse piezoelectricity}}{\left(\frac{\partial x_{ij}}{\partial E_k}\right)_{T,\Pi}} \mathrm{d}E_k, \tag{B.6}$$

$$\underset{\text{pyroelectric effect}}{\mathrm{d}D_i = \left(\frac{\partial D_i}{\partial T}\right)_{\Pi,E}} \mathrm{d}T + \underset{\text{direct piezoelectricity}}{\left(\frac{\partial D_i}{\partial \Pi_{jk}}\right)_{T,E}} \mathrm{d}\Pi_{ij} + \underset{\text{dielectric permittivity}}{\left(\frac{\partial D_i}{\partial E_j}\right)_{T,\Pi}} \mathrm{d}E_j. \tag{B.7}$$

Each of the partial derivatives in Eqns (B.5)–(B.7) identifies a physical effect [11] as indicated in the equations. Since the order in which derivatives are taken is irrelevant, it follows from (B.3) and (B.5)–(B.6) that, for example:

$$\underset{\text{converse piezoelectric effect}}{d_{ijk}^{T,\Pi} = \left(\frac{\partial x_{ij}}{\partial E_k}\right)_{T,\Pi}} = -\left(\frac{\partial^2 G}{\partial E_k \partial \Pi_{ij}}\right) = -\left(\frac{\partial^2 G}{\partial \Pi_{ij} \partial E_k}\right) = \underset{\text{direct piezoelectric effect.}}{\left(\frac{\partial D_k}{\partial \Pi_{ij}}\right)_{T,E}} = d_{kij}^{T,E}. \tag{B.8}$$

Equation (B.8) demonstrates the thermodynamic equivalence of the direct and converse piezoelectric effect. Using other thermodynamic potentials, which can be formed by taking Legendre transformations of the internal energy, it is possible to write a total of 27 relationships like (B.8), which are known as Maxwell relationships.

It is common to express Eqns (B.5)–(B.7) in the following integrated form, assuming that $\mathrm{d}E$ and $\mathrm{d}\Pi$ represent small deviations from the zero initial stress and field [11]:

$$\Delta S = \frac{c^{X,E}}{T}\Delta T + \alpha_{ij}^{T,E}\Pi_{ij} + p_i^{T,\Pi}E_i, \tag{B.9}$$

$$x_{ij} = \alpha_{ij}^{\Pi,E}\Delta T + s_{ijkl}^{T,E}\Pi_{kl} + d_{kij}^{T,\Pi}E_k, \tag{B.10}$$

$$D_i = p_i^{\Pi,E}\Delta T + d_{ijk}^{T,E}\Pi_{jk} + \varepsilon_{ij}^{T,\Pi}E_j. \tag{B.11}$$

Superscripts in Eqns (B.8)–(B.11) denote variables held constant, α_{ij} is the thermal expansion tensor, and c is the heat capacity. Relations (B.5)–(B.7) and (B.9)–(B.11) include only linear effects.

The set of independent variables (E, Π) chosen for the derivation of Eqns (4.6)–(4.7) is arbitrary. Other thermodynamic potentials and combinations of independent variables give six remaining isothermal piezoelectric constitutive equations:

$$\Pi_m = c^E_{mn} x_n - e^x_{im} E_i, \tag{B.12}$$

$$D_i = e^E_{im} x_m + \varepsilon^x_{ij} E_j, \tag{B.13}$$

$$\Pi_m = c^D_{mn} x_n - h^x_{im} D_i, \tag{B.14}$$

$$E_i = -h^D_{im} x_m + \beta^x_{ij} D_j, \tag{B.15}$$

$$x_m = s^D_{mn} \Pi_n + g^\Pi_{im} D_i, \tag{B.16}$$

$$E_i = -g^D_{im} \Pi_m + \beta^x_{ij} D_j, \tag{B.17}$$

where superscripts again indicate variables held constant. e, g, and h are piezoelectric tensors, and β is inverse dielectric susceptibility ($= \chi^{-1}$). One important result of the thermodynamics of piezoelectric materials is that piezoelectric coefficients of the same type are thermodynamically equivalent: $d^\Pi = d^E$, $g^D = g^\Pi$, $e^x = e^E$, and $h^D = h^x$, and the superscripts are usually omitted.

Consider, as an illustration, the difference between g and d coefficients, while omitting matrix indices for simplicity. Relation $D = \mathrm{d}\Pi$ gives piezoelectric charge measured on shorted samples, with free flow of the charge into an external electric circuit. If the sample is open circuited, this charge will accumulate on the sample surface and will generate an electric field E across the sample. This field depends on capacitance (permittivity) of the sample (charge = capacitance × voltage) and is related to the stress by $E = -g\Pi$ where $g = d/\varepsilon$. Which of relations (B.12)–(B.17) is to be used in a particular problem depends on the elastic and electric boundary conditions.

The coefficients of piezoelectric tensors are mutually related by the following relationships:

$$d_{im} = e_{in} s^E_{nm} = \varepsilon^\Pi_{ij} g_{jm} \text{ (m/V or C/N)}, \tag{B.18}$$

$$e_{im} = d_{in} c^E_{nm} = \varepsilon^x_{ij} h_{jm} \text{ (C/m}^2 \text{ or Vm/N)}, \tag{B.19}$$

$$g_{im} = h_{in} s^D_{nm} = \beta^\Pi_{ij} d_{jm} \text{ (m}^2\text{/C or N/(Vm))}, \tag{B.20}$$

$$h_{im} = g_{in} c^D_{nm} = \beta^x_{ij} e_{jm} \text{ (N/C or V/m)}. \tag{B.21}$$

Because of the piezoelectric coupling between the electrical and elastic fields, the values of the dielectric permittivity and elastic compliance (or

stiffness) measured under different experimental conditions will not be the same [187].

ACKNOWLEDGEMENT

The author gratefully acknowledges contributions from his students, collaborators, and colleagues: Abdolghaffar Barzegar, Fan Chu, Matthew Davis, Marlyse Demartin, Jonas Dorn, Pedro Duran Martin, Jamasp Jhabvala, Maxim Morozov, Juliette Müller, Gilles Robert, Nava Setter, Bharadwaja Srowthi, Alexandar Taganstev, David Taylor, and Cyril Voisard. Many results presented in this chapter have been obtained in the framework of the projects financed by the Swiss National Science Foundation.

References

1. M. E. Lines and A. M. Glass, *Principles and Applications of Ferroelectrics and Related Materials*, Clarendon, Oxford (1979).
2. J. M. Herbert, *Ferroelectric Transducers and Sensors*, Gordon and Breach, New York (1982).
3. J. M. Herbert, *Ceramic Dielectrics and Capacitors*, Gordon and Breach, New York (1985).
4. P. Ge and M. Jouaneh, 'Modeling hysteresis in piezoceramic actuators', Precission Engineering 17, 211–221 (1995).
5. P. Ge and M. Jouaneh, 'Generalized Preisach model for hysteresis nonlinearity of piezoceramic actuators', Precission Engineering 20, 99–111 (1997).
6. D. Hughes and J. T. Wen, 'Preisach modeling of piezoceramic and shape memory alloy hysteresis', Smart Mater. Str. 6, 287–300 (1997).
7. L. Cima, E. Laboure, and P. Muralt, 'Characterization and model of ferroelectrics based on experimental Preisach density', Review of Scientific Instruments 73, 3546–3552 (2002).
8. A. T. Bartic, D. J. Wouters, H. E. Maes, J. T. Rickes, and R. M. Waser, 'Presiach model for the simulation of ferroelectric capacitors', J. Appl. Phys. 89, 3420–3425 (2001).
9. A. Stancu, D. Ricinschi, L. Mitoseriu, P. Postolache, and M. Okuyama, 'First-order reversal curves diagrams for the characterization of ferroelectric switching', Applied Physics Letters 83, 3767–3769 (2003).
10. I. D. Mayergoyz, *Mathematical Models of Hysteresis*, Springer-Verlag, New York (1991).

11. J. F. Nye, *Physical Properties of Crystals*, Oxford University, Oxford (1985).
12. P. Muralt, 'Piezoelectric thin films for MEMS', Integrated Ferroelectrics 17, 297–307 (1997).
13. A. Barzegar, D. Damjanovic, N. Ledermann, and P. Muralt, 'Piezoelectric response of thin films determined by charge integration technique: substrate bending effects', J. Appl. Phys. 93, 4756–4760 (2003).
14. T. Mitsui, I. Tatsuzaki, and E. Nakamura, *An Introduction to the Physics of Ferroelectrics*, Gordon and Breach, London (1976).
15. R. Resta, '*Ab initio* simulation of the properties ferroelectric materials', Modelling Simul. Mater. Sci. Eng. 11, R69–R96 (2003).
16. F. Jona and G. Shirane, *Ferroelectric Crystals*, Pergamon, New York (1962).
17. B. A. Strukov and A. P. Levanyuk, *Ferroelectric Phenomena in Crystals: Physical Foundations*, Springer, Berlin (1998).
18. R. J. Nelmes and W. F. Kuhs, 'The crystal structure of tetragonal $PbTiO_3$ at room temperature and at 700K', Solid State Comm. 54, 721–723 (1985).
19. S. Stemmer, S. K. Streiffer, F. Ernst, and M. Rühle, 'Atomistic structure of 90° domain walls in ferroelectric $PbTiO_3$ thin films', Phil. Mag. A 71, 713–724 (1995).
20. M. Foeth, A. Sfera, P. Stadelmann, and P.-A. Buffat, 'A comparison of HREM and weak beam transmission electron microscopy for the quantitative measurement of the thickness of ferroelectric domain walls', J. Electron. Microsc. 48, 717–723 (1999).
21. M. Foeth, 'Determination of the thermal broadening of ferroelectric domain walls using quantitative transmission electron microscopy', PhDI, Swiss Federal Institute of Technology-EPFL, Lausanne, Switzerland (1999).
22. J. C. Burfoot and G. W. Taylor, *Polar Dielectrics and Their Applications*, Macmillan, London (1979).
23. G. Arlt, 'Twinning in ferroelectric and ferroelastic ceramics: stress relief,' J. Mat. Sci. 25, 2655–2666 (1990).
24. R. E. Newnham, *Structure–Property Relations*, Springer-Verlag, Berlin (1975).
25. J. Fousek and V. Janovec, 'The orientation of domain walls in twinned ferroelectric crystals,' J. Appl. Phys. 40, 135–142 (1969).

26. A. K. Tagantsev, I. Stolichnov, N. Setter, J. S. Cross, and M. Tsukuda, 'Non-Kolmogorov–Avrami switching kinetics in ferroelectric thin films', Phys. Rev. B 66, 214109 (2002).
27. M. E. Caspari and W. J. Merz, 'The electromechanical behavior of $BaTiO_3$ single-domain crystals', Phys. Rev. 80, 1082–1089 (1950).
28. B. Jaffe, W. R. Cook, and H. Jaffe, *Piezoelectric Ceramics*, Academic, New York (1971).
29. T. Tsurumi, Y. Kumano, N. Ohashi, T. Takenaka, and O. Fukunaga, '90° domain reorientation and electric-field-induced strain of tetragonal lead zirconate titanate ceramics', Jpn. J. Appl. Phys. 36, 5970–5975 (1997).
30. M. J. Zipparo, K. K. Shung, and T. R. Shrout, 'Piezoceramics for high-frequency (20 to 100 MHz) single-element imaging transducers', IEEE Trans. UFFC 44, 1038–1048 (1997).
31. K. Uchino, 'Electrostrictive actuators: materials and applications', Am. Ceram. Soc. Bull. 65, 647–652 (1986).
32. V. Y. Shur and E. L. Rumyantsev, 'Kinetics of ferroelectric domain structure during switching: theory and experiment', Ferroelectrics 151, 171–180 (1994).
33. V. Y. Shur, 'Fast polarization reversal process: evolution of ferroelectric domain structure in thin films', in: *Ferroelectric Thin Films: Synthesis and Basic Properties*, vol. 10, C. P. de Araujo, J. F. Scott and G. W. Taylor Eds, Gordon and Breach, Amsterdam (1996), pp. 153–192.
34. V. Shur and E. Rumyantsev, 'Arising and evolution of the domain structure in ferroics', J. Korean Phys. Soc. 32, S727–S732 (1998).
35. T. J. Yang, V. Gopalan, P. J. Swart, and U. Mohadeen, 'Direct observation of pinning and bowing of a single ferroelectric domain wall', Phys. Rev. Lett. 82, 4106–4109 (1999).
36. V. S. Postnikov, V. S. Pavlov, and S. K. Turkov, 'Internal friction in ferroelectrics due to interaction of domain boundaries and point defects', J. Phys. Chem. Sol. 31, 1785–1791 (1970).
37. J. Fousek and B. Brezina, 'Relaxation of 90° domain walls of $BaTiO_3$ and their equation of motion', J. Phys. Soc. Jap. 19, 830–838 (1964).
38. J. Fousek, 'The contribution of domain walls to the small-signal complex permittivity of $BaTiO_3$', Czech. J. Phys. 15, 412–417 (1965).
39. G. Arlt and N. A. Pertsev, 'Force constant and effective mass of 90° domain walls in ferroelectric ceramics', J. Appl. Physics. 70, 2283–2289 (1991).

40. G. Arlt, H. Dederichs and R. Herbeit, '90°-domain wall relaxation in tetragonally distorted ferroelectric ceramics', Ferroelectrics 74, 37–53 (1987).
41. H. Z. Ma, W. J. Kim, J. S. Horwitz, S. W. Kirchoefer, and J. Levy, 'Lattice-scale domain wall dynamics in ferroelectrics', Physical Review Letters 91, 217601 (2003).
42. E. I. Bondarenko, V. Y. Topolov, and A. V. Turik, 'The role of 90° domain wall displacements in forming physical properties of perovskite ferroelectric ceramics', Ferroelectr. Lett. 13, 13 (1991).
43. D. Damjanovic and M. Demartin, 'Contribution of the irreversible displacement of domain walls to the piezoelectric effect in barium titanate and lead zirconate titanate ceramics', J. Phys.: Condens. Matter 9, 4943–4953 (1997).
44. L. E. Cross, 'Ferroelectric ceramics: tailoring properties for specific applications', in *Ferroelectric Ceramics*, N. Setter and E. L. Colla Eds, Birkhäuser, Basel (1993), pp. 1–86.
45. Q. M. Zhang, H. Wang, N. Kim, and L. E. Cross, 'Direct evaluation of domain-wall and intrinsic contributions to the dielectric and piezoelectric response and their temperature dependence on lead zirconate-titanate ceramics', J. Appl. Phys. 75, 454–459 (1994).
46. Q. M. Zhang, W. Y. Pan, S. J. Jang, and L. E. Cross, 'Domain wall excitations and their contributions to the weak-signal response of doped lead zirconate titanate ceramics', J. Appl. Phys. 64, 6445–6451 (1988).
47. M. Stula, J. Fousek, H. Kabelka, M. Fally, and H. Warhanek, 'Extrinsic contribution to piezoelectric properties of RbH_2PO_4 crystals in the ferroelectric phase', J. Korean Phys. Soc. 32, S758–S760 (1998).
48. R. Hayakawa and Y. Wada, 'Piezoelectricity and related properties of polymers films', in *Advances in Polymer Science*, vol.11, H. J. Cantow, G. Dall'Asta, J. D. Ferry, H. Fujita, W. Kern, G. Natta, S. Okamura, C. G. Overberger, W. Prins, G. V. Schulz, W. P. Slichter, A. J. Stavermasn, J. K. Stille Eds, Springer, Berlin (1973), pp. 1–56.
49. G. Arlt, 'Piezoelectric relaxation', Ferroelectrics 40, 149–157 (1982).
50. R. Lakes, 'Shape-dependent damping in piezoelectric solids', IEEE Trans. Sonics. Ultrason. SU-27, 208–213 (1980).
51. G. E. Martin, 'Dielectric, piezoelectric and elastic losses in longitudinally polarized segmented ceramics tubes', U.S. Navy J. Underwater Acoustics 15, 329–332 (1965).

52. C. E. Land, G. W. Smith, and C. R. Westgate, 'The dependence of the small-signal parameters of ferroelectric ceramics resonators upon state of polarization', IEEE Trans. Sonics Ultrason. SU-11, 8–19 (1964).
53. R. Holland and E. P. EerNisse, 'Accurate measurement of coefficients in a ferroelectric ceramic', IEEE Trans. Sonics Ultrason. SU-16, 173–181 (1969).
54. J. W. Waanders, *Piezoelectric Ceramics – Properties and Applications*, Philips Components, Eindhoven (1991).
55. A. Schnell, 'Nonlinear charge release of piezoelectric ceramics under uniaxial pressure', Ferroelectrics 28, 351–353 (1980).
56. S. Sherrit, D. B. van Nice, J. T. Graham, B. K. Mukherjee, and H. D. Wiedrick, 'Domain wall motion in piezoelectric materials under high stress', in: *Proceedings of the 8th ISAF*, Greenville, 1982, M. Liu, A. Safari, A. I. Kingon and G. Haertling Eds, IEEE Service Center, Piscataway, NJ (1992), pp. 167–170.
57. D. Damjanovic, 'Stress and frequency dependence of the direct piezoelectric effect in ferroelectric ceramics', J. Appl. Phys. 82, 1788–1797 (1997).
58. D. Damjanovic, M. Demartin Maeder, C. Voisard, and N. Setter, 'Maxwell–Wagner piezoelectric relaxation in ferroelectric heterostructures', J. Appl. Phys. 90, 5708–5712 (2001).
59. V. D. Kugel and L. E. Cross, 'Behavior of soft piezoelectric ceramics under high sinusoidal electric fields', J. Appl. Phys. 84, 2815–2830 (1998).
60. D. V. Taylor, D. Damjanovic and N. Setter, 'Nonlinear contributions to dielectric and piezoelectric properties in lead zirconate titanate thin films', Ferroelectrics 224, 299–306 (1999).
61. J. Meixner and H. G. Reik, *Handbuch der Physik III/2*, Springer, Heidelberg (1959).
62. A. S. Nowick and W. R. Heller, 'Dielectric and anelastic relaxation of crystals containing point defects', Adv. Phys. 14, 101–166 (1965).
63. T. Yamaguchi and K. Hamano, 'Piezoelectric relaxation in ferroelectric $AgNa(NO_2)_2$', J. Phys. Soc. Japan 50, 3956–3963 (1981).
64. J. G. Smits, 'Influence of moving domain walls and jumping lattice defects on complex material coefficients of piezoelectrics', IEEE Trans. Sonics Ultrasonics SU-23, 168–174 (1976).
65. K. Hamano and T. Yamaguchi, 'Piezoelectric relaxation in ferroelectrics and polymers', Ferroelectrics 42, 23–33 (1982).

66. T. Furukawa, K. Ishida, and E. Fukada, 'Piezoelectric properties in the composite systems of polymers and PZT ceramics', J. Appl. Phys. 50, 4904–4912 (1979).
67. C. J. Dias and D. K. Das-Gupta, 'Piezo- and pyroelectricity in ferroeletric ceramic–polymer composites', in *Key Engineering Materials. Ferroelectric Polymers and Ceramic–Polymer Composites*, D. K. Das-Gupta Ed., Trans Tech Publications, Switzerland (1994), pp. 181–216.
68. A. Daniel, *Dielectric Relaxation*, Academic, London (1967).
69. C. J. F. Böttcher and P. Bordewijk, *Theory of Polarization – Vol. II. Dielectrics in Time-dependent Fields*, Elsevier Amsterdam (1978), pp. 1–128.
70. R. Holland, 'Representation of dielectric, elastic, and piezoelectric losses by complex coefficients', IEEE Trans. Sonics Ultrason. SU-14, 18–20 (1967).
71. D. Damjanovic, T. R. Gururaja, and L. E. Cross, 'Anisotropy in piezoelectric properties of modified lead titanate ceramics', Am. Ceram. Soc. Bull. 66, 699–703 (1987).
72. M. Demartin Maeder, D. Damjanovic, C. Voisard, and N. Setter, 'Piezoelectric properties of $SrBi_4Ti_4O_{15}$ ferroelectric ceramics', J. Mat. Res. 17, 1376–1384 (2002).
73. H. E. Mueser and H. Schmitt, 'Measurements of complex piezoelectric constants in ferroelectric crystals', J. Phys. (France) 33, C2/103–C2/104 (1972).
74. H. E. Müser and J. Petersson, 'Thermodynamic theory of relaxation phenomena', Fortschritte der Physik 19, 559–612 (1971).
75. G. Bertotti, *Hysteresis in Magnetism*, Academic Press, San Diego (1998).
76. W. C. Elmore and M. A. Heald, *Physics of Waves*, Dover, New York (1985).
77. R. Lakes, 'Discussion', IEEE Transactions on Sonics and Ultrasonics SU-27, 208 (1980).
78. F. B. Hildebrand, *Methods of Applied Mathematics*, Prentice Hall, Englewood Clifs, NJ (1952).
79. D. A. Berlincourt, D. R. Curran, and H. Jaffe, 'Piezoelectric and piezomagnetic materials and their function in transducers', in: *Physical Acoustics – Principles and Methods*, vol. I, Part A, W. P. Mason Ed., Academic, New York (1964), pp. 170–270.
80. A. V. Turik and V. Y. Topolov, 'Ferroelectric ceramics with a large piezoelectric anisotropy', J. Phys. D: Appl. Phys. 30, 1541–1549 (1997).

81. R. Hilfer, 'Analytical representations for relaxation functions of glasses', Journal of Non-Crystalline Solids 305, 122–126 (2002).
82. A. K. Jonscher, *Dielectric Relaxation in Solids*, Chelsea Dielectric Press, London (1983).
83. J.-L. Déjardin, 'Fractional dynamics and nonlinear harmonic responses in dielectric relaxation of disordered liquids', Phys. Rev. E 68, 031108 (2003).
84. R. Metzler and J. Klafter, 'From stretched exponential to inverse power-law: fractional dynamics, Cole–Cole relaxation processes, and beyond', Journal of Non-Crystalline Solids 305, 81–87 (2002).
85. J. van Turnhout and M. Wübbenhorst, 'Analysis of complex dielectric spectra. II. Evaluation of the activation energy landscape by differential sampling', Journal of Non-Crystalline Solids 305, 50–58 (2002).
86. O. Bidault, M. Maglione, M. Actis, M. Kchikech, and B. Salce, 'Polaronic relaxation in perovskites', Phys. Rev. B 52, 4191 (1995).
87. M. S. Islam, 'Ionic transport in ABO_3 perovskite oxides: a computer modelling tour', J. Mater. Chem. 20, 1027–1038 (2000).
88. H. S. Shulman, D. Damjanovic, and N. Setter, 'Niobium doping and dielectric anomalies in bismuth titanate', J. Am. Ceram. Soc. 83, 528–532 (2000).
89. B. Meyer and D. Vanderbilt, '*Ab initio* study of ferroelectric domain walls in $PbTiO_3$', Phys. Rev. B 65, 104111 (2002).
90. A. V. Turik, O. V. Pugachev, V. V. Volgin, and M. S. Novikov, 'Infralow--frequency dispersion of piezoelectric and dielectric constants in $PbTiO_3$-based ferreoelctric ceramics', J. Europ. Ceram. Soc. 19, 1175–1177 (1999).
91. B. Jimenez and J. M. Vicente, 'Oxygen defects and low-frequency mechanical relaxation in Pb-Ca and Pb-Sm titanates', J. Phys. D: Appl. Phys. 31, 446–452 (1998).
92. K. Hamano, 'Electromechanical properties of order–disorder type ferroelectrics. I. Piezoelectric and elastic properties', J. Phys. Soc. Jpn. 41, 1670–1678 (1976).
93. A. R. Von Hippel, *Dielectrics and Waves*, MIT Press, Cambridge, MA (1954).
94. A. V. Turik and G. S. Radchenko, 'Maxwell–Wagner relaxation in piezoactive media', J. Phys. D: Appl. Phys. 35, 1188–1192 (2002).

95. H. Ueda, E. Fukada, and F. E. Karasz, 'Piezoelectricity in three-phase sytems: effect of the boundary phase', J. Appl. Phys. 60, 2672–2677 (1986).

96. G. R. Strobl, *The Physics of Polymers*, Springer, Berlin (1996).

97. J. G. Smits, 'High-accuracy determination of real and imaginary parts of elastic, piezoelectric and dielectric constants of ferroelectric Plzt (11/55-45) ceramics with iterative method,' Ferroelectrics 64, 275–291 (1985).

98. J. G. Smits, 'Iterative method for accurate determination of real and imaginary parts of materials coefficients of piezoelectric ceramics,' IEEE Transactions on Sonics and Ultrasonics 23, 393–402 (1976).

99. D. Damjanovic, 'An equivalent electric circuit of a piezoelectric bar resonator with a large piezoelectric phase angle', Ferroelectrics 110, 129–135 (1990).

100. A. V. Mezheretskii, 'Energy losses in piezoelectric ceramic during electrical excitation', Elektrichestvo 10, 5–7 (1984). (in Russian).

101. B. Noheda, D. E. Cox, G. Shirane, J. A. Gonzalo, L. E. Cross, and S.-E. Park, 'A monoclinic ferroelectric phase in the $Pb(Zr_{1-x}Ti_x)O_3$ solid solution', Appl. Phys. Lett. 74, 2059–2061 (1999).

102. B. Noheda, J. A. Gonzalo, L. E. Cross, *et al.*, 'Tetragonal-to-monoclinic phase transition in a ferroelectric perovskite: the structure of $PbZr_{0.52}Ti_{0.48}O_3$', Phys. Rev. B 61, 8687–8695 (2000).

103. M. J. Haun, E. Furman, S. J. Jang, and L. E. Cross, 'Thermodynamic theory of the lead zirconate-titanate solid solution system, part V: theoretical calculations', Ferroelectrics 99, 63–86 (1989).

104. R. Guo, L. E. Cross, S.-E. Park, B. Noheda, D. E. Cox, and G. Shirane, 'Origin of the high piezoelectric response in $PbZr_{1-x}Ti_xO_3$', Phys. Rev. Lett. 84, 5423–5426 (2000).

105. V. Mueller and Q. M. Zhang, 'Nonlinearity and scaling behavior in donor-doped lead zirconate titanate piezoceramic', Appl. Phys. Lett. 72, 2692–2694 (1998).

106. V. Mueller and Q. M. Zhang, 'Shear response of lead zirconate titanate piezoceramics', J. Appl. Phys. 83, 3754–3761 (1998).

107. V. Perrin, M. Troccaz, and P. Gonnard, 'Non-linear behavior of the permittivity and of the piezoelectric strain constant under high electric field drive', J. Electroceramics 4, 189–194 (2000).

108. D. V. Taylor and D. Damjanovic, 'Evidence of domain wall contribution to the dielectric permittivity in PZT thin films at sub-switching fields', J. Appl. Phys. 82, 1973–1975 (1997).

109. D. V. Taylor and D. Damjanovic, 'Domain wall pinning contribution to the nonlinear dielectric permittivity in Pb(Zr, Ti)O_3 thin films', Appl. Phys. Lett. 73, 2045–2047 (1998).

110. D. A. Hall, 'Nonlinearity in piezoelectric ceramics', J. Mat. Sci. 36, 4575–4601 (2001).

111. D. A. Hall, 'Rayleigh behavior and the threshold field in ferroelectric ceramics', Ferroelectrics 223, 319–328 (1999).

112. D. Damjanovic and M. Demartin, 'The Rayleigh law in piezoelectric ceramics', J. Phys. D: Appl. Phys. 29, 2057–2060 (1996).

113. R. S. Lord Rayleigh, 'XXV. Notes on electricity and magnetism-III. On the behaviour of iron and steel under the operation of feeble magnetic forces', Phil. Mag. 23, 225–245 (1887).

114. F. Preisach, 'Über die magnetische Nachwirkung', Z. Physik 94, 277–302 (1935).

115. L. Néel, 'Théories des lois d'aimantation de Lord Rayleigh', Cahiers Phys. 12, 1–20 (1942).

116. H. Kronmüller, 'Statistical theory of Rayleigh's law', Z. Angew. Phys. 30, 9–13 (1970).

117. F. Colaiori, A. Gabrielli, and S. Zapperi, 'Rayleigh loops in the random-field Ising model on the Bethe lattice', Phys. Rev. B 65, no. 224404 (2002).

118. S. Zapperi, A. Magni, and G. Durin, 'Microscopic foundations of the Rayleigh law of hysteresis', J. Magnetism and Magnetic Mat. 242–245, 987–992 (2001).

119. A. V. Turik, 'Theory of polarization and hysteresis of ferroelectrics', Soviet Phys. – Solid State 5, 885–887 (1963).

120. A. V. Turik, 'A statistical method for the investigation of repolarization processes in ferroelectric ceramics', Soviet Phys. – Solid State 5, 1751–1753 (1964).

121. A. V. Turik, 'Experimental investigation of the statistical distribution of domains in a ferroelectric ceramic', Soviet Phys. – Solid State 5, 2141–2143 (1964).

122. O. Boser, 'Statistical theory of hysteresis in ferroelectric materials', J. Appl. Phys. 62, 1344–1348 (1987).

123. M. Sjöström, 'Frequency analysis of classical Preisach model', IEEE Transactions on Magnetics 35, 2097–2103 (1999).

124. J. Dec, W. Kleemann, S. Miga, *et al.*, 'Probing polar nanoregions in $Sr_{0.61}Ba_{0.39}Nb_2O_6$ via second-harmonic dielectric response', Phys. Rev. B 68, no. 092105 (2003).

125. K. Kuramoto and E. Nakamura, 'Nonlinear dielectric constant of KH_2PO_4 in the ferroelectric phase', Ferroelectrics 157, 57–62 (1994).

126. D. V. Taylor, 'Dielectric and piezoelectric properties of sol-gel derived Pb(Zr, Ti)O_3 thin films', PhD Thesis no. 1949I, Swiss Federal Institute of Technology-EPFL, Lausanne (1999).

127. G. Robert, D. Damjanovic, and N. Settter, 'Separation of nonlinear and friction-like contributions to the piezoelectric hysteresis', in *Proc. 12th IEEE International Symposium on Application of Ferroelectrics*, Honolulu, IEEE Service Center. Piscataway, NJ, pp. 699–702.

128. G. Robert, D. Damjanovic, and N. Setter, 'Piezoelectric hysteresis analysis and loss separation', J. Appl. Phys. 90, 4668–4675 (2001).

129. L. B. Ioffe and V. M. Vinokur, 'Dynamics of interfaces and dislocations in disordered media', Journal of Physics C – Solid State Physics 20, 6149–6158 (1987).

130. T. Nattermann, Y. Shapir, and I. Vilfan, 'Interface pinning and dynamics in random systems', Phys. Rev. B 42, 8577–8586 (1990).

131. D. Damjanovic, 'Logarithmic frequency dependence of the piezoelectric effect due to pinning of ferroelectric-ferroelastic domain walls', Phys. Rev. B 55, R649–R652 (1997).

132. W. Kleemann, J. Dec, S. Miga, T. Woike, and R. Pankrath, 'Non-Debye domain wall induced dielectric response in $Sr_{0.61-x}Ce_xBa_{0.39}Nb_2O_6$', Phys. Rev. B 65, no. 220101 (2002).

133. V. Mueller, Y. Shchur, H. Beige, A. Fuith, and S. Stepanow, 'Non-Debye domain wall response in KH_2PO_4', Europhysics Letters 57, 107–112 (2002).

134. V. Mueller, Y. Shchur, and H. Beige, 'Logarithmic domain-wall dispersion', Ferroelectrics 269, 201–206 (2002).

135. A. K. Tagantsev, private communication (2004).

136. A. V. Shil'nikov, N. M. Galiyarova, S. V. Gorin, D. G. Vasil'ev, and L. K. Vologirova, 'Domain-wall motion in low- and infralow-frequency electric fields', Izv. Akad. Nauk SSSR, Ser. Fiz. 55, 578–582 (1991).

137. A. K. Tagantsev and J. Fousek, 'Permittivity enhancement due to domain walls interacting with repulsive defects', Ferroelectrics 221, 193–198 (1999).

138. R. C. Miller and A. Savage, 'Motion of 180° domain walls in metal electroded barium titanate crystals as a function of electric field and sample thickness'. J. Appl. Phys. 31, 662–669 (1960).

139. T. Tybell, P. Paruch, T. Giamarchi, and J.-M. Triscone, 'Domain wall creep in epitaxial ferroelectric $Pb(Zr_{0.2}Ti_{0.8})O_3$ thin films', Phys. Rev. Lett. 89, 097601 (2002).

140. A. A. Fedorenko, V. Mueller, and S. Stepanow, 'Dielectric response due to stochastic motion of pinned domain walls', Phys. Rev. B70, 224104 (2004).

141. A. K. Tagantsev, private communication (2004).

142. G. Robert, D. Damjanovic, N. Setter, and A. V. Turik, 'Preisach modeling of piezoelectric nonlinearity in ferroelectric ceramics', J. Appl. Phys. 89, 5067–5074 (2001).

143. N. S. Akulov and P. P. Galenko, 'About theory of rectangular hysteresis loops in ferromagnetics', Dokl. Acad. Nauk BSSR 6, 551–555 (1962).

144. G. Robert, D. Damjanovic, and N. Setter, 'Preisach distribution function approach to piezoelectric nonlinearity and hysteresis', J. Appl. Phys. 90, 2459–2464 (2001).

145. G. Robert, private communication (2001).

146. G. Robert, 'Extrinsic contributions to the piezoelectric response of lead-based ferroelectrics', PhD Thesis, Swiss Federal Institute of Technology, Lausanne (2001).

147. W. L. Warren, D. Dimos, B. A. Tuttle, R. D. Nasby, and G. E. Pike, 'Electronic domain pinning in $Pb(Zr, Ti)O_3$ thin films and its role in fatigue', Appl. Phys. Lett. 65, 1018–1020 (1994).

148. H. N. Al-Shareef, B. A. Tuttle, W. L. Warren, *et al.*, 'Effect of B-site cation stochiometry on electrical fatigue of $RuO_2/Pb(Zr_xTi_{1-x})O_3/RuO_2$ capacitors', J. Appl. Phys. 79, 1013–1016 (1996).

149. W. L. Warren, D. Dimos, and B. A. Tuttle, 'Electronic and ionic trapping at domain walls in $BaTiO_3$', J. Am. Ceram. Soc. 77, 2753–2757 (1994).

150. W. L. Warren, D. Dimos, G. E. Pike, K. Vanheusden, and R. Ramesh, 'Alignment of defect dipoles in polycrystalline ferroelectrics', Appl. Phys. Lett. 67, 1689–1691 (1995).

151. W. L. Warren, G. E. Pike, K. Vanheusden, D. Dimos, B. A. Tuttle, and J. Robertson, 'Defect-dipole alignment and tetragonal strain in ferroelectrics', J. Appl. Phys. 79, 9250–9257 (1996).

152. W. L. Warren, K. Vanheusden, D. Dimos, G. E. Pike, and B. A. Tuttle, 'Oxygen vacancy motion in perovskite oxides', J. Am. Ceram. Soc. 79, 536–538 (1996).

153. K. Carl and K. H. Haerdtl, 'Electrical after-effects in $Pb(Ti, Zr)O_3$ ceramics', Ferroelectrics 17, 473–486 (1978).

154. L. Sagalowicz, F. Chu, P. Duran Martin, and D. Damjanovic, 'Microstructure, structural defects and piezoelectric response of $Bi_4Ti_3O_{12}$ modified by Bi_3TiNbO_9', J. Appl. Phys. 88, 7258–7263 (2001).

155. W. R. Buessem, L. E. Cross, and A. K. Goswami, 'Phenomenological theory of high permittivity in fine-grained barium titanate', J. Am. Ceram. Soc. 49, 33–36 (1966).

156. M. Demartin and D. Damjanovic, 'Dependence of the direct piezoelectric effect in coarse and fine grain barium titanate ceramics on dynamic and static pressure', Appl. Phys. Lett. 68, 3046–3048 (1996).

157. M. Liu and K. J. Hsia, 'Locking of electric-field-induced non-180° domain switching and phase transition in ferroelectric materials upon cyclic electric fatigue', Appl. Phys. Lett. 83, 3976–3978 (2003).

158. S. E. Park and T. R. Shrout, 'Ultrahigh strain and piezoelectric behavior in relaxor based ferroelectric single crystals', J. Appl. Phys. 82, 1804–1811 (1997).

159. K. Nakamura, T. Tokiwa, and Y. Kawamura, 'Domain structures in $KNbO_3$ crystals and their piezoelectric properties', J. Appl. Phys. 91, 9272–9276 (2002).

160. S. Wada, S. Suzuki, T. Noma, *et al.*, 'Enhanced piezoelectric property of barium titanate single crystals with engineered domain configuration', Jpn. J. Appl. Phys. 38, 5505–5511 (1999).

161. D.V. Taylor and D. Damjanovic, 'Piezoelectric properties of rhombohedral $Pb(Zr, Ti)O_3$ thin films with (100), (111) and ''random'' crystallographic orientation', Appl. Phys. Lett. 76, 1615–1617 (2000).

162. X.-H. Du, J. Zheng, U. Belegundu, and K. Uchino, 'Crystal orientation dependence of piezoelectric properties of lead zirconate titanate near the morphotropic phase boundary', Appl. Phys. Lett. 72, 2421–2423 (1998).

163. X. Du, U. Belegundu, and K. Uchino, 'Crystal orientation of piezoelectric properties in lead zirconate titanate: theoretical expectation for thin films', Jpn. J. Appl. Phys. 36, 5580–5587 (1997).

164. D. Damjanovic, F. Brem, and N. Setter, 'Crystal orientation dependence of the piezoelectric d_{33} coefficient in tetragonal $BaTiO_3$ as a function of temperature', Appl. Phys. Lett. 80, 652–654 (2002).

165. M. Budimir, D. Damjanovic, and N. Setter, 'Piezoelectric anisotropy-phase transition relations in perovskite single crystals', J. Appl. Phys. 94, 6753–6761 (2003).

166. H. Janocha, K. Kuhnen, 'Real-time compensation of hysteresis and creep in piezoelectric actuators', Sensors and Actuators A 79, 83–89 (2000).

167. A. Daniele, S. Salapaka, M. V. Salapaka, and M. Dahlel, 'Piezoelectric scanners for atomic force microscopes: design of lateral sensors, identification and control', in *Proceedings of the 1999 ACC Conference*, San Diego, IEEE Service Center, Piscataway, NJ (1999), pp. 253–257.

168. J. F. Scott, *Ferroelectric Memories*, Springer, Berlin (2000).

169. A. K. Tagantsev, I. Stolichnov, E. L. Colla and N. Setter, 'Polarization fatigue in ferroelectric films: basic experimental findings, phenomenological scenarios, and microscopic features', J. Appl. Phys. 90, 1387–1402 (2001).

170. A. K. Tagantsev, 'Size effects in polarization switching in ferroelectric thin films', Integrated Ferroelectrics 16, 237–244 (1997).

171. J. F. Scott, 'Ferroelectric thin films and thin film devices', in *Ferroelectric Ceramics*, N. Setter and E. Colla Eds, Birkhaüser, Basel (1993) pp. 185–212.

172. R. Ramesh, W. K. Chan, B. Wilkens, *et al.*, 'Fatigue and retention in ferroelectric' Y-Ba-Cu-O/Pb-Zr-Ti-O/Y-Ba-Cu-O heterostructures', Appl. Phys. Lett. 61, 1537–1539 (1992).

173. Y. Ishibashi, 'Polarization reversal in ferroelectrics', in *Ferroelectric Thin Films*: *Synthesis and Basic Properties*, vol. 10, C. P. de Araujo, J. F. Scott and G. W. Taylor Eds, Gordon and Breach, Amsterdam (1996) pp. 135–151.

174. Y. Ishibashi and Y. Takagi, 'Note on ferroelectric domain switching', J. Phys. Soc. Jap. 31, 506–510 (1971).

175. O. Lohse, M. Grossmann, U. Boettger, D. Bolten, and R. Waser, 'Relaxation mechanism of ferroelectric switching in $Pb(Zr, Ti)O_3$ thin films', J. Appl. Phys. 89, 2332–2336 (2001).

176. I. Stolichnov, A. K. Tagantsev, N. Setter, J. S. Cross, and M. Tsukada, 'Crossover between nucleation-controlled kinetics and domain wall motion kinetics of polarization reversal in ferroelectric films', Appl. Phys. Lett. 83, 3362–3364 (2003).

177. A. K. Tagantsev, M. Landivar, E. Colla, and N. Setter, 'Identification of passive layer in ferroelectric thin films from their switching parameters', J. Appl. Phys. 78, 2623–2630 (1995).

178. U. Robels, J. H. Calderwood, and G. Arlt, 'Shift and deformation of the hysteresis curve of ferroelectrics by defects: an electrostatic model', J. Appl. Phys. 77, 4002–4008 (1995).

179. S. L. Miller, J. R. Nasby, J. R. Schwank, M. S. Rodgers, and P. V. Dressendorfer, 'Device modeling of ferroelectric capacitors', J. Appl. Phys. 68, 6463–6471 (1990).

180. A. K. Tagantsev, M. Landivar, E. Colla, K. G. Brooks, and N. Setter, 'Depletion, depolarizing effects and switching in ferroelectric thin films', *Science and Technology of Electroceramic Thin Films*, O. Auciello and R. Waser Eds, Kluwer, Boston (1995), pp. 301–314.

181. U. Robels and G. Arlt, 'Domain wall clamping in ferroelectrics by orientation of defects', J. Appl. Phys. 73, 3454–3460 (1993).

182. G. E. Pike, W. L. Warren, D. Dimos, *et al.*, 'Voltage offsets in (Pb, La)(Zr, Ti)O_3', Appl. Phys. Lett. 66, 484–486 (1995).

183. H. N. Al-Shareef, D. Dimos, W. L. Warren, and B. A. Tuttle, 'A model for optical and electrical polarization fatigue in $SrBi_2Ta_2O_9$ and Pb(Zr, Ti)O_3', Integrated Ferroelectrics 15, 53–67 (1997).

184. N. Balke, Y. Genenko, H. Rauh, D. Lupascu, and J. Roedel, 'Ferroelectric aging by drift of charge carriers', presented at *Electroceramics IX*, Cherbourg, France, June (2004).

185. G. Robert, D. Damjanovic, and N. Setter, 'Preisach modeling of ferroelectric pinched loops', Appl. Phys. Lett. 77, 4413–4415 (2000).

186. D. Damjanovic, A. K. Tagantsev, J. Dorn, M. Morozov, J. Müller, and N. Setter, 'Order–disorder transition in hard Pb(Zr, Ti)O_3', unpublished (2002).

187. D. Damjanovic, 'Ferroelectric, dielectric and piezoelectric properties of ferroelectric thin films and ceramics', Rep. Prog. Phys. 61, 1267–1324 (1998).